Norwegian University
of Life Sciences

**Master's Thesis 2021 60 ECTS**
Faculty of Chemistry, Biotechnology and Food science

# Microenvironment Models and the Effect of Metformin on Energy Metabolism in Cervical Cancer Cell Lines

Andrine Myklebust Lindseth
Biotechnology (M.Sc.) – Molecular Biology

# Microenvironment Models and the Effect of Metformin on Energy Metabolism in Cervical Cancer Cell Lines

Andrine Myklebust Lindseth

Supervisors:
Heidi Lyng,
Eva- Katrine Aarnes,
Siv Kjølsrud Bøhn

Oslo University Hospital,
Department of Radiation Biology
and
Norwegian University of Life Sciences,
Faculty of Chemistry, Biotechnology and Food science

## Acknowledgements

The work presented was carried out in the Clinical Radiation Biology group at the Department of Radiation Biology, Institute for Cancer research, Norwegian Radium Hospital, Oslo University Hospital from August 2020 until May 2021. The thesis is part of the Master program in Biotechnology at the Faculty of Chemistry, Biotechnology and Food Sciences (KBM) at the Norwegian University of Life Sciences (NMBU).

First and foremost, I would like to thank my supervisors Dr. philos Heidi Lyng and M.Sc Eva-Katrine Aarnes. I am grateful to be allowed to join the research group and for valuable guidance, encouragement and help with the study both in the lab and with writing. I would also like to thank the rest of the Clinical Radiation Biology group members for insights during presentations. I am grateful to Tine Raabe and Senior scientist Theodossis Theodossiou for help and guidance with the Seahorse instrument, and Senior scientist Sebastian Patzke for help with live cell microscopy and imaging. I would also like to thank my internal supervisor at NMBU, Associate Professor Siv Kjølsrud Bøhn, for helpful advice and encouragement. Furthermore, I am grateful for the company of the fellow master students at office K06 67.

I would also like to thank my family, especially my mom Mette Myklebust, for always supporting and encouraging me. Final thanks go to my partner Þorsteinn Grétar Eiríksson for all the help with illustrations, the love and for always believing in me.

Oslo, May 2021
Andrine Myklebust Lindseth

# Sammendrag

**Bakgrunn:** På tross av gode prognoser for livmorhalskreft hvis oppdaget tidlig, får en tredjedel av pasienter med avanserte stadier tilbakefall etter behandling med kjemoradioterapi. Det er derfor et behov for å forstå biologien bak disse tumorene for å forbedre resultatet av behandling. Ved å omprogrammere metabolismen kan kreftceller utvikle fordeler ovenfor normale celler, som økt proliferasjon og overlevelse under spesialiserte mikromiljø med trekk som hypoksi, høy laktatkonsentrasjon og lav pH. Dette bidrar til kreftprogresjon. Metformin, en vanlig diabetes-medisin, har fått økt interesse innen kreftbehandling ettersom den har vist seg å hemme kreft-metabolisme. Denne studien hadde som mål å undersøke *in vitro* effekter av forskjellige mikro-miljøforhold og metformin på to livmorhalskreftcellelinjer. Spesielt ble nytten av Seahorse-teknologi, som er spesielt egnet til studier av metabolisme, for disse undersøkelsene evaluert.

**Metoder:** Cellelinjene HeLa og SiHa ble brukt som modeller for livmorhalskreft. Tre mikro-miljømodeller ble etablert ved å dyrke cellene under ulike forhold: 1) hypoksi, 2) høy laktat-konsentrasjon (laktosis) og 3) høy laktatkonsentrasjon og lav pH (laktisk acidose). Hypoksi-modellen ble etablert ved å stabilisere HIF-1α, et viktig protein i hypoksiresponsen, ved å bruke $CoCl_2$. Laktat ble tilsatt +/- HCl for å etterligne mikromiljøene rike på laktat ved normal og lav pH. Effekter på proliferasjon ble undersøkt gjennom celletelling, og mitokondriell masse ble studert ved hjelp av fluorescenssignal fra et fluorokrom som binder seg til mitokondriene (MitoTracker Green), detektert av en plateleser. Effekter på metabolismen ble studert ved hjelp av et Seahorse-instrument.

**Resultater:** Resultatene avslørte at proliferasjon ble hemmet av $CoCl_2$ i SiHa-celler, men hadde ingen effekter på HeLa-celler. Laktisk acidose reduserte proliferasjon i begge cellelinjer, mens laktosis ble funnet å øke mitokondriell masse i HeLa-celler. Ingen effekter av metformin ble funnet på proliferasjon eller mitokondriell masse i noen av mikromiljømodellene. Derimot ble metformin funnet å påvirke cellulær metabolisme ved å hemme oksidativ fosforylering på en doseavhengig måte ved bruk av Seahorse-instrumentet.

**Konklusjoner:** Resultatene indikerer at Seahorse-teknologi bør implementeres i fremtidig forskning for å øke forståelsen av cellulær metabolisme under forskjellige mikromiljøforhold og for å avdekke de metabolske effektene av metformin.

# Abstract

**Background:** Although the prognosis is good for cervical cancer if detected early, about one third of the patients with advanced cervical cancer stages relapse after chemoradiotherapy treatment. There is therefore a need to understand the biology of these tumours better to improve treatment outcome. By reprogramming cellular metabolism cancer cells can develop advantages over normal cells, increasing proliferation rates and survival under specialised tumour microenvironments with features such as hypoxia, high lactate concentration and low pH. This contributes to cancer progression towards increased malignancy. The diabetic drug metformin has recently received increased interest for cancer treatment as it has been found to target cellular metabolism. This study aimed to investigate *in vitro* effects of different microenvironmental conditions and metformin on two cervical cancer cell lines. In particular, the usefulness of Seahorse technology, which is especially useful for studies of metabolism, was evaluated.

**Methods:** The cell lines HeLa and SiHa were used as models for cervical cancer. Three microenvironment models were established by culturing the cells under different conditions: 1) hypoxia, 2) high lactate concentration (lactosis) and 3) high lactate concentration and low pH (lactic acidosis). The hypoxia model was established using $CoCl_2$ to stabilize HIF-1α, which is crucial in the hypoxia response. Lactate was added +/- HCl to mimic microenvironments rich in lactate at normal and low pH. Effects on proliferation were investigated through cell counting, and mitochondrial mass was studied using fluorescence signal from Mitotracker Green, as detected by a plate reader. Effects on metabolism was studied using a Seahorse analyser.

**Results:** The results revealed that proliferation was inhibited by $CoCl_2$ in SiHa cells but had no effects on HeLa cells. Lactic acidosis decreased proliferation in both cell lines, while lactosis was found to increase mitochondrial mass in HeLa cells. No effects of metformin were found on proliferation or mitochondrial mass in any of the microenvironment models investigated. However, using the Seahorse analyser metformin was found to affect cellular metabolism by inhibiting oxidative phosphorylation in a dose dependent manner.

**Conclusions:** The results indicate that Seahorse analyser should be implemented in future research to better understand cellular metabolism under different microenvironmental conditions and to reveal the metabolic effects of metformin.

# Abbreviations and units

| | |
|---|---|
| **µg** | Microgram |
| **µL** | Microliter |
| **µm** | Micrometer |
| **µM** | Micromolar |
| **3-D** | Three-Dimensional |
| **ADP** | Adenosine diphosphate |
| **AE** | Anion Exchanger |
| **ATP** | Adenosine triphosphate |
| **BSA** | Bovine serum albumin |
| **CA IX** | Carbonic anhydrase 9 |
| **$CO_2$** | Carbon dioxide |
| **$CoCl_2$** | Cobalt(II)Chloride |
| **CoQ** | Coenzyme Q |
| **$ddH_2O$** | Double distilled water |
| **DMEM** | Dulbecco's Modified Eagle Medium |
| **DMSO** | Dimethyl sulfoxide |
| **DNA** | Deoxyribonucleic acid |
| **DTT** | Dithiothreitol |
| **ECAR** | Extracellular acidification rate |
| **ETC** | Electron transport chain |
| **$FADH_2$** | dihydro- flavin adenine dinucleotide |
| **FBS** | Fetal bovine serum |
| **FCCP** | Trifluoromethoxy carbonyl cyanide phenylhydrazone |
| **g** | Gram |
| **GLUT** | Glucose transporter |
| **$H^+$** | Proton |
| **$H_2PO_4^-$** | Dihydrogen phosphate |
| **HCl** | Hydrochloric acid |
| **HEPES** | 4-(2-hydroxyethyl)-1-piperazineethanesulfonic acid |
| **HIF** | Hypoxia inducible factor |
| **HPV** | Human papillomavirus |
| **HRP** | Horseradish peroxidase |
| **kDa** | Kilodaltons |
| **LA** | Lactic acidosis |
| **LAF** | Laminar airflow |
| **M** | Molar (Moles per litre) |
| **MCT** | Monocarboxylate transporter |
| **mg** | Milligrams |
| **min** | Minutes |
| **Mm** | Millimetres |
| **mM** | Millimolar |

| | |
|---|---|
| **mL** | Millilitre |
| **M-PER** | Mammalian protein extraction reagent |
| **mpH** | Milli pH units |
| **MTOR** | Mechanistic target of rapamycin |
| **MTT** | 3-(4,5-dimethylthiazol-2-yl)-2,5-diphenyltetrazolium bromide |
| **mV** | Millivolt |
| **MYC** | MYC proto-oncogene |
| **NaCl** | Sodium chloride |
| **NADH** | Nicotinamide adenine dinucleotide + hydrogen |
| **NF-κB** | Nuclear factor kappa-light-chain-enhancer of activated B cells |
| **NHE** | Sodium-Hydrogen antiporter |
| **Nm** | Nanometres |
| **nM** | Nanomolar |
| **NO** | Nitric oxide |
| **OCR** | Oxygen consumption rate |
| **OCT** | Organic cation transporter |
| **PBS** | Phosphate buffered saline |
| **PHD** | Prolyl hydroxylase |
| **$pH_e$** | Extracellular pH |
| **$pH_i$** | Intracellular pH |
| **pKa** | Negative log of the acid dissociation constant |
| **pmol** | picomoles |
| **PS** | Penicillin and Streptomycin solution |
| **PVDF** | Polyvinylidene fluoride |
| **RB** | Retinoblastoma-associated protein |
| **ROS** | Reactive oxygen species |
| **RPMI** | Roswell Park Memorial Institute |
| **SDS** | Sodium dodecyl sulphate |
| **TBS-T** | Tris Buffered Saline with Tween |
| **TCA** | Citric acid cycle (Tricarboxylic acid cycle) |
| **$T_D$** | Doubling time |
| **TME** | Tumour microenvironment |
| **TP53** | Tumour protein p53 |
| **Treg** | Regulatory T cell |
| **UPR** | Unfolded protein response |
| **V** | Volt |
| **VEGFA** | Vascular endothelial growth factor A |
| **VHL** | von Hippel–Lindau protein |

# Table of Contents

# 1. INTRODUCTION

## 1.1 Cancer

Cancer is a disease where abnormal cells divide uncontrollably and can spread to other tissues or parts of the body [1]. Cells are controlled by the genetic information stored in their DNA. Therefore, if normal cells accumulate damage to their DNA cancer can develop. Cell growth and proliferation are controlled through the cell cycle, which encompasses a protein network that aims to prevent damaged cells from proliferating. Cancer cells are known to escape the control mechanisms of the cell cycle and sustain genomic damage. Furthermore they undergo further alterations of the genome, transcriptome, proteome and epigenome [2].

The characteristics of cancer are often divided into eight biological capabilities, termed the hallmarks of cancer. These hallmarks are presented in Figure 1.1 and include: sustaining proliferative signalling, evading growth suppressors, resisting cell death, enabling replicative immortality, inducing angiogenesis, activating invasion and metastasis, evading immune destruction, and reprogramming of energy metabolism. This thesis will focus on the energy metabolism hallmark, which will be described in detail later in section 1.2. Central to the development of these hallmarks are genomic instability and inflammation [3].

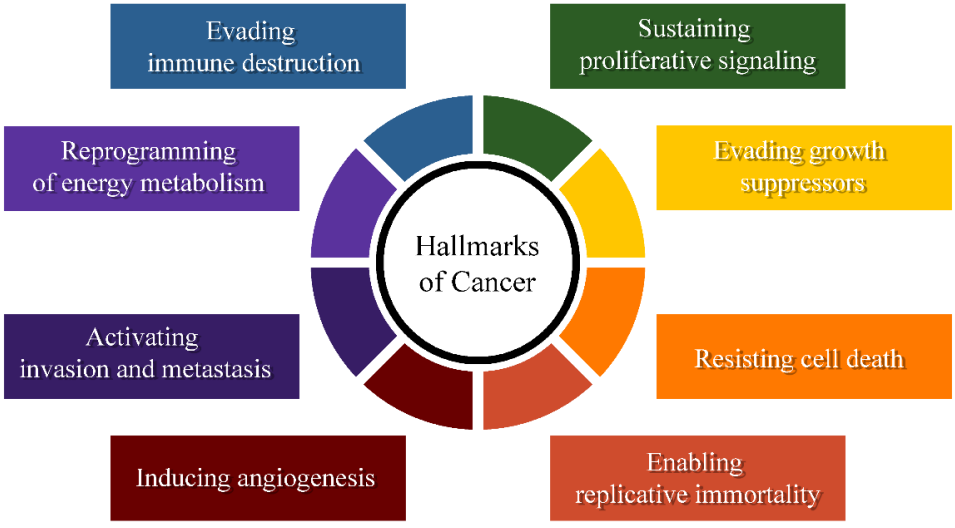


**Figure 1.1 The hallmarks of cancer.** The figure includes the six original hallmarks proposed by Hanahan and Weinberg in 2000 [4] with the addition of the two emerging hallmarks presented in "Hallmarks of Cancer: The Next Generation" (2011) [3]. The figure is based on a figure from [3].

Genomic instability, meaning a high frequency of genomic changes, is crucial to the development of cancer. Typically, a cancer has been growing and developing for years by the time it is detected. A tumour is often derived from a single cell that experienced a heritable change in its genome. Through cell division more changes accumulate, and the cells eventually become cancerous. During a typical lifetime, every human gene is estimated to have gone through a mutation on approximately $10^{10}$ different occasions. It is therefore clear that a mutation in any single gene is not enough to develop cancer [5].

Genes that are critical to the development of cancer are often grouped into two classes: proto-oncogenes and tumour suppressor genes. If these so-called cancer-critical genes are mutated, cancer may arise. Oncogenes are the overactive and overexpressed mutant of proto-oncogenes [5]. An example of a proto-oncogene is the MYC gene which promotes cell growth and proliferation [6]. Tumour suppressors limit cell growth and proliferation. Two quintessential examples of tumour suppressor genes encode the RB (retinoblastoma-associated) and TP53 proteins. These proteins are important to the control of regulatory pathways that allow the cells to grow and proliferate [3].

Inflammation is linked to genomic instability and can also lead to development of cancer. Inflammation is complex and can be defined as the interactions occurring in a tissue that has experienced injury or infection [7]. When a tissue has sustained damage, cell proliferation will be increased to repair the wound. Enhanced proliferation alone does not cause cancer, but chronic inflammation can lead to repetitive damage and regeneration of tissue and promote cancer development. The microenvironment plays an important role and can lead to damage, as well as promote survival, proliferation, and migration. Microenvironment can be defined as the immediate environment of a cell or tissue [8]. A microenvironment with an abundance of growth factors, inflammatory cells, and agents capable of causing DNA damage can increase the risk of cancer development [9]. Chronic inflammation is commonly caused by autoimmune diseases, e.g. inflammatory bowel disease which is tightly linked to development of colon cancer, or infections like for example papilloma viruses leading to cervical cancers [10].

### 1.1.1 Cervical cancer

Cervical cancer is globally the fourth most common cancer in women, and is the second most common cancer specific to women [11]. Cervical cancer arises in the outer layer of the cervix: the cervical epithelium. This epithelial layer consists of glandular and squamous cells, which constitutes the inner (columnar) epithelium and the outer (squamous) epithelium respectively (Figure 1.2) [12]. Squamous cell cancer is the most common among cervical carcinomas, constituting around 70-80% of all cases. The second most common is adenocarcinoma, which starts in the gland cells, and constitutes around 20% of cervical carcinomas [13].

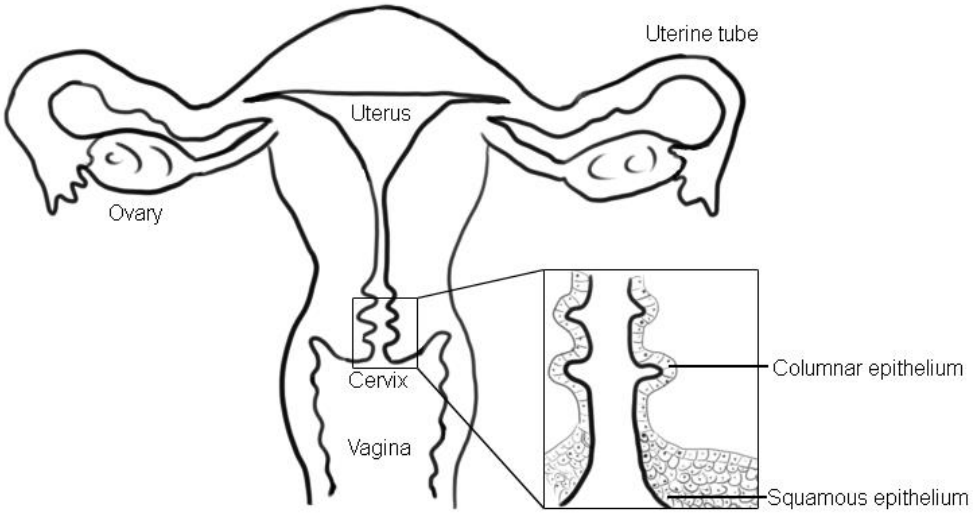


**Figure 1.2 Illustration of the female reproductive system and the epithelial cells of the cervix.** The figure is based on [12].

Human papilloma viruses (HPVs) are considered to be the causative agents of most cervical cancers (over 99%). It is estimated that most people that have been sexually active have been infected with an HPV unless vaccinated. However, most HPV infections are controlled and cleared by the immune system [14]. There are several types of these small viruses, and 15 are categorised as high risk, with HPV16 and HPV18 causing approximately 70% of all cervical cancers. Cervical cancer can occur if an infection with a high risk HPV persists for years without successful immune control [15]. Preventative treatments against cervical cancer include HPV-vaccination and smear tests of the cervix [16]. Vaccination especially could lead to elimination of most cervical cancer in the next generation [17, 18]. However, this presupposes that vaccination is available and that enough people receive it.

The HPV viral proteins that are most important for cancer development are the oncoproteins E5, E6 and E7. E6 and E7 are the primary transforming proteins, which targets the RB and TP53 proteins and induce genomic instability. E6 leads to loss of tumour suppression and resistance to apoptosis by degradation of TP53 through ubiquitination. E7 binds and targets RB for ubiquitination, leading to the release of transcription factors which facilitate cell proliferation [19]. E5 is known to enhance proliferation. The oncoproteins keep the infected cells in a proliferative state where genome mutations accumulate. This can eventually lead to transformation of the cells into cancer cells, and typically takes 15-20 years in women with a functioning immune system [15, 20].

Treatment of cervical cancer in Norway usually constitutes surgery, chemotherapy, radiation, or a combination of these modalities. The treatment of choice depends on how far the cancer has progressed (the cancer stage). At stage I, cervical conization surgery to remove the abnormal cells is preferred. Chemotherapy can be an option if the cancer has reached stage two, has spread to distant organs, or reoccurs after treatment. Radiation, most often combined with the chemotherapeutic drug cisplatin, is often used at stages II, III and IV. Cervical cancer is usually highly curable when detected at an early stage, while patients with cancers in the latest stage will often receive only palliative care. Patients with stages I-IVa, where distant metastases have not been detected, receive treatment with curative intent. The 5-year survival rate for these patients decreases with increasing cancer stage. If detected at stage I, the survival rate in Norway is higher than 90%, while at stage IVa, the survival rate is around 50% [21].

In addition to the risk of dying from cervical cancer, radiation constitutes a risk of severe damage to crucial organs in the pelvis, as the gastrointestinal and urinary systems can be affected [22]. The radiation dose utilised today is high to increase the probability of tumour control, and should not be any higher [23]. Approximately one third of patients receiving radiotherapy relapse, and most recurrences arise within two years of treatment [24]. Research on better treatment for these patients is therefore highly important, especially for women that do not have access to or avoid health services.

## 1.2 Cellular energy metabolism

Cells get energy by oxidizing organic molecules, such as sugar, fat, and proteins in a series of reactions catalysed by enzymes. These reactions are coupled to the production of ATP, which is the energy currency in all cells [5]. Two central processes in the cellular energy metabolism, which both produce ATP, are glycolysis and oxidative phosphorylation. Together they can produce a maximum of 38 molecules of ATP; 2 molecules from glycolysis and 36 from oxidative phosphorylation. Glycolysis occurs in the cytoplasm of the cell, while the process of oxidative phosphorylation occurs in the inner mitochondrial membrane and mitochondrial matrix.

The citric acid cycle, which occurs in the mitochondrial matrix, connects the pathways through its production of reducing equivalents. The reducing equivalents NADH (Nicotinamide Adenine Dinucleotide) and $FADH_2$ (Flavin Adenine Dinucleotide), as well as $CO_2$. All the organic molecules that a cell can use for energy production get broken down differently, but eventually converge onto the citric acid cycle [25]. A simplified overview of cellular energy metabolism relevant for this study can be seen in Figure 1.3.

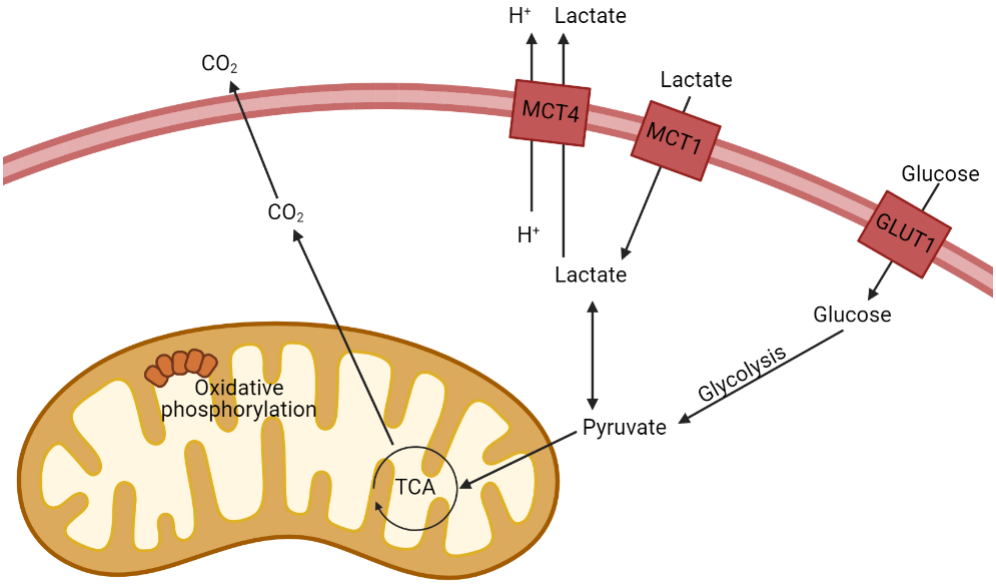


**Figure 1.3 Overview of the cellular energy metabolism.** The figure presents part of a cell with the cell membrane shown in pink, a mitochondrion in yellow, relevant molecules and essential transport proteins. TCA: Citric acid cycle. The presented protein complexes that transport glucose and lactate across the cell membrane are: MCT4: Monocarboxylate transporter 4. MCT1: Monocarboxylate transporter 1. GLUT1: Glucose transporter 1. The Figure is based on [26] and was created using biorender.com.

Glycolysis is a 10-step pathway that breaks down a molecule of glucose into two molecules of pyruvate, while storing the energy released in ATP and in the electrons of the electron carrier NADH (Figure 1.4). Uptake of glucose is done through glucose transporters (GLUTs) [25]. Glycolysis leads to the net synthesis of 2 ATP and 2 NADH molecules per glucose molecule. If the cells are oxygenated the pyruvate will normally be fed into the citric acid cycle in the mitochondrial matrix where NADH and $FADH_2$ are produced. Under anaerobic conditions, fermentation occurs and lactate is produced to regenerate NAD+ from NADH [5]. Lactate can also be used as a metabolite, as it can be converted back into pyruvate. Lactate is transported over the cell membrane through monocarboxylate transporters (MCTs) (Figure 1.3).

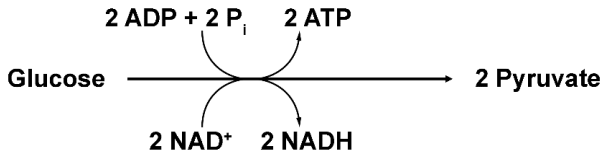


**Figure 1.4 Simplified illustration of glycolysis.** 1 glucose molecule is broken down into 2 pyruvate molecules in glycolysis, and 2 molecules of ATP and NADH are produced.

In normal cells, the main source of ATP production is through oxidative phosphorylation which occurs in the mitochondrial matrix. In the oxidative phosphorylation pathway electrons are transported through a series of protein complexes, known as the electron transport chain (ETC) in the inner membrane of the mitochondria. The reducing equivalents NADH and $FADH_2$ produced in glycolysis and the citric acid cycle are used as electron donors for the ETC [27, 28]. These molecules are therefore crucial to the ATP production by oxidative phosphorylation [29].

### 1.2.1 The mitochondrion

Mitochondria, being the powerhouses of the cell, are the main producer of ATP. Mitochondria also regulate cellular processes like cell death, proliferation, cell signalling, $Ca^{2+}$ homeostasis and metabolic adaptation [30]. Being important for normal cellular function, they are dependent on constant renewal and mitophagy (autophagy of mitochondria). Mitochondria have their own genome and can therefore auto replicate and control mitochondrial biogenesis, meaning growth and division of mitochondria. Fusion and fission events are also important in these processes. The shape, the number and the size of mitochondria are regulated by the cells in response to environmental factors (e.g. toxins) and cellular stress, and differ in relation to energetic and

metabolic needs [31]. Changes in mitochondrial mass, meaning size and number of mitochondria, have been related to many pathological conditions [32, 33].

Mitochondria consist of two membranes, creating two spaces within the organelle: the matrix and the intermembrane space (Figure 1.5). The outer mitochondrial membrane connects the mitochondrion to other organelles in the cell by functioning as a signalling platform. Pores in the membrane make it permeable to small proteins and ions, which can work as signals to adapt metabolism or control cell death. The outer membrane is also a site of phosphorylation and regulation of the innate immune system [30]. The inner membrane is highly impermeable compared to the outer membrane, and membrane transport proteins specific to a given ion or molecule carry out transport across the membrane. The membrane forms mitochondrial cristae (folds) that provides a big surface area, making the inner membrane far more extensive than the outer membrane (Figure 1.5). The number of cristae in the membrane depends on the energy demand in the tissue where the mitochondrion is located. Another important feature of the inner membrane is the electrochemical membrane potential of about 180mV created by the proton gradient in the ETC [30].

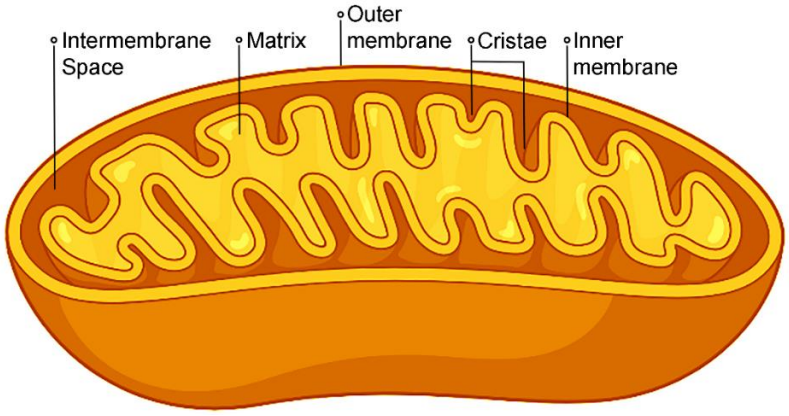


**Figure 1.5 The mitochondrion**. The figure shows a representation of a mitochondrion with relevant structures labelled. Created using biorender.com.

The inner mitochondrial membrane has a high protein content due to the complexes needed for oxidative phosphorylation, fusion and fission of the mitochondria as well as transport of molecules across the membrane. The ETC consists of five complexes through which electrons are transferred to their final acceptor, $O_2$. The complexes in the ETC are arranged in order of increasing reduction potential, so that electrons are passed from a high energy state to a lower

energy state. As electrons are transported across the ETC, an electrochemical gradient also called a proton motive force is created as protons are pumped across the membrane into the inner membrane space against their concentration gradient. This gradient is utilised by ATP synthase to generate ATP [27, 28, 30].

The ETC complexes include NADH dehydrogenase (complex I), succinate dehydrogenase (complex II), cytochrome bc1 complex (complex III), cytochrome c oxidase (complex IV) and ATP synthase (complex V) (Figure 1.6). In addition, coenzyme Q (CoQ) and cytochrome c transport electrons between complexes. Complex I receives two electrons from NADH which are then transferred to CoQ. The energy released is used by complex I to pump four protons over the membrane into the intermembrane space. Complex II receives an additional two electrons transferred via $FADH_2$ from oxidation of succinate. These electrons are also transferred to CoQ. Complex III receives the electrons from CoQ and passes them on to cytochrome c while also pumping four protons across the membrane. Complex IV transfers the four electrons to $O_2$, resulting in the reduction of $O_2$ and formation of two $H_2O$ molecules [30]. Most of the protons pumped across the inner membrane, return to the matrix through ATP synthase. The energy released from the electrochemical potential of the protons when they are returned is used as mechanical energy to change the shape of the ATP synthase which then produces ATP from ADP, $H_2PO_4$- and H+ [30].

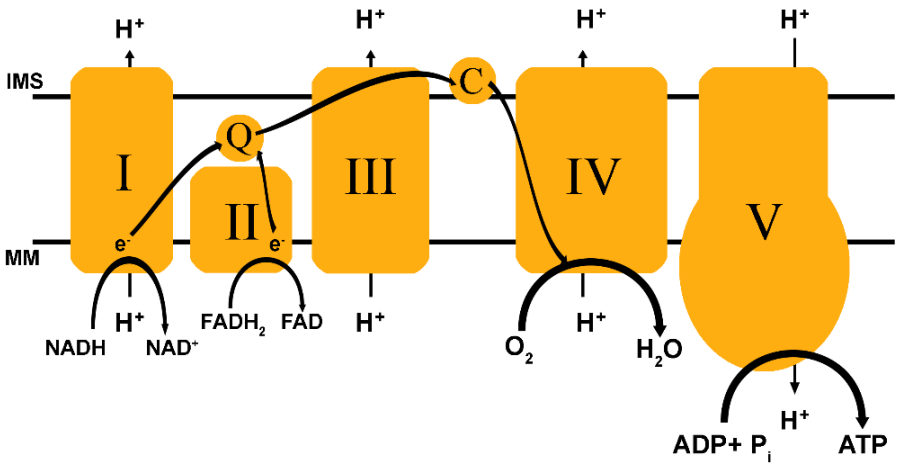


**Figure 1.6 The electron transport chain (ETC).** The five ETC complexes are shown. The two electron transporters coenzyme Q (Q) and cytochrome C (C), the flow of electrons from the reducing equivalents NADH and $FADH_2$ and the generation of $H_2O$ and ATP are indicated. IMS: Intermembrane space. MM: Mitochondrial matrix.

### 1.2.2 Reprogramming of cellular energy metabolism in cancer

To cope with high proliferation rates, cancer cells adapt their metabolism. Reprogramming of energy metabolism is therefore an important hallmark of cancer. Cancer cells often show an increased metabolism of lipids, glutamine, amino acids, and glucose. They also often have accumulation of lactate and reactive oxygen species (ROS) addiction [34]. The purpose of altered metabolism is to improve cellular fitness to provide a selective advantage for the cancer cells. It supports the cells' survival under stressful conditions and allows the cells to grow and divide at a high rate. Reprogramming of energy metabolism can be in response to microenvironmental factors like hypoxia or high lactate concentrations, but can also happen through genetic regulation due to changes in oncogenes and tumour suppressors [35].

An example of metabolic reprogramming is aerobic glycolysis, also called the Warburg effect, where the cancer cells have upregulated glycolysis and glucose uptake even when oxygen is present [28]. This is advantageous, as it gives the cells more intermediates that can be used for biosynthesis of new cells, allowing for increased proliferation [36]. However, the Warburg effect has been shown to only be a small part of the alterations in energy metabolism. It has also been found that tumours can contain cells that utilize different energy-generating pathways, creating symbiotic relationships. An example of this is when glycolytic cells secrete lactate, which is then utilised as main energy source by other cells in the tumour [3].

With glycolysis being upregulated it has been assumed that oxidative phosphorylation is downregulated in all cancers. However, oxidative phosphorylation is not necessarily downregulated, and can even be upregulated in certain cancers [28]. Findings in humans and mice both support the idea that mitochondrial metabolism is required for tumour growth, and research in over 30 cancer types shows that functional mitochondria are positively selected for [36, 37]. It has been found that cells termed cancer stem cells or tumour-initiating cells are especially dependent on their mitochondrial function, and that oxidative phosphorylation is used by invasive and metastatic cells to produce large amounts of ATP [30, 38]. Studying mitochondrial function and mass will lead to a better understanding of mitochondria in cancer and can therefore provide valuable information leading to better targeting and treatment.

Like other cancers, cervical cancers also adapt their metabolism. A virus is dependent on the host cell as it is an intracellular parasite and needs an abundance of energy and substrates to replicate. Therefore, metabolic reprogramming is a crucial part of many viral infections, giving the viruses what they need to replicate [39]. After HPV induced malignant transformation in cervical cancer, the cells go through metabolic reprogramming to fulfil their new metabolic needs. The HPV oncoproteins are involved in this reprogramming by their targeting of various cellular pathways, which again adapt cellular metabolism [40].

## 1.3 Tumour microenvironment and metabolic stress

The tumour microenvironment (TME) consists of non-malignant cells, vessels, metabolites, and intercellular components like collagen fibres [34, 41]. The non-malignant cells in the TME, or stromal cells, include endothelial cells, immune cells, fibroblasts, and specialised mesenchymal cells [42]. The TME is created, adapted and recruited by cancer cells as a response to internal and external stress and to assist the development of cancer hallmarks [34].

This thesis has focused on three common metabolic characteristics of the microenvironments: hypoxia, high lactate concentration in normal pH (lactosis) and high lactate concentration in low pH (lactic acidosis). These characteristics cause metabolic stress in cancer cells and are crucial for the progression of the disease. Hence, hypoxia, high lactate concentrations and low pH have been associated with treatment resistance, increased metastasis, poor prognosis, tumour recurrence and evasion of the immune system in cancer patients [28, 43, 44]. Understanding the TME may therefore be just as important for future cancer therapies as understanding the genetic abnormalities seen in cancer [42].

### 1.3.1 Hypoxia

Cervical squamous cell carcinoma is regarded as one of the most hypoxic types of cancer [45]. Hypoxia occurs due to an inefficient vascular network, poor oxygen supply as well as high oxygen demand in the tumour cells. Hypoxia is a specific TME, which can be a target for cancer treatment. There have been attempts at alleviating hypoxia by increasing oxygen supply without much success. It could therefore be a good alternative to instead decrease the cells' oxygen

consumption [28]. Mathematical models even suggest that this is a more efficient way of improving oxygenation of the tumour [46].

As a response to hypoxia the cells will go through metabolic reprogramming. This reprogramming allows for quicker growth of the cancer cells [47], and this is important for how the disease can progress towards increased malignancy [28]. Anaerobic glycolysis is favoured for energy production over oxidative phosphorylation under hypoxia. However, oxidative phosphorylation is not limited by $O_2$ levels until approximately 0.4-0.7% [48]. The metabolic reprogramming under hypoxia is largely controlled by transcription factors called hypoxia inducible factors (HIFs), especially the master transcriptional regulator hypoxia inducible factor 1 (HIF-1). The HIF gene family encode alpha (α) and beta (β) subunits which form heterodimers capable of regulating transcription, and consist of three HIF-1α paralogues (HIF-1α, -2α and -3α) and two HIF-1β paralogues (ARNT and ARNT2) [49].

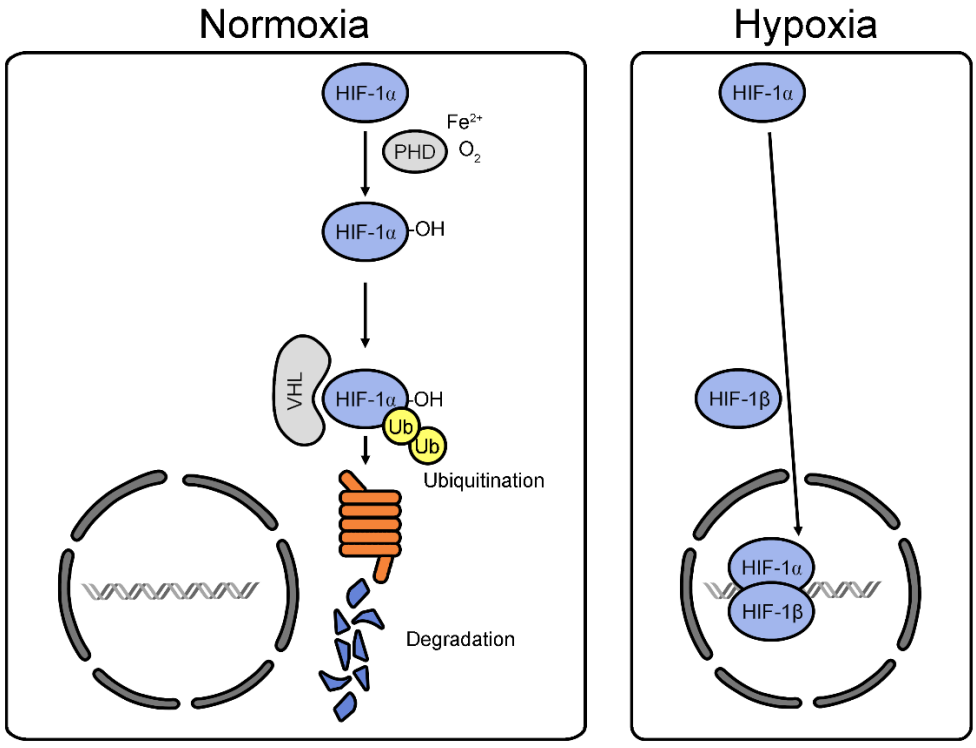


**Figure 1.7 Degradation pathway of HIF-1α.** Under normoxia, PHDs hydroxylate HIF-1α, which triggers VHL-mediated ubiquitination and degradation in the cytosol. Under hypoxia, PHD hydroxylation is inhibited, and HIF-1α can dimerize with HIF-1β, thus forming an active HIF-1 complex that can regulate transcription of target genes. The figure is inspired by [50].

HIF-1 activates transcription of genes involved in angiogenesis, glucose metabolism, increased proliferation, and survival. HIF-1 is built up of two subunits: HIF-1α and HIF-1β. Under normoxic conditions HIF-1α is quickly broken down by prolyl hydroxylases (PHDs). This is done by hydroxylating proline residues on HIF-1α, which leads to ubiquitination, recognition by the von Hippel-Lindau protein (VHL), and degradation of the subunit in proteasomes (Figure 1.7). PHDs are dependent on $O_2$, $Fe^{2+}$ ions, ascorbate and 2-oxoglutarate. Under hypoxic conditions PHDs are therefore unable to hydroxylate HIF-1α, which then leads to its stabilisation and accumulation. HIF-1α can then move into the nucleus along with HIF-1β, where they together can activate transcription of certain genes (Figure 1.7) [51, 52].

### 1.3.2 Lactate and low pH

The Warburg effect states that cancer cells produce more lactate than normal cells through excessive aerobic glycolysis. Lactate is produced through conversion of pyruvate to lactate (Figure 1.8). This study has modelled two microenvironments rich in lactate; lactosis and lactic acidosis. Lactosis is in this thesis defined as a microenvironment with high lactate concentration around the typical healthy pH of 7.4 [53]. Lactic acidosis is defined here as a microenvironment with high lactate concentrations around pH values considered to be at low physiological pH (<7.0) [54]. Lactate in the tumour microenvironment is usually co-located with low pH, as lactate and $H^+$ are co-transported through MCTs (Figure 1.8) [55]. However, tumour tissue is typically highly heterogeneous, and it is possible that certain areas will retain lactate without retaining $H^+$. Lactosis and low pH are therefore not necessarily present simultaneously, and gene analysis in human mammalian endothelial cells have revealed that the genetic response to lactosis is distinct from that of lactic acidosis [56].

High cellular exportation of lactate leads to high proton concentrations and therefore an acidic extracellular pH [57]. Under normal conditions the extracellular pH in tissues is typically kept at 7.4, while in almost all tumour tissues this pH drops to values ranging between 6.3 and 6.9 [53]. Acidity in the microenvironment is a common feature of inflammation as well as of solid tumour tissue. Extracellular acidity triggers pain in tissues with inflammation and in tumours. Further contributions to an increase in acidity can be poor perfusion, leading to inefficient removal of acid, and increased expression of $H^+$ transporters [56, 58]. Cells in an acidic microenvironment

need to maintain a higher intracellular pH, typically between 7.3-7.7, leading to a reversed pH-gradient commonly observed in proliferating cells [34]. All enzymes have an optimal pH. Cytoplasmic enzymes, like those involved in glycolysis, function optimally at a pH of 7.3, and intracellular pH is therefore strictly regulated around this value. Cancer cells need to facilitate transport of acids over the membrane to keep the intracellular pH at a desirable level (Figure 1.8). [58]

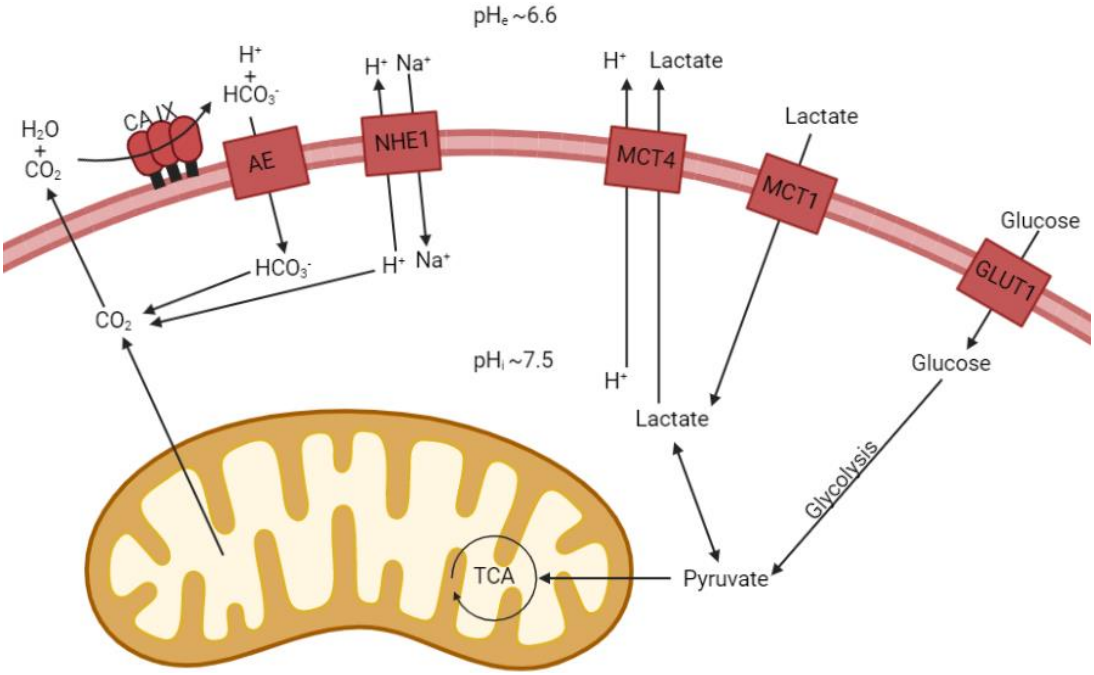


**Figure 1.8 Overview of cellular pH regulation**. The figure presents an overview of pH regulation in a cancer cell. TCA: Citric acid cycle. The presented protein complexes that contribute to pH regulation are CA IX: Carbonic anhydrase 9. AE: Anion exchanger. NHE1: Sodium-Hydrogen antiporter 1. MCT4: Monocarboxylate transporter 4. MCT1: Monocarboxylate transporter 1. GLUT1: Glucose transporter 1. The Figure is based on [26] and [59] and was created using biorender.com.

In cancer, and other proliferating cells, aerobic glycolysis converts up to 85% of its glucose into lactate. This can lead to concentrations as high as 40mM lactate, compared to the normal range of 1.5-3mM. High lactate concentration and low pH are often co-located with hypoxia, as cells become more glycolytic and produce more lactate in the absence of oxygen [53]. However, hypoxia and extracellular lactate accumulation are not always co-located, as glycolysis also can be upregulated under non-hypoxic conditions [60]. Interestingly cervical cancer cells with access to high concentrations of lactate *in vitro* has been shown to alter their metabolism towards oxidative phosphorylation showing further evidence that lactate can be a favoured metabolite

under certain conditions [61, 62]. Upregulated oxidative phosphorylation can also lead to an increased acidity, especially in poorly perfused tissue. This is due to the required production of reducing equivalents in the citric acid cycle also generating large amounts of $CO_2$ which can contribute to acidification of the TME (Figure 1.8) [63].

Research shows that lactate may be able to reprogram cancer and stromal cells in the TME, and is no longer considered to be only a waste product [34]. In addition to previously mentioned correlations, high lactate concentration also inhibits dendritic cell activation, cytokine release and monocyte migration. Lactate functions as an intrinsic inflammatory mediator, and therefore also promotes chronic inflammation in the tumour. Furthermore, lactate enhances the motility of tumour cells, angiogenesis, induction of vascular endothelial growth factor (VEGFA), survival of hypoxic cells and radiation resistance [34, 57]. Lactate can also be used as fuel under physiological conditions, and is frequently used by multiple organs in the human body, and can also be converted into glucose in the liver through the Cori cycle [43].

## 1.4 Targeting oxidative phosphorylation in cancer

Because cancer cells do rely on oxidative phosphorylation for ATP production, inhibition of this ETC dependent process could be a useful therapeutic approach [64]. This approach can be effective in multiple cancer subtypes, including hypoxic tumours of the cervix and cancer stem cells who are dependent on oxidative phosphorylation [38]. Within the same tumour, some cells are more reliant on oxidative phosphorylation than others, and this heterogeneity adds to the complexity of the tumour [28]. Inhibition of ETC also inhibits the citric acid cycle, thus decreasing synthesis of metabolic intermediates needed for tumour growth [36].

Multiple inhibitors of oxidative phosphorylation are proven to have therapeutic potential, and some are presented in Figure 1.9. Complex I has been shown to be an attractive target and inhibitors include metformin and phenformin. Atovaquone, which is used to treat malaria, is an inhibitor of complex III, whereas arsenic trioxide, NO and hydrocortisone are complex IV inhibitors. Many more inhibitors have also been studied *in vitro*, and some also *in vivo* [28]. Metformin was chosen for this study, as there is an ongoing clinical trial at the Norwegian Radium hospital with this drug in patients with cervical cancer.

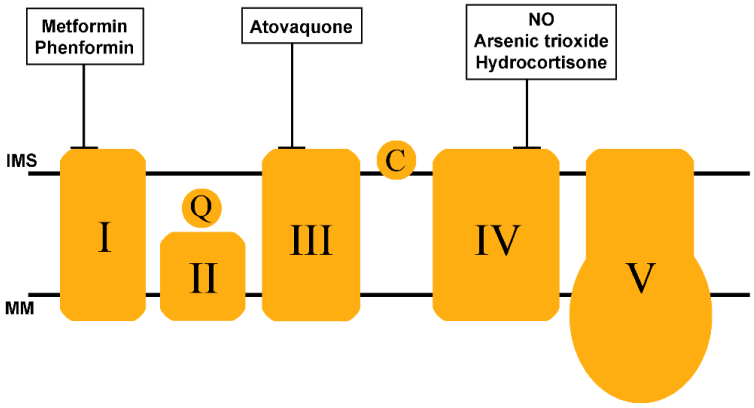


**Figure 1.9 A selection of ETC inhibitors used in clinical trials.** The figure shows the 5 complexes of the ETC, and which complexes the displayed inhibitors have been shown to inhibit [28].

### 1.4.1 Metformin

Metformin is a water soluble, strong base that is originally used to treat type II diabetes mellitus. It is developed from a guanidine derivative called galegine found in *Galega officinalis* (french lilac) [65]. Metformin enters the cell via organic cation transporters (OCTs) and is reversibly accumulated in the mitochondrial matrix at normal pH when there is a robust mitochondrial membrane potential [36, 66]. Otherwise, metformin is mostly located in the cytoplasm [67]. The mechanisms of metformin are not fully understood, but it has been found to inhibit oxidative phosphorylation and have a negative effect on cancer [66]. The use of metformin in cancer therapy is a way of drug repurposing. Such new use of established drugs is advantageous as it (1) lowers costs of development of a new drug, (2) reduces risks due to sufficient safety and known toxicity, (3) and is easier to introduce to the market once an effect on cancer has been established [34].

In diabetics, metformin reduces blood sugar by inhibiting gluconeogenesis in the liver [66]. By decreasing the hepatic glucose production, as well as the absorption of glucose in the intestine, metformin also improves insulin sensitivity. Metformin serves as the most popular initial therapy for type II diabetes mellitus patients and is typically safe for patients without severe renal disease. It is also inexpensive, contributing to its widespread use [68]. Metformin was first synthesised in 1922 and started being used as medicine for diabetes in 1957 [69]. The more potent phenformin and buformin were more popular initially, but these drugs were taken off the

market due to reports of systemic lactic acidosis. Metformin has been found to also lower cancer risk, which has led to a renewed interest in this established drug [68].

### 1.4.2 Use of metformin in cancer therapy

Metformin has become an area of interest after fewer cancer incidents were detected in diabetes patients treated with metformin [38]. There is a general belief that metformin can inhibit tumour progression and cell survival under hypoxic conditions. However, clinical trials have yielded conflicting results [70]. Understanding the effects of metformin and finding the tumours that are susceptible to metformin treatment is therefore important to research. Two widely accepted mechanisms in which metformin exerts an antitumour effect are the (1) lowering of glucose and insulin in circulation and (2) the inhibition of mitochondrial complex I.

Many studies have confirmed mitochondrial complex I inhibition by metformin both *in vitro* and *in vivo* [36]. Metformin has for example been shown to have antitumour effect in ovarian cancer by the targeting of mitochondrial metabolism [71], and in breast cancer by inhibiting complex I and thereby diminished TCA cycle intermediates production [72]. The use of metformin as an oxidative phosphorylation inhibitor is in clinical trials and the focus of the presented work has been on this direct mechanism. Metformin has been proposed as a strategy to alleviate tumour hypoxia by decreasing the cellular oxygen consumption rate through the inhibition of the ETC [28, 66, 73]. It has been demonstrated that metformin therefore increases the response to radiation, since hypoxia limits the radiation efficiency [73].

Metformin may also target the acidic environments, as it has been shown to inhibit proliferation and formation of colonies in acidic melanoma cells. In addition, metformin has been found to impair the cells' metabolic reprogramming, evasion of immune destruction as well as resistance to chemotherapy [34]. Other effects of metformin that have been proposed are reduced HIF-1 stability, inhibition of protumourigenic Treg lymphocytes, increased lymphocyte cytotoxicity towards tumour cells, and downregulation and blocking of crucial cancer pathways, including NF-κB and MTOR pathways [70]. Some effects of metformin found in studies can be seen in Figure 1.10. To fully understand the potential of metformin in cancer therapy, further research on its effects is important.

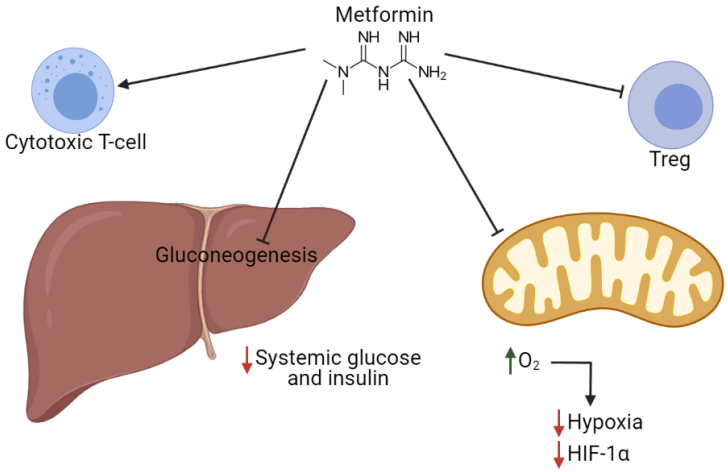


**Figure 1.10 Effects of metformin on cancer.** The figure shows effects of metformin that affect cancer progression and survival. The figure is based on [66] and [70] and was created using biorender.com.

## 1.5 Measurements of energy metabolism

Historically the processes of cellular metabolism have been largely unknown, and it was only in the 20th century, when enzymes were first described that this field of biochemical research arose [74]. Since then, knowledge of the biochemical pathways that control our energy metabolism have grown rapidly. To describe the energy metabolism pathways and the controls that govern their rate, many methods have been utilised. A lot of these methods include cell lysates, where cell walls and debris has been removed to study e.g. proteins, or to provide better access for external materials to cellular components [75].

Agilent Technologies Seahorse, referred to as Seahorse from here on out, is a metabolic analyser used to measure live cellular bioenergetic functions in real time [76]. This technology was first introduced in 2006 and has been used in various studies for investigating the critical role of metabolism regulation in cancer development and progression [77]. The ability to study metabolic changes and adaption in real time provides novel data on cellular metabolism, allowing for more accurate assessment of metabolic function. This is unlike previous studies where the data obtained typically gives a view of the metabolism in a cell at a given time [75].

Seahorse measures the oxygen consumption rate (OCR) and the extracellular acidification rate (ECAR), which are used to investigate mitochondrial respiration and glycolytic activity, respectively. Another system able to detect respiration rate is the high-resolution Oxygraph-2k

(O2k) which is also capable of measuring OCR in live cells. These technologies (Seahorse and O2k) have been predicted to provide novel insights into complex diseases, like cancer, and assist in development of therapeutic strategies [78].

Seahorse detects changes in $O_2$ and proton ($H^+$) concentrations using a solid-state sensor material [79]. Probes containing fluorophores embedded in polymer measures concentrations of dissolved $O_2$ and protons in the wells where cells are growing (Figure 1.11). Light excites the fluorophores, and the fluorophore emission can be measured giving information on $O_2$ and proton levels. During measurements, the sensor cartridge with probes containing fluorophores is lowered to 200µm above the cells, creating a small and contained chamber where the recording can take place quickly. Between two measurements the sensor cartridge is raised allowing the well content to mix before the next measurement takes place [76]. The technology also provides the opportunity and protocol to study cells under hypoxia, but this opportunity requires that the equipment is placed in a hypoxia chamber [80].

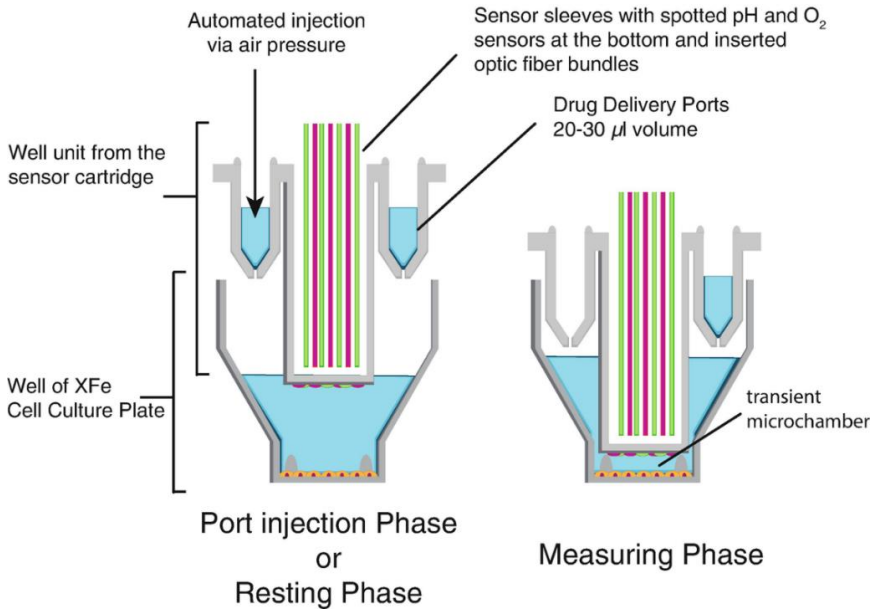


**Figure 1.11 Illustration of Seahorse wells, probes, and delivery ports.** The figure shows a labeled schematic of the important features of the Seahorse system, and was obtained from [81].

Seahorse technology provides the means to study many features of cellular metabolism and 9 different assay and test kits are offered. For example, using the Seahorse XF Glycolysis Stress Test, it is possible to calculate parameters regarding glycolytic function, including glycolysis,

glycolytic capacity and glycolytic reserve. The assay utilised in this study was the Mito stress assay, which measures mitochondrial function and gives information on the use and capacity for oxidative phosphorylation in cells.

An important feature of Seahorse is that the instrument injects drugs during recording, giving results in real time. This allows for addition of substrates, inhibitors or stimulators that can give valuable information on the cell metabolism of the cultured cells. Some drugs that are typically used for studying mitochondrial function can be seen in Figure 1.12. The effects of the drugs utilised in this study are further explained in the methods section.

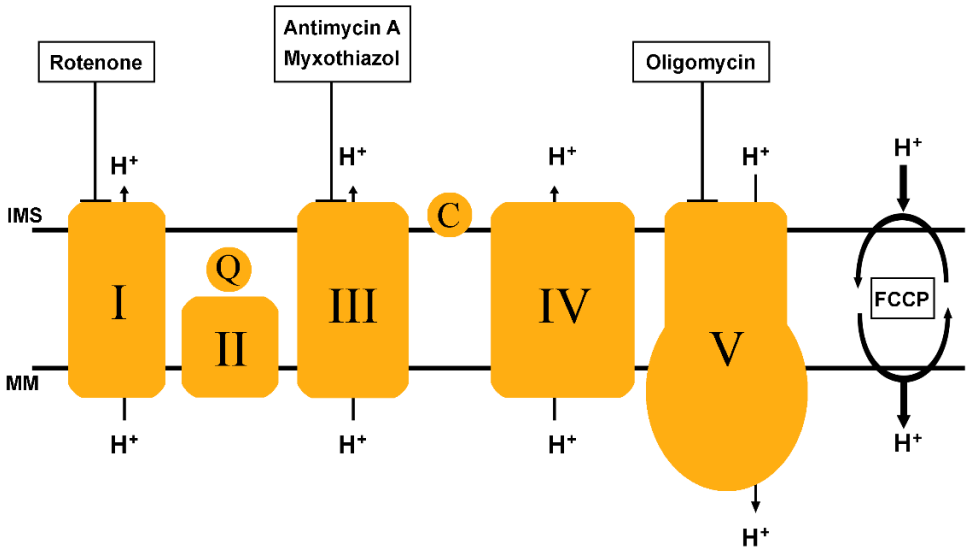


**Figure 1.12 Targets of drugs commonly used with Seahorse.** The figure shows the targets of Rotenone, Myxothiazol, Antimycin A, Oligomycin and FCCP (Trifluoromethoxy carbonyl cyanide phenyl-hydrazone). Antimycin A and Rotenone were not utilised in this thesis. The figure is inspired by [82].

# 2. AIMS

The overall aim of this study was to investigate *in vitro* effects of different cellular microenvironments and effects of metformin in two cervical cancer cell lines; HeLa and SiHa.

An important part of the study was to establish relevant microenvironment models to investigate metabolism and the impact of drugs for cancer treatment. Such models better mimic the TME and are more relevant to cancer research than cells grown under normal culturing conditions optimised for cell growth. The modelled microenvironments were hypoxia, lactosis and lactic acidosis. These conditions were compared with cells grown under normal culturing conditions, which entailed conventional growth medium. The models were created by chemically inducing hypoxia in cervical cancer cell lines and by growing them under conditions of elevated lactate concentration with and without acidic pH. Chemically induced hypoxia was used since growing cells under low oxygen concentrations in a hypoxia chamber could not be combined with the Seahorse instrument available.

To study targeting of cellular energy metabolism the drug metformin was chosen. This was due to the suggested anticancer effects and potential advantage for treatment of tumours in specific microenvironments. There is also an ongoing clinical trial at the Norwegian Radium hospital with this drug in cervical cancer patients. Since Seahorse technology is a powerful tool for metabolism studies, a part of the study included establishment of a protocol for Seahorse experiments.

The study was separated into four specific aims:

1) Establish protocols for chemical induction of hypoxia, detection of mitochondrial mass, and studies of cell metabolism.
2) Study the effect on cell proliferation and mitochondrial mass in the TME models compared to cells cultured under normal conditions.
3) Study the effect of metformin on HIF-1α stabilisation, proliferation, and mitochondrial mass in the TME models.
4) Investigate metabolic changes in cells with and without chemically induced hypoxia, and with metformin treatment using Seahorse technology and evaluating its usefulness.

# 3. METHODS

A schematic overview of the methods used in this study can be seen in Figure 3.1. Methodological approaches included four main methods used to establish protocols, characterize proliferation, detect mitochondrial mass, and investigate the usefulness of Seahorse for further metabolic studies. Instruments, software, kits, reagents, media, solutions, equipment, antibodies, and cells used are listed in Appendix A.

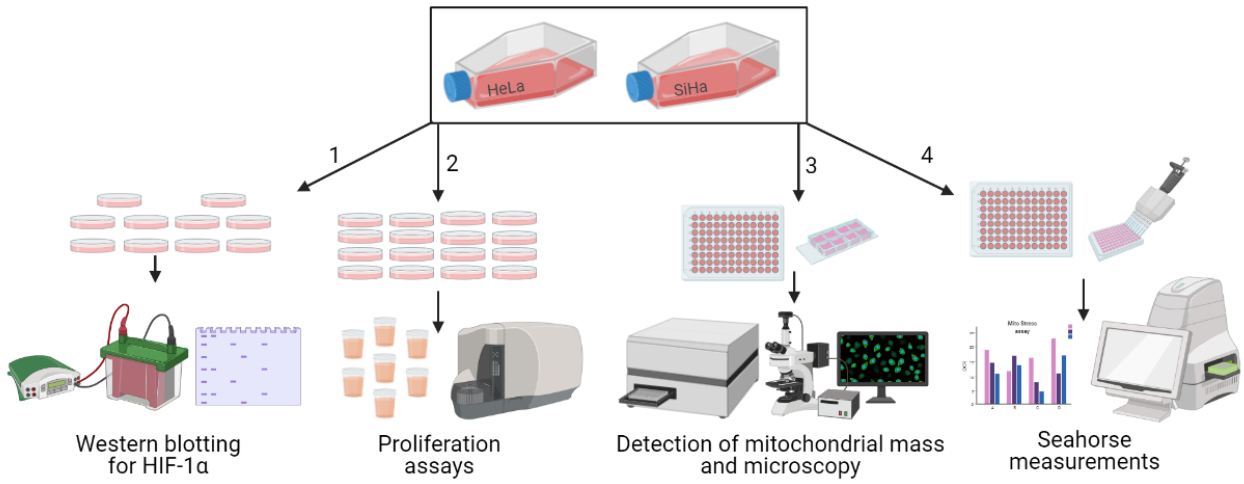


**Figure 3.1 Schematic overview of methods.** The figure shows the 4 main methods utilised in the study. Created using biorender.com.

## 3.1 Cell lines and culture

### 3.1.1 Cell lines

The cervical cancer cell lines HeLa and SiHa were used. Both are human epithelial cell lines obtained from cervical tumours. HeLa cells are adenocarcinoma cells with HPV18 sequences. SiHa cells derive from squamous cell carcinoma with HPV16 sequences [83, 84]. Further details on these cell lines can be found in Table A.1 in Appendix A. The HeLa and SiHa cell lines were chosen because they are a common model system for cervical cancer and have been extensively used in studies by the Clinical radiation biology research group.

### 3.1.2 Culturing technique

Cell culturing is a method used for maintaining and growing cells under controlled conditions *in vitro*. The cells were incubated in a humidified incubator at 37°C with 5% $CO_2$, which are the standard conditions for cell culturing [85]. Cell lines differ and can therefore require different conditions or growth media. It is important that the growth medium provides the cells with nutrients and has the buffering capacity to keep the pH in a desirable range for the cells (7.0-7.6). It is common to supplement media with animal serum, most commonly foetal bovine serum (FBS), to stimulate growth, metabolism and proliferation [86]. It is also common to add antibiotics that do not harm the cells, such as penicillin and streptomycin (PS), to the medium to prevent bacterial infection [87].

The cells were cultured in T75 culture flasks with filtered caps, allowing for gas exchange. Cells were grown as adherent monolayers in Dulbecco's Modified Eagle's Medium (DMEM) supplemented with 10% FBS and 1% PS, referred to as complete media. The cells were kept in an exponential growth phase by splitting them when they reached a confluency of 80%-90%. The cells' confluency and morphology were determined using a Nikon Diaphot microscope. Splitting was done by discarding the old medium and washing with phosphate-buffered saline (PBS) to remove trypsin inhibitors. Trypsin was added to remove cell-cell and cell-flask adhesion. Finally, fresh medium and cell suspension were added to a new flask. A full protocol for cell splitting can be found in Appendix B.1.

#### 3.1.2.1 Chemically induced hypoxia

To establish the hypoxia model, Cobalt(II)chloride ($CoCl_2$) was used to stabilise HIF-1α. The mechanism in which $CoCl_2$ stabilises HIF-1α is not completely understood. At least three hypotheses have been presented [52]. The most widely accepted one is the replacement hypothesis, proposing that $Co^{2+}$ from $CoCl_2$ replaces $Fe^{2+}$ as cofactor in the PHD active site, and makes it inactive. This further leads to HIF-1α stabilisation and accumulation [52].

Titrations of two different concentrations, 100µM and 200µM, and four different incubation times were done to establish a protocol for the $CoCl_2$ treatment. Cells were seeded the day prior to addition of $CoCl_2$. $CoCl_2$ was added to complete DMEM medium at the right concentration,

and this medium was carefully pipetted into the dishes with cells after removal of the seeding medium. The cells were then incubated for 4 hours, 6 hours, 18 hours and 24 hours before being lysed. A detailed protocol for $CoCl_2$ treatment can be found in Appendix B.2. Western blotting of the lysates was performed to confirm HIF-1α stabilisation.

#### 3.1.2.2 Lactosis and lactic acidosis

Lactate is the conjugate base of lactic acid. The pKa of the pair (lactate/lactic acid) is 3.8 at normal physiological pH, where lactic acid dissociates into lactate and a proton ($H^+$) [43]. Two different culturing conditions with lactate were used to model TME: lactosis and lactic acidosis, which involved medium supplemented with 10mM lactate at pH≈7.4 (lactosis) or pH≈6.6 (lactic acidosis). A concentration of 10mM was chosen, as this has been used in other studies where a microenvironment high in lactate has been studied [43, 88]. The pH value of 6.6 was used, as this is in the middle of the low pH range found in tumours and have also been used in other studies to mimic an acidic microenvironment [53, 89-91]. The media were prepared according to a protocol developed in previous studies by the Clinical radiation biology research group (unpublished). Freshly made complete media was supplemented with 10mM sodium lactate and HEPES buffer. HCl was added to the lactic acidosis medium to lower the pH to approximately 6.6. Cells were seeded in lactosis or lactic acidosis medium 24 hours prior to experiments. A detailed protocol for media preparation can be found in Appendix B.3.

### 3.1.3 Freezing and thawing of cells

Cryopreservation of cells at a regular basis is important to ensure reproducibility of the model system over time. If cells are kept in continuous culture genetic drift will occur, and cells can reach senescence. Furthermore, an instrument, like the cell incubator, can fail and subject the cells to damage, or a contamination of the cells can occur. Keeping a stock of frozen cells is therefore necessary [92]. The cells can be stored in liquid nitrogen tanks for a period of many years without significant impairment [93]. To prevent the cells from being damaged by the freezing process the cells are frozen in freezing media, which contains a cryoprotectant. In this study, the cells were frozen in media containing 20% dimethyl sulfoxide (DMSO), which is amphipathic, and easily penetrates the cell membrane and prevents damage from the crystallization of liquids [94]. However, DMSO is toxic to cells at room temperature, so it is important to work quickly. After addition of freezing media, the cells were quickly placed in a

cryopreservation unit (Mr. Frosty) at -80°C. The unit ensures a steady decrease in temperature, which prevents crystallization of liquids, additional cellular stress and cell death [95]. After 24 hours, the cells were transferred to liquid nitrogen ($N_2$) containers for long time storage.

Thawing of the cells was done by heating the tube with cells in a water bath at 37°C before quickly transferring the content to a 15mL tube. Growth medium was added to dilute the DMSO and the cells were pelletised using a centrifuge. The supernatant was removed, and growth medium was added. The pellet was dissolved, and the content was transferred to a filtered T25 bottle, which was placed in an incubator. Cells need some days before they achieve normal proliferation rate [85]. Protocols for freezing and thawing of cells can be found in Appendix B.4 and B.5 respectively.

## 3.2 Proliferation assays

The effect of different microenvironments (chemical hypoxia, lactosis and lactic acidosis), and of metformin, on cell proliferation was studied by use of a cell counter. Three independent biological replicates were done for each condition. The cells were seeded in 3mL medium in 60mm petri dishes 24 hours before they were counted. The number of cells seeded in each dish was calculated using Equation 3.1, where $C_1$ and $V_1$ are the starting concentration and volume respectively, while $C_2$ and $V_2$ are the final concentration and volume. $CoCl_2$, lactosis or lactic acidosis medium was added during seeding, while 3mM Metformin was added 18 hours before counting.

$$C_1V_1=C_2V_2 \qquad \text{Equation 3.1}$$

### 3.2.1 Cell quantification

Cell quantification was done using a Coulter Counter (Beckman Coulter, Z2 Coulter Counter), which counts the number of cells per mL. This was first done before seeding to calculate the number of cells required for the experiment, and after 24 hours to study the proliferation. Before counting, 1mL of cell suspension was diluted in NaCl solution to ensure that only one cell enters the detection area at a time [96]. The Counter was also flushed with NaCl solution prior to counting, as this functions as a baseline. The counter counts cells by moving them through an

electrical current and measuring the electrical conductivity. It detects cells within a pre-set range of sizes based on the electrical conductivity difference between the cells and the suspending fluid [97]. A standard setting of 8-24µm was used for all experiments. A detailed protocol for cell quantification can be found in Appendix B.6.

### 3.2.2 Cellular doubling time

Cellular doubling time ($T_D$) was calculated from the proliferation assay results using Equation 3.2. Growth rate (X) is the number of counted cells after 24 hours divided by number of cells seeded.

$$T_D(hours) = \frac{Log2}{\log(1+(X-1))} * 24 \qquad \text{Equation 3.2}$$

## 3.3 Protein methods

### 3.3.1 Protein extraction

Cells were lysed to release the proteins of interest. The lysis buffer was Mammalian Protein Extraction Reagent (M-PER), which was supplemented with Halt Protease Inhibitor Cocktail. According to the producer, this lysis buffer extracts cytoplasmic and nuclear proteins. As HIF-1α can be localised both in the cytoplasm and nucleus, this buffer is appropriate. It is recommended to use approximately 100µL lysis buffer per 1 million cells, but lower volumes can be used if a more concentrated lysate is desired [98]. After addition of lysis buffer to cells in monolayer, the cells were scraped off, and the lysate was collected in an Eppendorf tube. The lysate was centrifuged to pellet cell debris. The supernatant was transferred to a clean tube and the pellet was discarded. The lysates were stored at -80°C. A detailed protocol for lysing of cells can be found in Appendix B.7.

### 3.3.2 Total protein concentration

Protein concentration in the lysates was determined so that an approximately equal amount of protein could be added to each lane for gel electrophoresis as part of the western blotting procedure. There are several ways to quantify protein concentration. For this study, a Bradford assay method was utilised, which was quick and easy to use. However, one disadvantage is that

a standard curve needs to be created for each new assay. The Bradford assay is a dye binding assay which relies on a shift in absorbance that occurs when a dye binds to the proteins in the sample [99].

Quantification of protein concentration was done using Pierce™ Coomassie Plus (Bradford) Assay Kit from Thermo Scientific, which accurately measures concentrations between 100-1500µg/mL. Bovine serum albumin (BSA) was used as a protein standard. Cell lysates and dilutions with different known concentrations of BSA were added to a 96-well plate. Coomassie Plus Reagent was added to all wells and the plate was shaken and incubated at room temperature. The absorbance was measured at 595nm using a Gen5™ Microplate Reader. A standard curve was created from the absorbances of different BSA dilutions and used to estimate protein concentrations in the cell lysates. A detailed protocol can be found in Appendix B.8.

### 3.3.3 Western blotting

Western blotting or protein immunoblotting is used to identify and quantify proteins by using specific antibodies. Solutions with total protein are first denatured and separated based on size by gel electrophoresis. The proteins are then transferred from the gel onto a membrane made of polyvinylidene fluoride (PVDF). Antibodies against the proteins of interest are applied to the membrane. The proteins of interest are visualised as separate bands on the membrane by using secondary antibodies and detection reagents [100]. In this study, western blot was performed to confirm stabilisation of HIF-1α, and to investigate if metformin had an effect on this stabilisation in the hypoxia model of HeLa and SiHa cells after pre-treatments. By including the endogenous protein γ-tubulin as a loading control, the method allows for determination of relative amounts of HIF-1α protein expression between the samples.

After quantification of total protein concentration, the samples were prepared for loading into gels. Sample loading buffer was added in a 1:4 ratio to the cell lysates before they were boiled at 95°C. This is done to denature and give the proteins a uniform negative charge. The sample loading buffer contains an anionic denaturing detergent, sodium dodecyl sulphate (SDS), which binds to the proteins and gives it a negative charge. This charge is proportionate to the length of the denatured protein. Another component of the buffer, Dithiothreitol (DTT), denatures the

proteins further by also reducing disulphide bonds [101]. The sample loading buffer also contains glycerol, which increases the density of the sample, allowing for more even gel loading as well as keeping the sample at the bottom of the desired well [100].

For this study, ready-made 7.5% precast polyacrylamide gels from Bio-Rad were used. The polyacrylamide creates pores that the proteins can migrate through. This allows for separation of proteins by size, as smaller proteins wander through the gel faster. By using a ladder, it is possible to identify protein size, and serve as a positive control if the sizes are known. The Precision Plus Protein Dual Color Standards ladder was used. The antibodies used and sizes of the proteins of interest are listed in Table 3.1. The loading of approximately equal amounts of total protein allows for determination of relative amounts of protein expression between the samples, and the protein γ-tubulin was used as loading control as loading of samples will not be completely equal. A loading control should be expressed at the same level in all samples regardless of treatment. The gels are submerged in a running buffer (or migration buffer), which contains ions that conduct a current through the gel. The running buffer was made using the 10x Tris/Glycine/SDS premixed electrophoresis buffer from Bio-Rad and distilled deionised water. The gels were run at 200V for approximately 40 minutes before the proteins were transferred to a membrane. This transfer is called blotting and is performed by an electrical field.

**Table 3.1 Antibodies used for immunoblotting.** The table contains protein size, host and dilution used for this study. Further information on the antibodies used can be found in Table A.8 in Appendix A.

| | Name | Target protein size (kDa) | Host | Dilution |
|---|---|---|---|---|
| Primary antibodies | HIF-1α | 120 | Mouse | 1:800 |
| | γ-tubulin | 48 | Mouse | 1:5000 |
| Secondary antibody | Donkey Anti-Mouse | | Donkey | 1:10000 |

Blotting was done in semi-wet conditions using the Bio-Rad Trans-Blot® Turbo™ Transfer System. The blotting sandwich, made up of filter paper, a membrane, the gel and another filter paper, was placed between positive and negative electrodes. The membrane was blocked using a 5% skim milk solution to prevent non-specific binding of antibodies.

Primary antibodies were added and left overnight at 4°C. The secondary antibody was left for an hour at room temperature post primary antibody treatment. The secondary antibodies are

horseradish peroxidase (HRP) -conjugated. A luminol-based chemiluminescent substrate developing solution, SuperSignal West Dura, was used to detect HRP on the membrane. A picture of the membrane was created using a ChemiDoc MP Imaging System. A detailed protocol for the procedure can be found in Appendix B.9. Quantification of the protein bands on the membrane was done in Image Lab according to recommendations [102].

## 3.4 Metformin treatment

Cells were treated with metformin to investigate its effect on proliferation, mitochondrial mass, HIF-1α stabilisation in TME models, as well as its effect on mitochondrial function with the help of Seahorse.

### 3.4.1 Preparation of metformin solution

The metformin solution was prepared using metformin (1,1-Dimethylbiguanide hydrochloride) and sterilised water. Metformin is soluble in water, and a stock solution of 100mM was made according to recommendations [103]. The amount of metformin needed was calculated using Equation 3.3. Metformin has a molecular weight of 165.62 g/mol. Stock solutions were kept in 1.5mL Eppendorf tubes at -20°C for up to 1 month, as recommended [103]. The procedure was done in a laminar airflow (LAF) bench, and the solution was sterile filtered before being added to the Eppendorf tubes. A detailed protocol can be found in Appendix B.10.

$$Mass\ (g) = \frac{Concentration\ (mM) * Volume\ (mL) * Molecular\ Weight\ (\frac{g}{mol})}{1000} \qquad \text{Equation 3.3}$$

## 3.5 Detection of mitochondrial mass and microscopy

Fluorescence was used to detect mitochondrial mass in cells using MitoTracker Green and a Tecan plate reader. Live cell imaging in a fluorescence microscope was also done to ensure correct staining at the chosen concentration of MitoTracker Green. Fluorescence is a short-lived emission of light created by electromagnetic excitation and was first discovered in 1852. Fluorescence is created when a fluorescent substance (a fluorophore) absorbs light and then emits light, typically $10^{-9}$ to $10^{-8}$ seconds afterwards. The emitted light typically has a longer

wavelength, and therefore lower energy, than the light used for excitation. Each fluorophore has a specific excitation and emission spectrum, which shows the specific wavelength it will absorb and emit energy most efficiently. The difference between the peaks of the two spectra is known as the Stokes shift [104]. The excitation and emission spectra for MitoTracker Green are shown in Figure 3.2.

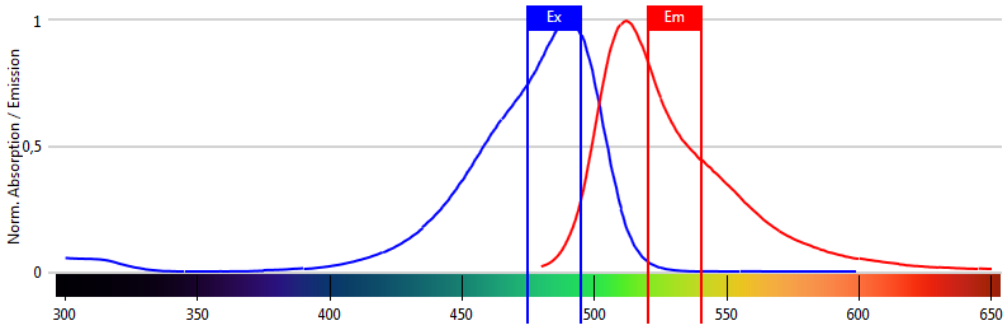


**Figure 3.2 Excitation and emission spectra for MitoTracker Green.** The excitation and emission peaks are at 490nm and 516nm, respectively. The chosen excitation and emission wave lengths, 485nm and 530nm, are visualised with the Ex and Em columns. The figure is obtained from Spark Control Magellan (Tecan software).

MitoTracker green localizes to mitochondria in live cells and can therefore be used to detect mitochondrial mass [105]. The cells were seeded 24 hours prior to the experiment in a Seahorse microplate. Before measuring fluorescence signal, the cells were incubated with 200nM MitoTracker Green for 30 minutes at 37°C. The measurements were done using a Tecan Spark microplate reader. A detailed protocol for this procedure can be found in Appendix B.11.

Live cell microscopy was done using a Zeiss cell observer microscope system with a Plan-Apochromat 20x/NA0.8 Ph2 lens, a 2.5x tube lens, a HXP120 illumination unit and a filter with appropriate excitation and emission wavelengths for MitoTracker Green (Figure 3.2). Images were captured using an ORCA FLASH 4.0 V3 Digital CMOS camera. Z-stacks covering the whole cell, with sections spaced 0.31mm apart, were recorded. Cells were seeded 24 hours prior to microscopy and imaging under normal conditions in an 8 well microscopy slide. A total of 12000 cells were seeded per well in 300µL medium. MitoTracker Green treatment was done in the same way as described above and in Appendix B.11. After removal of MitoTracker Green, RPMI medium without phenol red, supplemented with FBS (10%) and glutamine (1%), was added to the cells before microscopy and imaging.

## 3.6 Analysis of mitochondrial function by Seahorse

A protocol was established to analyse mitochondrial function using Seahorse. A cell Mito stress assay was performed using the Seahorse to measure mitochondrial function through OCR, as well as ECAR in untreated and metformin treated cells grown under normal culturing conditions and chemically induced hypoxia.

### 3.6.1 Seahorse Cell Mito Stress Assay

Flux assay kits and cell microplates from Seahorse were used (Figure 3.3). The flux assay kit contains a cartridge plate, which sits on a utility plate used for hydration and calibration. The cartridge plate contains sensor material and four injection ports (Figure 3.3). The kit also includes guide plates to ease loading of the injection solutions.

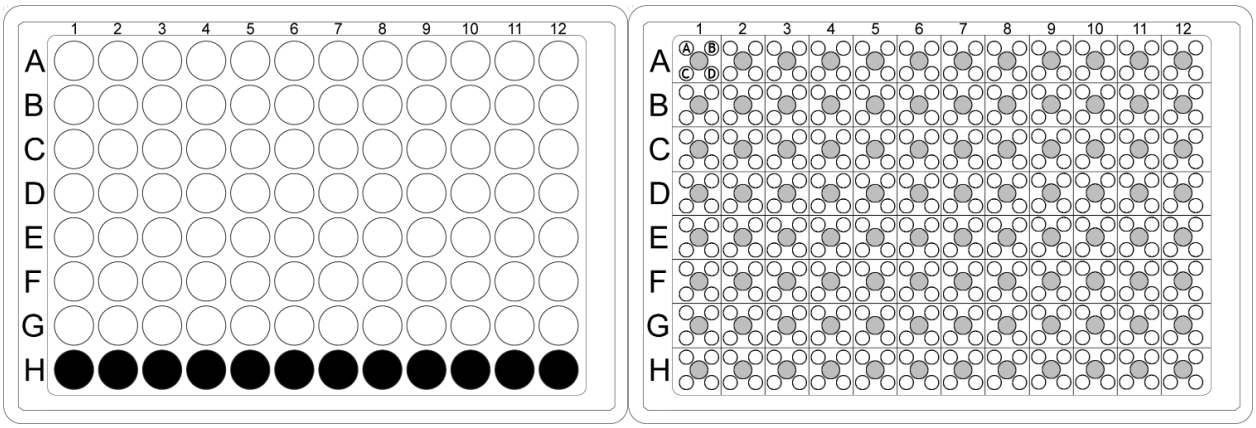


**Figure 3.3 Illustration of Seahorse XFe96 cell culture microplate and cartridge plate.** The left image shows the cell culture microplate where the background wells, which only receive media, are shown in black. The well bottom has a diameter of 3.81mm [106]. The right image shows the cartridge plate, which contains the sensor material, with the four injection ports labelled A, B, C and D.

The day prior to the measurements, the cells were seeded at the chosen density in the Seahorse cell culture microplate, leaving the bottom row empty (Figure 3.3 left), and placed in the standard cell incubator. Induction of chemical hypoxia was done by adding 200µM $CoCl_2$ during seeding, while metformin was added 18 hours before assay run. The cartridge was hydrated using Agilent Seahorse XF calibrant for the sensors to function correctly during the assay and placed in a non-$CO_2$ incubator overnight.

On the day of the assay, the assay medium was prepared by supplementing ready-to-use Agilent Seahorse XF DMEM assay media (pH 7.4). This media was used to provide consistent conditions, and with its low buffering capacity small changes in pH can be detected. The assay medium was prepared by adding glucose to a final concentration of 10mM, sodium pyruvate to a final concentration of 2mM and L-glutamine to a final concentration of 2mM. The medium in the cell plate was replaced with the assay medium. The cell plate was then placed in the non-$CO_2$ incubator for an hour to allow for degassing of the plate, medium and cells [107].

The assay was set up by creating an instrument protocol using the Wave software, and the injection solutions were prepared by diluting oligomycin, FCCP and myxothiazol in assay media (Table 3.2). Each solution was added to their designated injection ports (Figure 3.3 right), facilitated by the loading guide plates included in the kit. The A ports were loaded with oligomycin, the B ports with FCCP and the C ports with myxothiazol. Using these injections, fundamental parameters of mitochondrial function can be investigated.

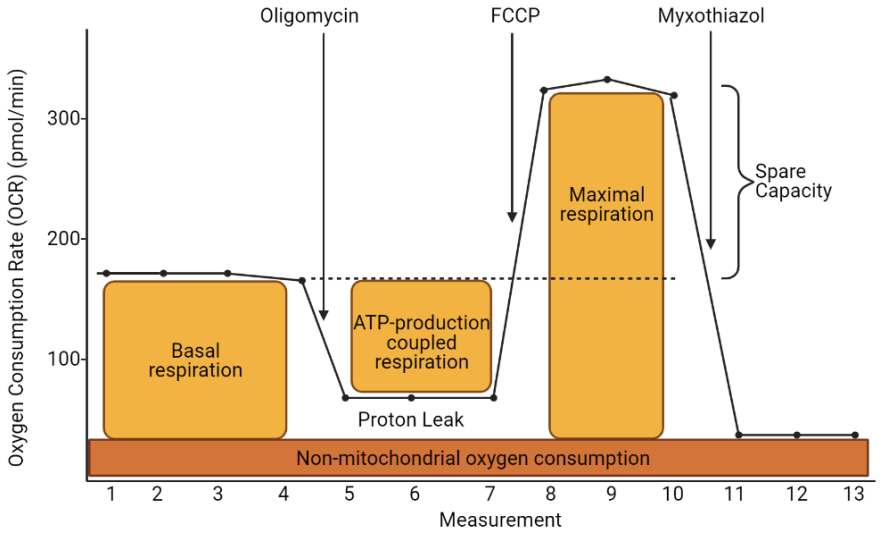


**Figure 3.4 Seahorse parameters.** The figure shows an OCR curve with some of the parameters that can be calculated from the OCR data obtained from a Mito stress assay. The shape is caused by the injection solution effects. The figure is inspired by [79].

The injection drugs and their targets are illustrated in Figure 1.12 in section 1.5 and allows for the calculation of the parameters presented in Figure 3.4: Basal respiration, ATP-production coupled respiration, maximal respiration, spare respiratory capacity, and non-mitochondrial

oxygen consumption. It is also possible to calculate a few other parameters, including proton leak (Figure 3.4). Oligomycin targets complex V, lowering the OCR, allowing for calculation of ATP-linked respiration. FCCP disrupts the mitochondrial membrane potential, allowing unrestricted flow of electrons through the ETC resulting in maximum oxygen consumption by complex IV. In this way FCCP imitates a high energy demand in the cell and makes the cell metabolism operate at its maximum. From this it is therefore possible to calculate maximal respiration and spare capacity of the cells. Myxothiazol is a mitochondrial poison that shuts down the ETC, allowing for calculation of non-mitochondrial oxygen consumption [82].

**Table 3.2 Mito Stress assay injection drugs.** The table shows the dilutions, final concentrations and loading amounts for the drugs used in the Mito Stress Test assay: Oligomycin, FCCP and Myxothiazol.

| Drug | Volume of stock solution (10mM) added to 5mL assay medium. | Working solution added to designated cartridge ports | Final well concentration |
|---|---|---|---|
| Oligomycin | 5µL | 20µL to port A | 1µM |
| FCCP | 5µL | 22.5µL to port B | 1µM |
| Myxothiazol | 10µL | 25µL to port C | 2µM |

A prompt is given by the software to place the cartridge on the instrument tray when the protocol setup is completed. Once calibration is done, another prompt will be given to remove the utility plate and place the cell plate on the tray. The instrument places the cartridge plate on top of the cell plate automatically. The assay is then run where measurements of dissolved oxygen and protons is done over 3-minute periods, calculating the OCR and ECAR automatically in real time and presenting them as a function of time on the computer screen. In this study, the protocol was set up to have 4 baseline measurement cycles, 3 injections (oligomycin, FCCP and myxothiazol) and 3 measurement cycles following each of these injections. Once the final measurement is done, the cell plate and cartridge is removed. The Mito stress assay protocol can be found in Appendix B.12.

### 3.6.2 Optimization of cell number and FCCP concentration

The number of HeLa and SiHa cells required for proper measurements were optimised by evaluating three different seeding numbers: 10 000, 20 000 and 40 000 cells. 100µL cell suspensions with desired concentrations were seeded to each well in a 96 well plate 24 hours prior to the Seahorse run, leaving the bottom row empty. Cells were then left to adhere

overnight. The optimal basal range for OCR is between 20 and 160pmol/min, while the desired basal ECAR range lies between 10 and 90mpH/min [108].

The cells were also optimised regarding FCCP concentration by evaluating four different concentrations: 0.5µM, 1.0µM, 1.5µM and 2.0µM. The optimal concentration of FCCP is the lowest concentration that gives the highest maximal respiration at the chosen seeding density [82, 109]. The Mito stress assay was run according to the protocol in Appendix B.12.

### 3.6.3 Analysis of OCR data

Analysis of Seahorse results was done using the web-based software Seahorse Analytics, the Seahorse software Wave and Microsoft excel. The equations used to calculate the parameters presented in Figure 3.4 can be seen in Table 3.3.

**Table 3.3 Seahorse Mito stress parameters.** Equations were obtained from [110].

| Parameter | Equation used for calculation |
|---|---|
| Basal respiration | (Last measurement before oligomycin injection) - (Non-mitochondrial oxygen consumption) |
| ATP-production coupled respiration | (Last measurement before oligomycin injection) - (Lowest measurement after oligomycin injection) |
| Maximal respiration | (Highest measurement after FCCP injection) – (Non-mitochondrial oxygen consumption) |
| Spare respiratory capacity | (Maximal respiration) – (Basal respiration) |
| Non-mitochondrial oxygen consumption | Lowest measurement after myxothiazol injection |

Quantification of mitochondrial ATP production rate was done using Equation 3.4 obtained from Agilent [111]. The ATP-production coupled respiration ($OCR_{ATP}$) calculated with the equation found in Table 3.3 was used for this calculation. To convert $OCR_{ATP}$ to mitochondrial ATP production rate, $OCR_{ATP}$ was multiplied by 2, for conversion from one $O_2$ molecule to two oxygen atoms. The rate was further multiplied by 2.75, which is the average number of ATP molecules synthesised per reduced oxygen atom [111].

Mitochondrial ATP Production Rate (pmol ATP/min) =
$OCR_{ATP}$ (pmol O2 /min) * 2 (pmol O/pmol O2) * 2.75 (pmol ATP/pmol O) Equation 3.4

## 3.7 Statistical analysis

Microsoft excel was used for all statistical analyses. Standard deviations were used to show how much the values deviate from the mean value. To search for significant differences between groups of the experiment, a paired two-sample student's t-test was used. All p-values are two-tailed, and therefore state whether the mean values of two groups differ. A paired t-test was used since each experiment included a sample of each group and could be directly compared. Pearson correlation coefficients were used to measure how related fluorescence signals were to cell numbers for establishment of a protocol for detection of mitochondrial mass. This was done using the CORREL function, which specifically calculates this coefficient.

# 4. RESULTS

## 4.1 Establishment of protocols

This section addresses the first aim of the study: the establishment of protocols for chemically induced hypoxia, detection of mitochondrial mass and Seahorse Mito stress assay in HeLa and SiHa cells.

### 4.1.1 Chemical induction of hypoxia

Using intracellular accumulation of HIF-1α proteins as an indicator of chemically induced hypoxia, different concentrations of $CoCl_2$ were tested to optimize and establish a culturing method. In order to verify HIF-1α accumulation, cells cultured in media containing 100µM or 200µM $CoCl_2$ for different lengths of time, were lysed for western blot analysis. The western blots revealed that $CoCl_2$ stabilised HIF-1α proteins in both HeLa and SiHa cells, leading to their accumulation. All the western blots done to verify HIF-1α stabilisation can be found in Appendix C in Figure C.1 and C.2. The antibodies utilised can be found in Appendix A Table A.8. Representative blots are shown in Figure 4.1A and B.

The western blot in Figure 4.1A shows that HIF-1α protein was detected in HeLa cells cultured with $CoCl_2$. Control cells showed no HIF-1α protein. Very little HIF-1α was detected in the cells cultured with 100µM $CoCl_2$. However, significant increase in HIF-1α with increasing incubation time was detected using 200µM $CoCl_2$. The HIF-1α accumulation therefore seems to be time and concentration dependent in HeLa cells. Cells cultured for 24 hours with 200µM $CoCl_2$ showed the strongest HIF-1α accumulation.

HIF-1α protein was detected in SiHa cells treated with $CoCl_2$ (Figure 4.1B). As with the HeLa cells, no HIF-1α protein was detected in untreated cells. Some HIF-1α was detected in the cells cultured with 100µM $CoCl_2$, and even more when using 200µM $CoCl_2$. The SiHa cells did not show the same time dependency in HIF-1α accumulation as observed in HeLa cells. However, the stabilisation was concentration dependent. Moreover, in these cells, HIF-1α accumulation tended to decline slightly after 6 hours. The decline was especially visible in cells treated with 100µM $CoCl_2$.

**A)**

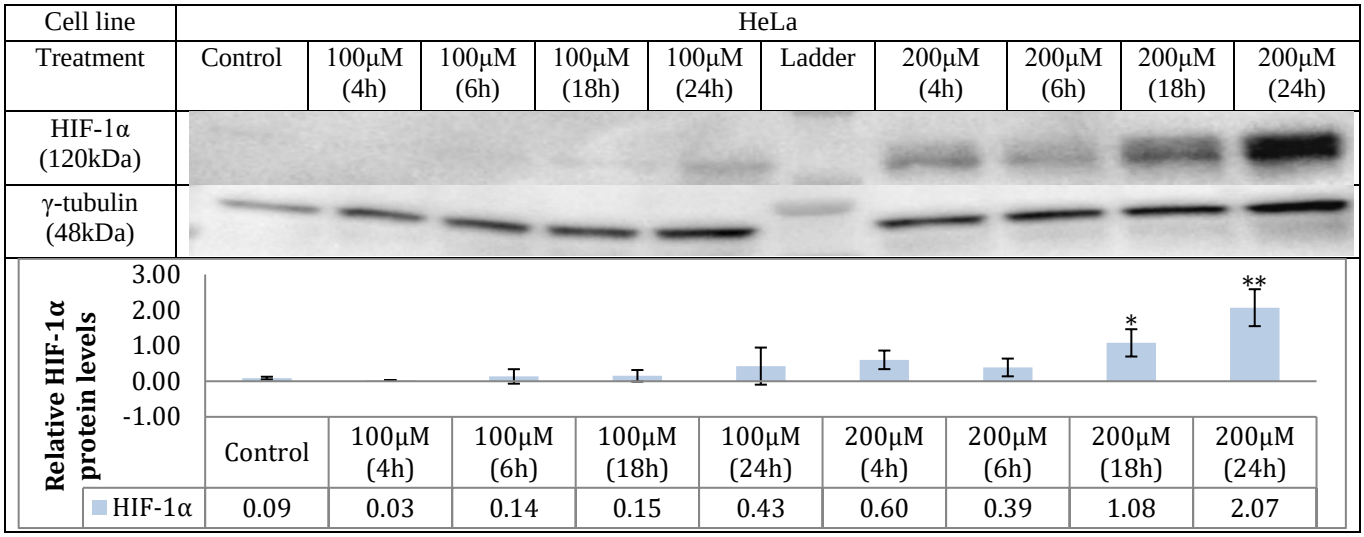


**B)**

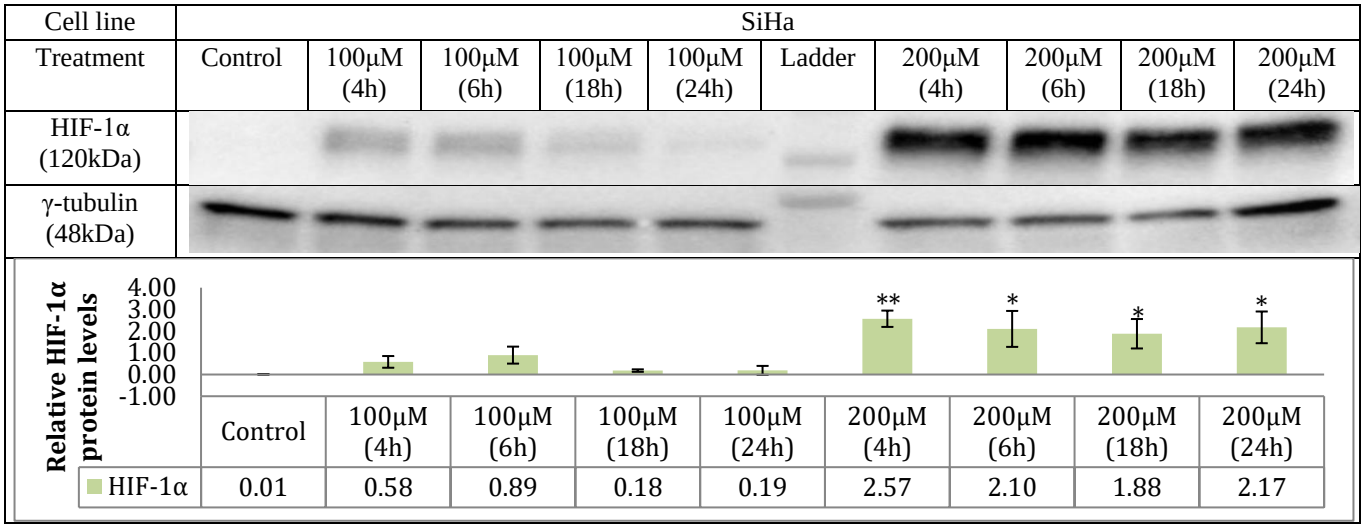


**Figure 4.1 Western blot and protein levels of HIF-1α in cells cultured with $CoCl_2$. A)** HeLa **B)** SiHa. The upper panels show representative western blots of detected HIF-1α and γ-tubulin (loading control) in HeLa- (A) and SiHa cell lysates (B) incubated for different amounts of time and with two different concentrations of $CoCl_2$. The lower panels show protein levels quantified based on all western blots performed with these setups. Mean values and standard deviations of normalised protein levels obtained from three biological replicates are presented. h: hours. *p<0.05. **p<0.01.

From the Western blots, it can also be seen that SiHa cells responded more strongly to treatment with $CoCl_2$ compared to HeLa cells as more HIF-1α accumulation can be seen at a lower concentration and after shorter incubation times (Figure 4.1). For further experiments, an incubation time of 24 hours, and a concentration of 200µM $CoCl_2$ were chosen for both cell lines, ensuring consistent HIF-1α stabilisation, and facilitating experimental set up for the other protocols.

### 4.1.2 Detection of mitochondrial mass

To verify correct staining with Mitotracker Green, live cell microscopy and imaging was done with HeLa cells using a Zeiss cell observer. Below, a superimposed image of a single-phase contrast section with deconvoluted fluorescence images is shown (Figure 4.2) indicating successful staining of organelles in the cytoplasm surrounding the cell nucleus. It was concluded that Mitotracker Green most likely exclusively stains the mitochondria.

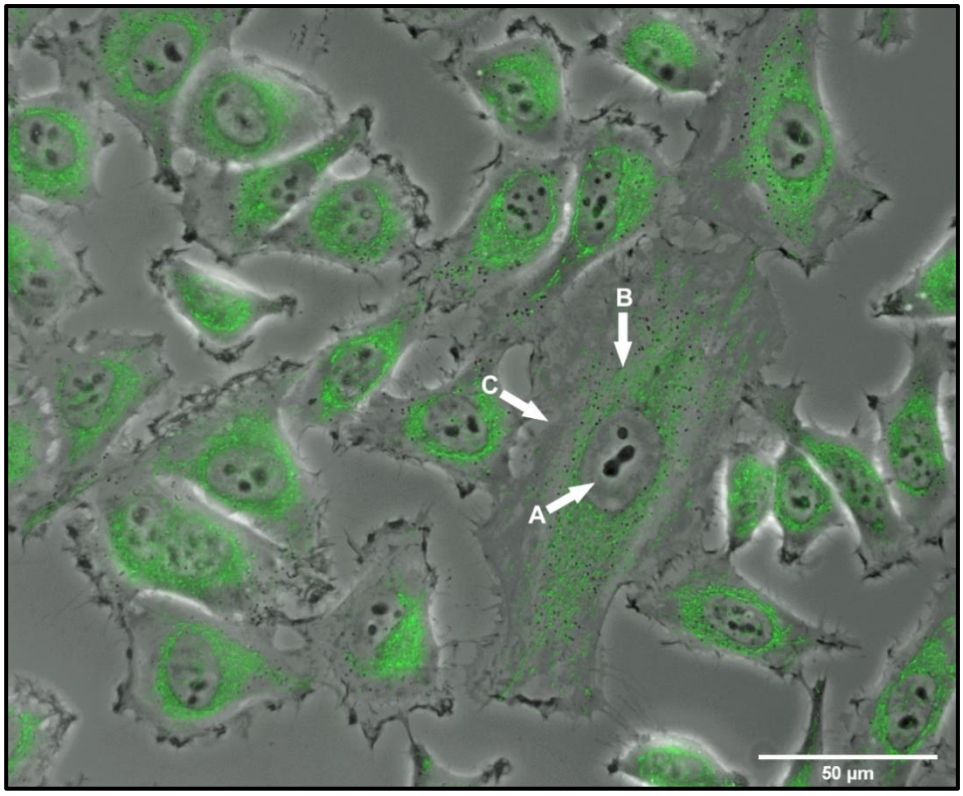


**Figure 4.2 Image of MitoTracker Green localization in HeLa cells.** The cells were seeded 24 hours prior to the imaging and treated with 200nM Mitotracker for 30 minutes. A single-phase contrast section merged with the fluorescence image (which was made through maximum projections of deconvoluted z-stacks) is shown. The labeled arrows point to a nucleus (A), a mitochondrion (B) and the cytoplasm (C) of a single cell. The image was acquired with assistance by Sebastian Patzke (OUH).

To investigate if fluorescence could be used to detect mitochondrial mass with a Tecan plate reader, different numbers of cells were seeded to investigate if the signal increased with increasing cell number. The results (Figure 4.3) are based on 6 technical replicates.

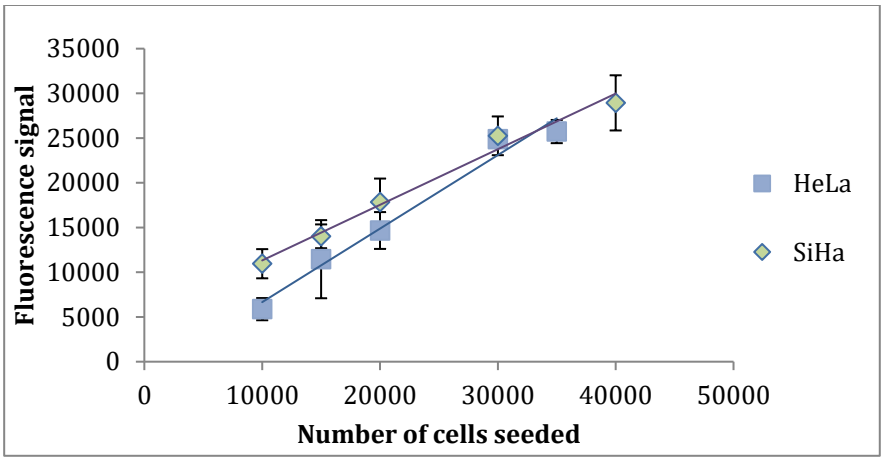


**Figure 4.3 Fluorescence signal detected at different seeding densities of HeLa and SiHa cells.** Mean fluorescence signals and standard deviations from 6 technical replicates are shown. Cells were treated with 200nM MitoTracker Green for 30 minutes prior to measurements by the Tecan plate reader. The cells were seeded approximately 24 hours prior to the measurements. HeLa cells were seeded with cell numbers of 10-, 15-, 20-, 30- and 35 000. SiHa cells were seeded with the cell numbers: 10-, 15-, 20-, 30- and 40 000.

Figure 4.3 shows that the fluorescence signal emitted in wells with increasing seeding densities increased in a linear fashion. A Pearson correlation coefficient (r) was calculated for each cell line, where the r-values were 0.99 and 1 for HeLa and SiHa respectively. The mitochondrial mass per cell seemed similar for both cell lines. For further experiments with MitoTracker Green the seeding densities chosen for HeLa and SiHa cells were 20 000 and 30 000, respectively. It was concluded that this method can be used to detect mitochondrial mass in HeLa and SiHa cells.

### 4.1.3 Seahorse assay

HeLa and SiHa cells were optimised with respect to cell number for the Seahorse assay by evaluating results based on 10-, 20- and 40 000 cells that were seeded 24 hours prior to the measurements. Below, the OCR and ECAR curves as well as the average values for basal respiration are presented for the three different seeding densities (Figure 4.4).

**A)**

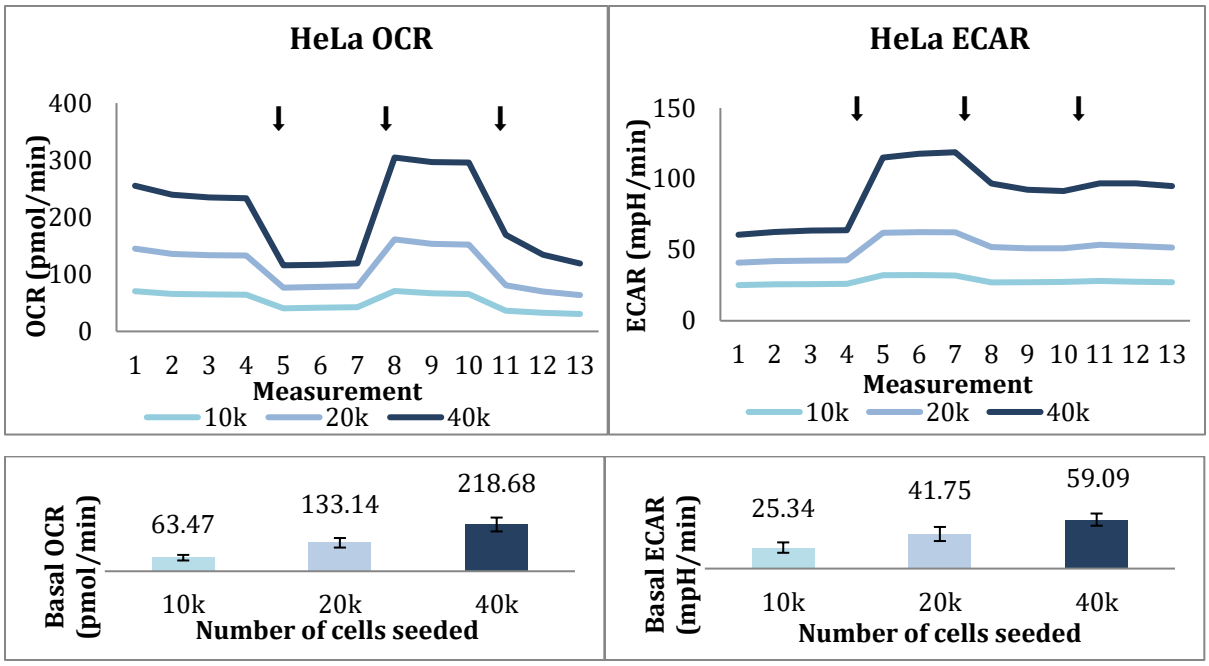


**B)**

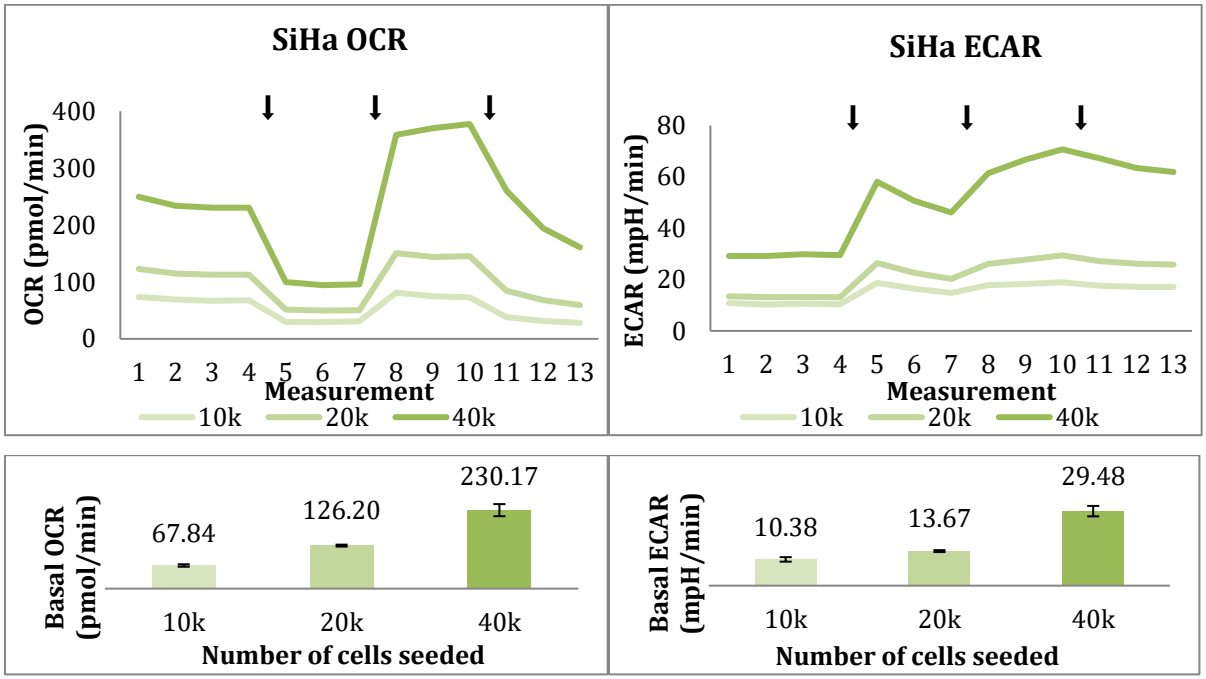


**Figure 4.4 OCR and ECAR measurements at different seeding densities of HeLa and SiHa cells.** Upper panels show the OCR and ECAR measurements at different cell numbers for HeLa cells (**A**) and SiHa cells (**B**). The arrows symbolize the injections shown in Figure 3.4. Lower panels show the average OCR values at the last basal measurement for HeLa cells (**A**) and SiHa cells (**B**). The values presented are mean values, and standard deviations are based on 1 biological replicate with 7 technical replicates for each cell number. k: x 1000.

The obtained Seahorse results presented in the upper left panels of Figure 4.4 show the characteristic OCR curve shape presented in Figure 3.4, which is due to the effect of the injected solutions. The measurements were consistent over time making them suitable for calculations, as well showing that the instrument functioned correctly. First, four measurements of basal respiration were done. Then oligomycin was injected, leading to an OCR decline in accordance with its inhibition of Complex V. After FCCP injection, which disrupts the mitochondrial membrane potential, the OCR increased in accordance with its effect. Further, the OCR decreased following injection of myxothiazol due to its inhibition of complex III. The Seahorse also measured ECAR, which can say something about the glycolytic compensation when mitochondrial function is altered. ECAR curves for both cell lines are presented in the upper right panels of Figure 4.4.

As shown in Figure 4.4, OCR and ECAR increased with increasing cell numbers in both cell lines. Based on these results, the cell number chosen for further experiments was 20 000. This number was chosen as the baseline OCR (133pmol/min for HeLa, 126pmol/min for SiHa) was within the recommended range of 20-160pmol/min. The baseline ECAR at a cell number of 20 000 (42mpH/min for HeLa, 14mpH/min for SiHa) was further within the recommended range of 10-90mpH/min.

The FCCP concentration to be injected during the assay was optimised by injecting four different FCCP concentrations: 0.5µM, 1µM, 1.5µM and 2µM. FCCP allows for measurements of maximal respiration, and the optimal FCCP concentration is therefore the concentration that gives the highest OCR values. The OCR results from both cell lines at seeding density 20 000 are shown for the different concentrations of FCCP in Figure 4.5.

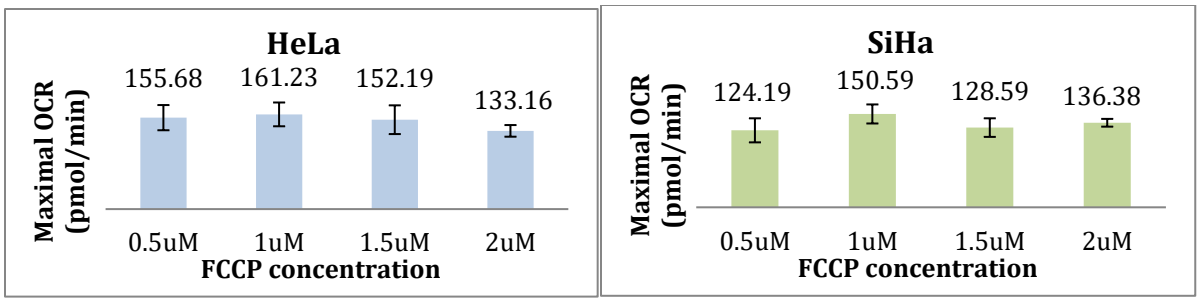


**Figure 4.5 Baseline OCR for HeLa and SiHa cells obtained for different FCCP concentrations.** 20 000 cells were seeded for both cell lines. Mean values and standard deviations are from the first measurement after FCCP injection (2nd injection) and are calculated from 5 technical replicates.

Based on these results, 1uM was chosen as the optimal FCCP concentration for further experiments for both cell lines, since this concentration led to the highest OCR in both HeLa and SiHa cells.

## 4.2 Effects of microenvironment

This section addresses the second aim of the study: To study the effects of different microenvironmental conditions on proliferation and mitochondrial mass. This was done by culturing cells under different conditions prior to the measurements. These culturing conditions were: 200µM $CoCl_2$ (chemically induced hypoxia), lactosis (10mM lactate with pH≈7.4) or lactic acidosis (10mM lactate with pH≈6.6).

### 4.2.1 Effects of microenvironment on proliferation

HeLa and SiHa cells cultured under the microenvironmental conditions were counted 24 hours after seeding and doubling times were calculated. The cell numbers and doubling times were used as a measure of proliferation. The doubling times presented in Table 4.1, and the graphs in Figure 4.6, show the microenvironmental effect on both cell lines.

**Table 4.1 HeLa and SiHa cell doubling times ($T_D$) for different microenvironmental conditions.** Mean values with standard deviations (±) are calculated from three biological replicates using Equation 3.2. The culturing conditions used were: normal growth conditions/Control (pH≈7.4), 200µM CoCl2 (chemically induced hypoxia), lactosis (10mM lactate with pH≈7.4) or lactic acidosis (LA) (10mM lactate with pH≈6.6).

| | **Control** | **$CoCl_2$** | **Lactosis** | **LA** |
|---|---|---|---|---|
| **$T_D$ (hours) HeLa** | 26.1±0.4 | 26.3±3.2 | 28.3±5.0 | 117.7±1.9 |
| **$T_D$ (hours) SiHa** | 31.3±3.3 | 44.6±3.9 | 30.6±2.5 | 125.4±39.2 |

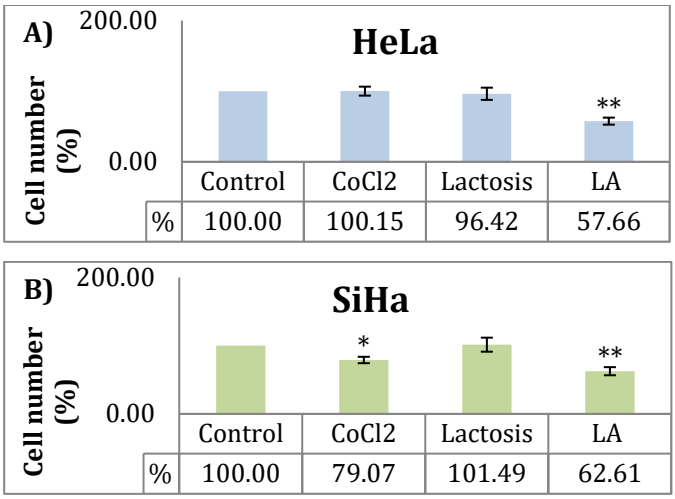


**Figure 4.6 HeLa and SiHa cell numbers under different culturing conditions. A)** Cell number relative to Control in HeLa cells **B)** Cell number relative to Control in SiHa cells. The culturing conditions used were: normal growth conditions/Control (pH≈7.4), 200µM CoCl2 (chemically induced hypoxia), lactosis (10mM lactate with pH≈7.4) or lactic acidosis (10mM lactate with pH≈6.6). Number of counted cells was derived as percentage of Control cell number for each replicate. Mean values and standard deviations are calculated from three biological replicates. Standard deviations for Control cells are not shown, as Control was used to normalize. *Statistically different from Control ($p<0.05$). **Statistically different from Control ($p<0.01$).

Figure 4.6A shows that $CoCl_2$ and lactosis did not significantly change HeLa proliferation in 24 hours, while the cells cultured in lactic acidosis had significantly lower cell numbers ($p=0.004$). Similar results were found for SiHa (Figure 4.6B), except that a decrease in cell number was also seen for cells cultured in media with $CoCl_2$ ($CoCl_2$: $p=0.024$ and LA: $p=0.009$). The inhibition of proliferation under these microenvironmental conditions was also reflected by the doubling times presented in Table 4.1. The table shows that the doubling times for cells cultured under LA, and $CoCl_2$ in the case of SiHa cells, are notably higher than the remaining conditions.

### 4.2.2 Effects of microenvironment on mitochondrial mass

Mitochondrial mass detected by using MitoTracker Green are presented below for cells cultured under the different microenvironmental conditions (Figure 4.7). Since the microenvironmental conditions had different effects on cell proliferation, the fluorescence signal was divided by the expected cell number after 24 hours based on the doubling times presented in Table 4.1.

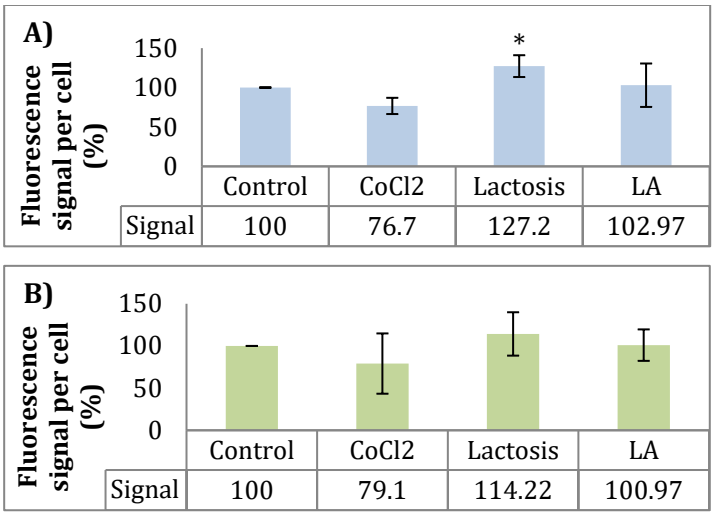


**Figure 4.7 Mitochondrial mass under different microenvironmental conditions. A)** HeLa **B)** SiHa. The cells were seeded in Seahorse cell microplates and treated with 200nM MitoTracker Green for 30 minutes before the plate was read. The culturing conditions used were: normal growth conditions/Control (pH≈7.4), 200µM CoCl2 (chemically induced hypoxia), lactosis (10mM lactate with pH≈7.4) or lactic acidosis (10mM lactate with pH≈6.6). Mean values and standard deviations calculated from 4 biological replicates are shown. The signals are normalised by the expected cell number for each condition, based on Table 4.1 and divided on the Control signal within each replicate. The values were then multiplied by 100 to show the relative percentage compared to Control. *Statistically different from Control ($p < 0.05$).

Figure 4.7A shows that cells cultured in lactosis had significantly higher fluorescence signal per cell than cells cultured under normal conditions (Control) in HeLa cells, indicating a larger mitochondrial mass per cell. On the other hand, no significant increase can be seen in the SiHa cells cultured under the same conditions (Figure 4.7B). Both cell lines tended to have a lower signal than Control cells cultured with $CoCl_2$, however these changes were not significant. Cells cultured with lactic acidosis showed no difference compared to Control cells in either cell line.

## 4.3 Effects of metformin

This section addresses the third aim of the study: To study the effects of metformin on HIF-1α stabilisation, as well as on cell proliferation and mitochondrial mass in HeLa and SiHa cells cultured under the microenvironmental conditions presented in section 4.2. For all the results presented in this section metformin treatment consisted of 3mM metformin for 18 hours as this was sufficient to have an effect on mitochondrial function using Seahorse (shown in section 4.4.3).

### 4.3.1 Effects of metformin on HIF-1α stabilisation

Because metformin has been proposed as a strategy to alleviate tumour hypoxia by decreasing the cellular OCR through the inhibition of the ETC, the treatment effect of metformin on HIF-1α stabilisation by $CoCl_2$ was investigated. Metformin-treated and untreated cells cultured with or without $CoCl_2$ were lysed, and HIF-1α was detected using Western blotting. Western blots for all three biological replicates can be found in Appendix C Figure C.3. One representative Western blot is shown in Figure 4.8.

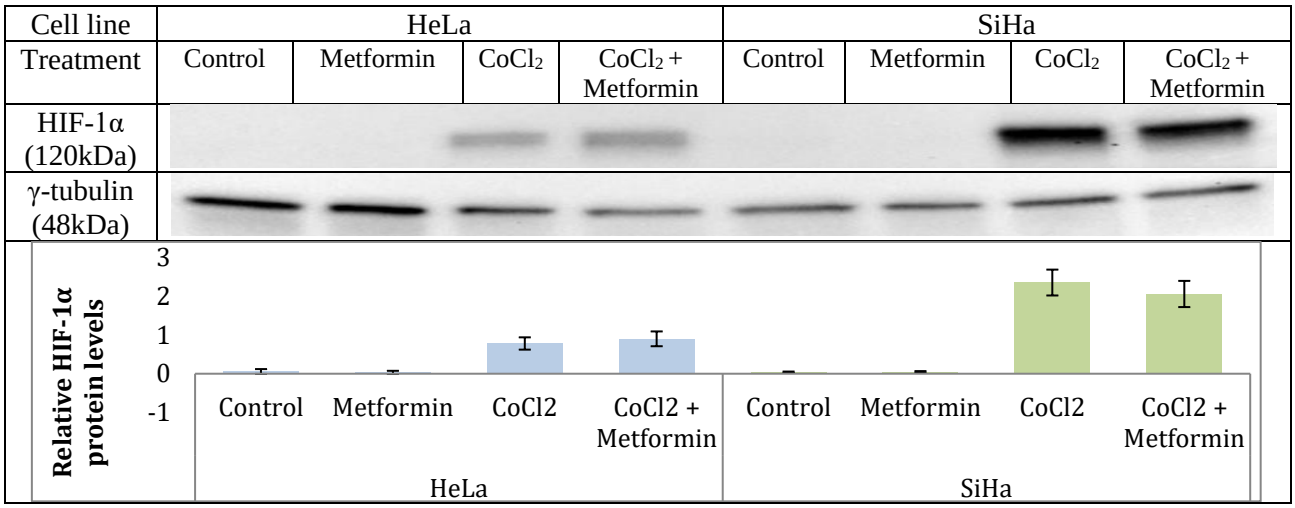


**Figure 4.8 Western blot and protein levels of HIF-1α in HeLa and SiHa cells treated with metformin and/or $CoCl_2$.** The upper panel shows a representative blot of detected HIF-1α and γ-tubulin in HeLa and SiHa lysates. The lower panel shows mean protein level with standard deviations quantified based on the three western blots presented in Appendix C Figure C.3.

The western blot presented in Figure 4.8 further shows that HIF-1α protein was detected in HeLa and SiHa cells cultured with $CoCl_2$, as shown in Figure 4.1. No HIF-1α was detected in untreated (Control) cells. This blot, like the previous blots presented (Figure 4.1), shows a bigger HIF-1α accumulation in SiHa compared to HeLa cells. However, no significant decrease or increase in HIF-1α stabilisation in cells treated with metformin was detected in either cell line, indicating that metformin was not able to alleviate this effect of the chemically induced hypoxia.

### 4.3.2 Effects of metformin on proliferation

As metformin has been shown to inhibit proliferation its effects were tested by counting the cells 18 hours following treatment with metformin. No significant effects of the drug were found under any of the microenvironmental conditions (Figure 4.9). The cell numbers and doubling

times were used as a measure of proliferation. The doubling times presented in Table 4.2, and the graphs in Figure 4.9, show the cell growth for HeLa and SiHa cells with metformin treatment under all the microenvironmental conditions. The cell growth presented in Figure 4.6 is also included in Figure 4.9 for comparison.

**Table 4.2 Doubling time ($T_D$) of HeLa and SiHa cells cultured under different microenvironmental conditions with metformin.** Mean values with standard deviations (±) are calculated from three independent biological replicates using Equation 3.2. Metformin treatment included treatment with 3mM metformin for 18 hours. The culturing conditions used were: normal growth conditions (pH≈7.4), 200μM CoCl2 (chemically induced hypoxia), lactosis (10mM lactate with pH≈7.4) or lactic acidosis (10mM lactate with pH≈6.6).

| | **Metformin** | **$CoCl_2$ + Metformin** | **Lactosis + Metformin** | **LA + Metformin** |
|---|---|---|---|---|
| **$T_D$ (hours) HeLa** | 25.6±1.1 | 26.6±2.6 | 28.8±3.5 | 562.8±470.6 |
| **$T_D$ (hours) SiHa** | 30.4±3.3 | 47.3±2.8 | 32.8±5.8 | 142.6±57.6 |

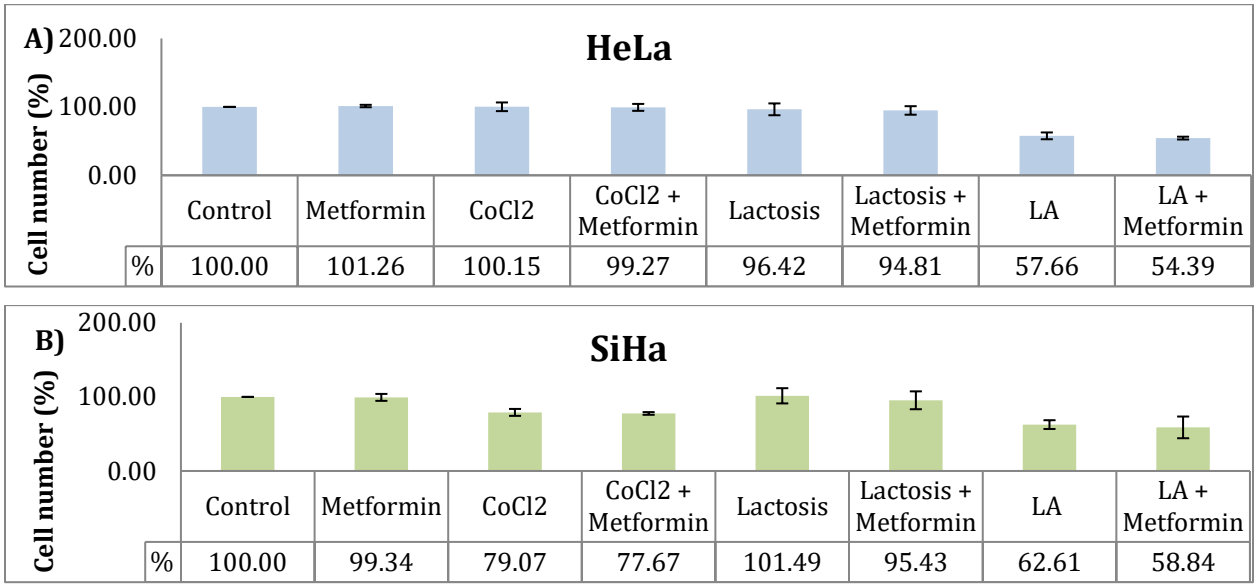


**Figure 4.9 HeLa and SiHa cell number under different culturing conditions with and without metformin treatment. A)** Cell number relative to Control in HeLa cells **B)** Cell number relative to Control in SiHa cells. Number of counted cells was derived as percentage of cell number of Control cells for each replicate. Mean values and standard deviations are based on three biological replicates. Metformin treatment included treatment with 3mM metformin for 18 hours. The culturing conditions used were: normal growth conditions/Control (pH≈7.4), 200μM CoCl2 (chemically induced hypoxia), lactosis (10mM lactate with pH≈7.4) or lactic acidosis (10mM lactate with pH≈6.6). The cells were counted 24 hours after being seeded.

There was no statistically significant effect of metformin under any of the conditions in either cell line. The doubling times (Table 4.2), when compared with those presented in Table 4.1, also showed that there is no notable difference when metformin treatment is added.

### 4.3.3 Effects of metformin on mitochondrial mass

As metformin previously has been shown to affect the ETC of mitochondria, its potential effect on mitochondrial mass was also investigated. Mitochondrial mass was detected in cells treated with metformin under all the microenvironmental conditions using MitoTracker Green and a Tecan plate reader (Figure 4.10). The fluorescence signals presented in Figure 4.7 are also included in Figure 4.10 for comparison. All signals were divided on the expected cell number after 24 hours in the given condition, derived from Table 4.1 and 4.2.

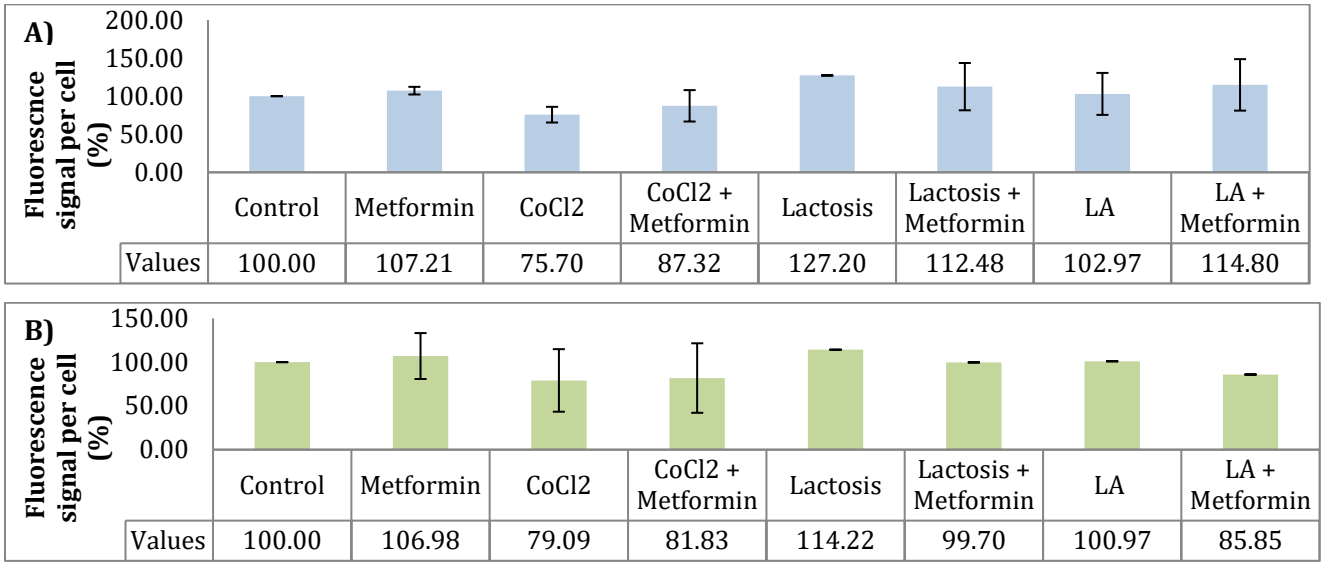


**Figure 4.10 Mitochondrial mass under different culturing conditions. A)** Fluorescence signals in HeLa cells. **B)** Fluorescence signals in SiHa cells. The cells were seeded in Seahorse cell microplates and treated with 200nM MitoTracker Green for 30 minutes before the plate was read. Metformin treatment included treatment with 3mM metformin for 18 hours. The culturing conditions used were: normal growth conditions/Control (pH≈7.4), 200µM CoCl2 (chemically induced hypoxia), lactosis (10mM lactate with pH≈7.4) or lactic acidosis (10mM lactate with pH≈6.6). Mean values and standard deviations calculated from 4 biological replicates are shown. The signals are normalised by the expected cell number for each condition, based on Table 4.1 and 4.2, and divided on the Control signal within each replicate. The values were then multiplied by 100 to show the relative percentage compared to Control.

Figure 4.10 shows that detection of mitochondrial mass following treatment with metformin showed no significant effect of the drug under any of the microenvironmental conditions. This can be seen by comparing each condition with and without metformin, which showed that 3mM metformin did not lead to a notable difference in fluorescence signal. In conclusion, the chosen metformin concentration cannot be said to alter mitochondrial mass in either cell line.

## 4.4 Metabolic studies in HeLa and SiHa cells by Seahorse

This section addresses the fourth aim of the study. Experiments were performed to investigate the usefulness of Seahorse in metabolic studies of cells cultured under normal conditions and chemically induced hypoxia. In addition, the ability of Seahorse technology to detect treatment effects of metformin was investigated. Due to time restraints the results presented are limited to few replicates.

### 4.4.1 Seahorse parameters in cells cultured under normal conditions

Figure 4.11 shows some of the parameters (Figure 3.4) that can be calculated from the Seahorse Mito stress assay, calculated as demonstrated in Table 3.3. This shows a range of information that can be obtained from Seahorse OCR data. The figure shows that both cell lines are similar when it comes to oxygen consumption rates; this is also reflected by Figure 4.4.

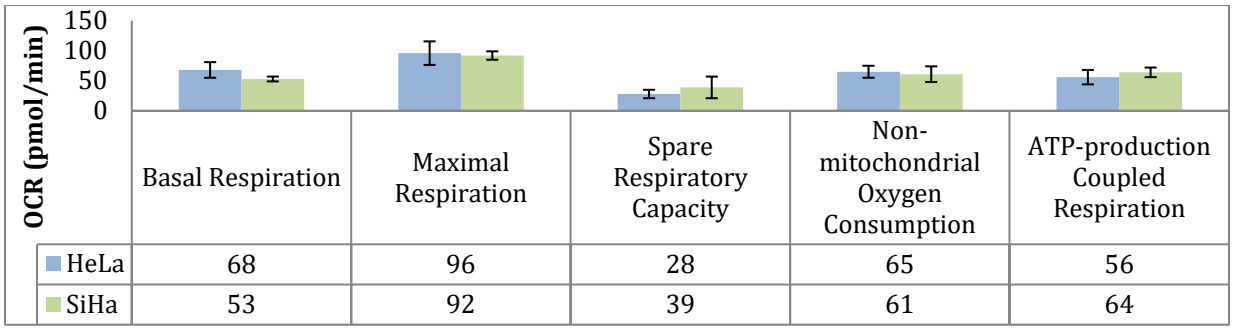


| | Basal Respiration | Maximal Respiration | Spare Respiratory Capacity | Non-mitochondrial Oxygen Consumption | ATP-production Coupled Respiration |
|---|---|---|---|---|---|
| HeLa | 68 | 96 | 28 | 65 | 56 |
| SiHa | 53 | 92 | 39 | 61 | 64 |

**Figure 4.11 Mito stress assay parameters in HeLa and SiHa cells.** Mean values and standard deviations are calculated from 7 technical replicates with HeLa and SiHa cells. The parameters were calculated using the equations presented in Table 3.3. Number of cells seeded was 20 000 for both cell lines.

Figure 4.11 shows that oxygen consumption rates are similar across all the parameters when comparing the two cell lines, meaning they show further similarities when it comes to oxygen consumption. Maximal respiration was shown to be very similar, implying an equal capacity for oxidative phosphorylation in HeLa and SiHa cells. This could further support the results presented in Figure 4.3 showing equal mitochondrial mass in the two cell lines. The same can be said for the OCR parameters describing spare respiratory capacity and ATP-production coupled respiration. Non-mitochondrial oxygen consumption was also shown to be similar. The ATP-production coupled respiration OCRs were further used to calculate ATP production rates for both cell lines. Figure 4.12 shows ATP production rates calculated using Equation 3.4 and was normalised on expected cell number.

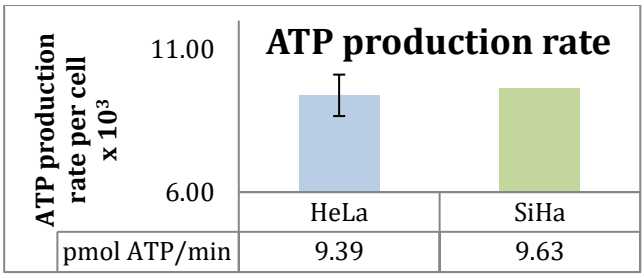


**Figure 4.12 Mitochondrial ATP production.** Mean values were calculated from measurements done before and after oligomycin injection on three biological replicates in the case of Hela, and one biological replicate on SiHa. The standard deviation shown for HeLa is based on the three biological replicates.

Figure 4.12 shows that the mitochondrial ATP production relative to cell number seems to be similar in both cell lines. This is again reflected by the similar OCR values presented in Figure 4.4 and 4.11. Even though OCR seems to be similar in the two cell lines, the results presented in Figure 4.4 indicate that ECAR differs. A ratio between the two parameters were therefore calculated for comparison of the two cell lines. OCR/ECAR ratios for HeLa and SiHa cells were calculated based on the values presented in Figure 4.4 (Figure 4.13). This ratio can be used to compare different cell lines and is independent of cell number, negating the necessity to normalize on expected cell number.

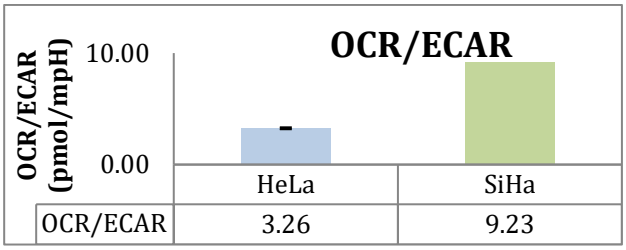


**Figure 4.13 OCR/ECAR ratios for HeLa and SiHa cells.** Mean values from three biological replicates (HeLa) and 5 technical replicates (SiHa) are presented. The seeding density was 20 000 for both cell lines.

From figure 4.13, it can be seen that the OCR/ECAR ratio for SiHa is 3 times higher than that of the HeLa cells. From Figure 4.4 it can be seen that this is due to low ECAR for SiHa cells.

### 4.4.2 Seahorse parameters in cells cultured under chemically induced hypoxia

As hypoxia is known to affect cellular energy metabolism, the effects of the hypoxia model on OCR and ECAR were measured. To investigate the effects, HeLa cells were cultured with 200µM $CoCl_2$ for 24 hours before Seahorse measurements.

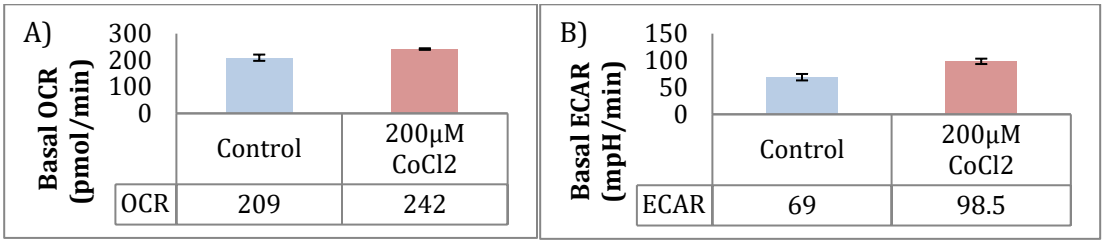


**Figure 4.14 OCR and ECAR results from HeLa cells treated with $CoCl_2$. A)** OCR **B)** ECAR. The cells were seeded approximately 40 hours and treated with 200µM $CoCl_2$ for 24 hours prior to the measurements. The values are based on one biological replicate with 5 technical replicates.

Figure 4.14 shows that HeLa cells cultured with $CoCl_2$ have a higher OCR and ECAR than Control cells. However, statistical significance cannot be claimed as the results are based on only one biological replicate. The OCR/ECAR ratio for cells treated with $CoCl_2$ is presented in Figure 4.15 along with the ratio for HeLa cells cultured under normal conditions from Figure 4.13.

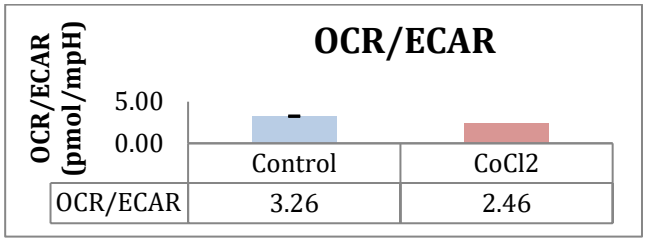


**Figure 4.15 OCR/ECAR ratios of HeLa cells cultured with $CoCl_2$.** Mean values from three biological replicates (Control) or 5 technical replicates ($CoCl_2$ treated cells) are presented. The standard deviation shown for Control is calculated from three biological replicates. The last basal measurements (measurement 4) were used in the calculations.

From Figure 4.15, it can be seen that the OCR/ECAR ratio for the HeLa cells treated with $CoCl_2$ is slightly lower than that of Control. As there is only one replicate of cells treated with $CoCl_2$, it is not possible to judge if this difference is significant or not.

### 4.4.3 Effects of metformin on Seahorse parameters

As metformin has been shown to inhibit complex I of the ETC, its effects on OCR and ECAR were measured by Seahorse. The measurements were done in HeLa cells treated with different concentrations (0, 1, 2, 3, 5 and 8mM) of metformin. The figures in section 4.4.3.1 visualizes the effects of metformin on OCR and ECAR in HeLa cells cultured under normal conditions.

Further, metformin effects under chemically induced hypoxia were investigated in HeLa cells, and the results are presented in section 4.4.3.2.

### 4.4.3.1 Cells cultured under normal conditions

Seahorse measurements of cells treated with the different metformin concentrations are shown in Figure 4.16. Based on the measurements presented in Figure 4.16, plots of how basal OCR and ECAR changed with increasing metformin concentration was generated, and is presented in Figure 4.17.

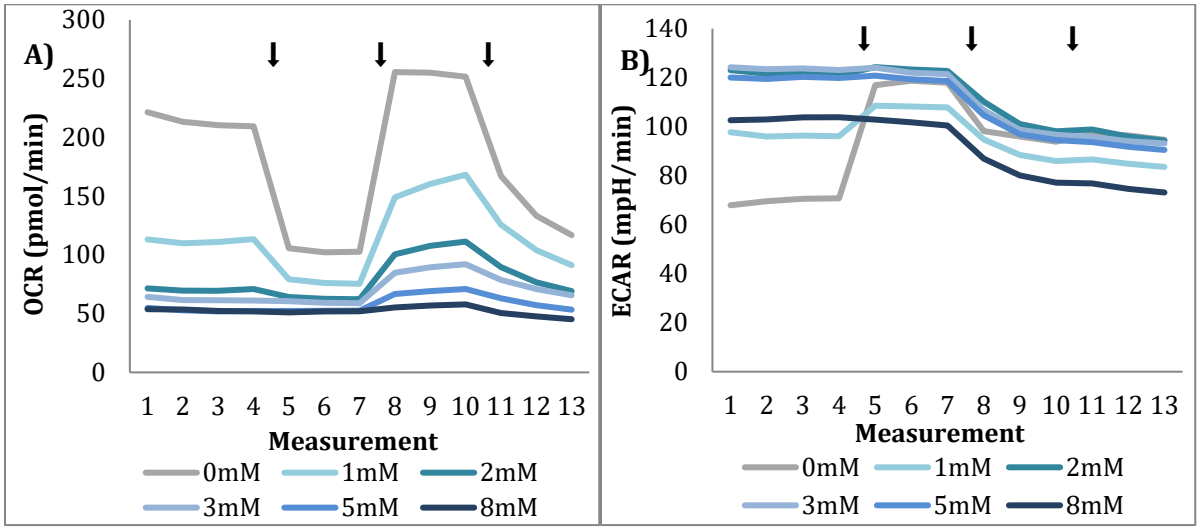


**Figure 4.16 OCR and ECAR measurements for HeLa cells treated with metformin.** OCR (**A**) and ECAR (**B**) measurements are shown in the left and right panel respectively, and arrows symbolize the Mito stress assay injections shown in Figure 3.4. The measurements were done approximately 40 hours after seeding, and metformin treatment entailed 18 hours with 3mM metformin. Mean values based on 5 technical replicates for each condition are shown.

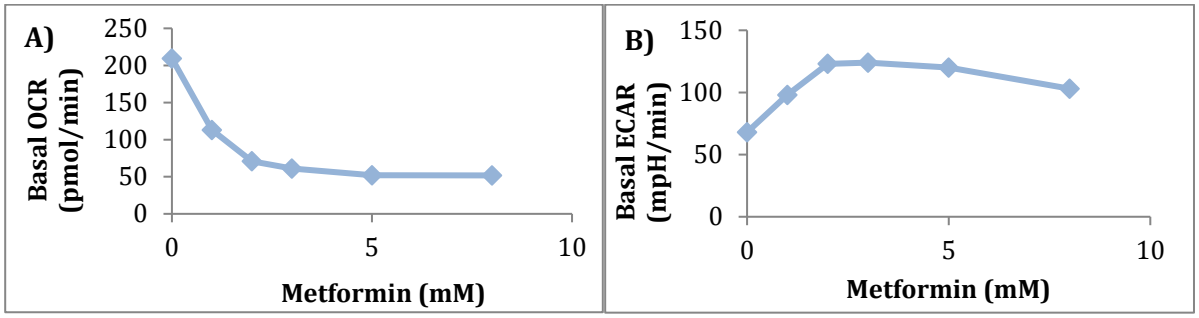


**Figure 4.17 Basal OCR and ECAR at increasing metformin concentrations. A)** Basal OCR **B)** Basal ECAR. Mean values of 5 technical replicates are presented. The cells were treated with either 0mM, 1mM, 2mM, 3mM, 5mM or 8mM metformin 18 hours prior to measurements. The cells were seeded approximately 40 hours prior to measurements.

The figures show that metformin affects the OCR and ECAR of HeLa cells in a concentration dependent manner. A reduction in OCR and increase in ECAR compared to Control were found (Figure 4.16 and 4.17). From the Figure 4.16, it can be seen that the OCR curves flatten with increasing concentrations of metformin. The curve representing cells treated with 8mM metformin was almost completely flat, while all other concentrations showed some capacity for oxygen consumption after FCCP injection (second injection). Figure 4.17 shows that maximal inhibition of basal OCR is almost reached at 3mM metformin, and that there is no further decrease in basal OCR after 5mM metformin, suggesting maximal inhibition of basal mitochondrial oxygen consumption.

ECAR was consistently higher in all cells treated with metformin compared to untreated cells (0mM), with cells treated with 2, 3 and 5mM having similar ECARs. Cells treated with 1mM and 8mM metformin had lower ECAR values than the other cells treated with metformin, but was still notably higher than untreated cells. Figure 4.17 also shows this trend showing that basal ECAR drops by approximatly 20 mpH/min in cells treated with 1 or 8mM metformin.

Figure 4.18 shows calculations of the seahorse parameters (Figure 3.4) of cells treated with five different concentrations of metformin. The parameters were calculated as demonstrated in Table 3.3.

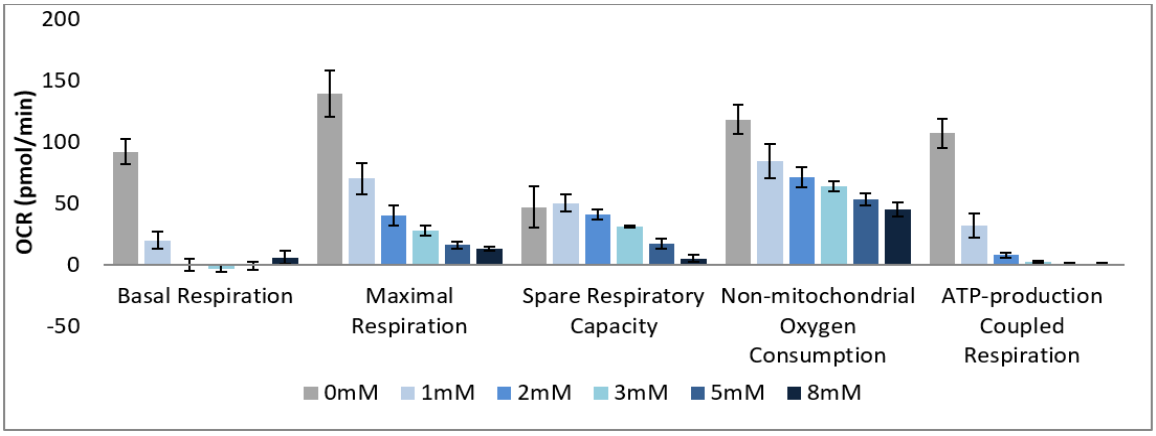


**Figure 4.18 Mito stress assay parameters under different metformin concentrations.** Mean values and standard deviations are calculated from 7 technical replicates. The cells were seeded approximately 40 hours, and treated with metformin 18 hours, prior to the measurements.

Figure 4.18 shows that all the OCR parameters decrease with increasing concentration. The basal respiration drastically decreases at 1mM metformin and is zero in the cells treated with 2mM metformin. It seems to be slightly increased at 8mM metformin, but not significantly so. The cells still have some spare respiratory capacity under all the concentrations, with the possible exception of cells treated with 8mM metformin. This is also reflected by the measurements of maximal respiration. A decrease in non-mitochondrial oxygen consumption by metformin was also observed with increasing metformin concentration. ATP-coupled respiration was again used to calculate mitochondrial ATP production rates using Equation 3.4. This is presented in Figure 4.19 and can give further insight into the altered energy metabolism caused by metformin treatment.

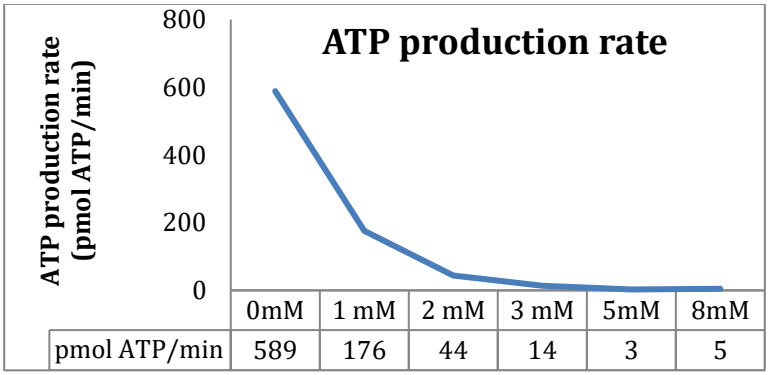


**Figure 4.19 Mitochondrial ATP production rate for HeLa cells treated with metformin.** The figure shows ATP production rates calculated using Equation 3.4 in HeLa cells treated with the indicated concentrations of Metformin for 18 hours before OCR measurements on the Seahorse. Cells were seeded 40 hours prior to the experiment.

Figure 4.19 shows that ATP production decreases with increasing metformin concentrations, which is also reflected by the decrease in mitochondrial oxygen consumption presented in the previous figures.

#### 4.4.3.2 Cells cultured under chemically induced hypoxia

To investigate the effects of metformin under chemically induced hypoxia, HeLa cells were cultured with 200µM $CoCl_2$ alone and with three different metformin concentrations: 1, 2 and 3mM.

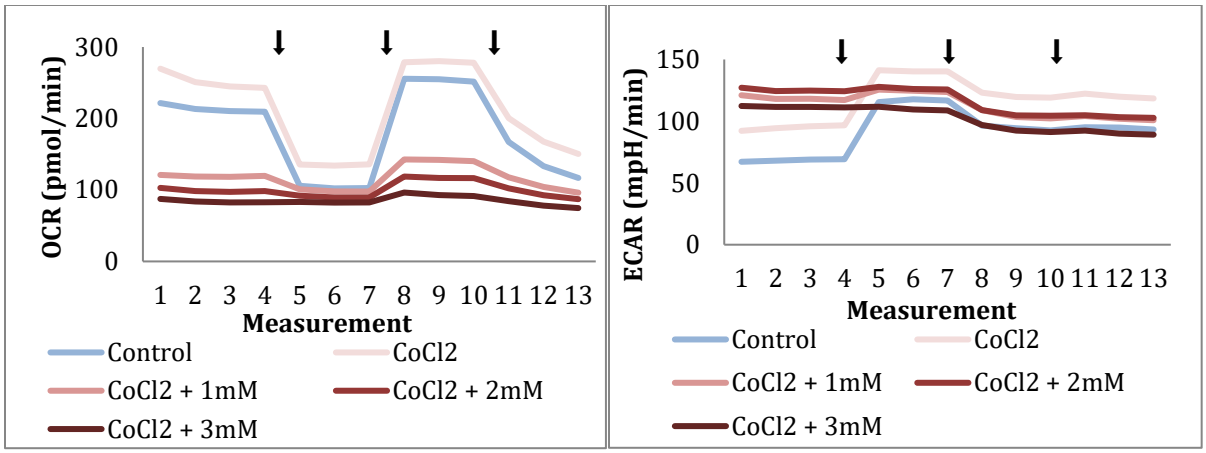


**Figure 4.20 OCR and ECAR measurements for HeLa cells cultured with $CoCl_2$ and metformin.** OCR and ECAR measurements are shown in the left and right panel respectively, and arrows symbolize the assay injections shown in Figure 3.4. The cells were seeded 40 hours prior to the experiment and were cultured with 200µM $CoCl_2$ for 24 hours and metformin at indicated concentrations 18 hours prior to the experiment. Mean values based on 5 technical replicates for each condition are shown.

Figure 4.20 shows the same trend in oxygen consumption inhibition, and increased ECAR, as under normal conditions (Figure 4.16) when the cells are treated with metformin. The OCR curves flatten showing a drastic decrease in oxygen consumption compared to untreated cells at all metformin concentrations. The ECAR increased, as under normal conditions. OCR and ECAR was also generally higher than under normal conditions (Control), something that is also shown in Figure 4.14.

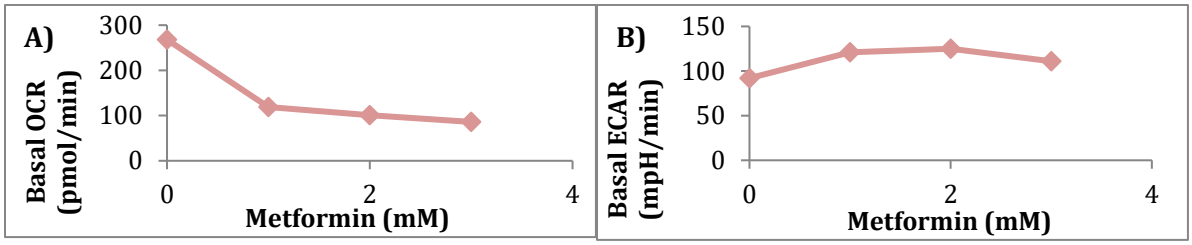


**Figure 4.21 Basal OCR and ECAR at increasing metformin concentrations in chemical hypoxia. A)** Basal OCR **B)** Basal ECAR. Mean values of 5 technical replicates from the last basal measurement are presented. The cells were seeded approximately 40 hours prior to measurements, and were treated with either 0, 1, 2 or 3mM metformin 18 hours prior to measurements.

Figure 4.21 shows that basal OCR decreased with increasing metformin concentrations, while basal ECAR increased. These results are similar to those of the cells cultured under normal conditions. However, ECAR does decrease slightly at 3mM metformin compared to 1mM and 2mM.

# 5. DISCUSSION

In this study, TME models were used to mimic microenvironment conditions in tumours and thereby increase the clinical relevance of the results. The study consisted of a methodological part, where protocols for chemical induction of hypoxia, assessment of proliferation and mitochondrial mass, and metabolic studies by use of the Seahorse technology were established. In addition, biological understanding of the TME models and the effect of metformin on cellular metabolism and chemical hypoxia was achieved.

## 5.1 Models

### 5.1.1 Choice of cell lines

HeLa and SiHa are two established *in vitro* model systems for cervical cancer. *In vitro* models were chosen as they allowed for studies by use of Seahorse technology, are easy to culture and allow for reproducibility. Furthermore, these cell lines have been characterised and studied by the Clinical radiation biology research group and other researchers allowing for direct comparison of results [112, 113]. The *in vitro* model also allowed for culturing under controlled conditions mimicking microenvironments, as well as allowing for metformin treatments with higher concentrations than those approved *in vivo* [112, 114].

The cell lines were grown as monocultures in two dimensions, are much less complex, and do not represent the heterogeneity found in tumours [112]. The models contain only monocultures of HeLa and SiHa cells, while a tumour consists of multiple cell types like for example fibroblasts and immune cells [42]. Furthermore, the genetically unstable nature of cancer cells leads to intra-tumour genetic heterogeneity, meaning that a tumour is made up of a collection of related subclones [115]. However, this heterogeneity in cell types and genetic variation is not represented by these cervical cancer models. Furthermore, such models cannot be used to study angiogenesis or metastasis, which are important factors influencing treatment outcome, and lack 3-D structure, cell-cell, or cell-matrix interactions found in a tumour [116, 117]. Tumours are therefore not perfectly modelled by using cell lines grown as monocultures in two dimensions.

### 5.1.2 Microenvironment models

Chemically induced hypoxia can be viewed as a shortcut to the hypoxia response related to activation of HIFs, especially the master regulator of hypoxia: HIF-1α [52]. Some ways to induce HIF-1α stabilisation and accumulation chemically are by using the chemicals $CoCl_2$, dimethyloxaloglycine and deferoxamine [52, 118]. These chemicals inhibit PHD activity, and therefore also the degradation of HIF-1α protein. However, $CoCl_2$ has been shown to promote HIF-1α accumulation more efficiently than the two other chemicals [52].

$CoCl_2$ has been shown to increase HIF-1α protein level in a dose- and time- dependent manner *in vitro*, and with a large variation in cell viability between cell lines [52]. It is therefore important to measure cell viability in addition to HIF-1α expression, when studying a new cell line. Our results demonstrated that $CoCl_2$ stabilised HIF-1α in both HeLa and SiHa cells. Based on the proliferation results, 200μM $CoCl_2$ had a negative effect on SiHa cell numbers after 24 hours, indicating an effect on cell viability. Therefore, it could be useful to test whether a lower $CoCl_2$ concentration stabilises HIF-1α without decreasing the cell number.

Sufficient oxygen levels are still present when culturing cells with $CoCl_2$. Therefore, this treatment will not induce an identical cell response to that of cells grown under low oxygen concentrations, e.g. in a hypoxia chamber. The cellular response to hypoxia is much more complex and constitute more than the HIF response, including activation of the unfolding protein response (UPR) and suppression of protein translation by MTOR [119, 120]. However, $CoCl_2$ and hypoxia have been found to induce similar alterations in cellular metabolism, including induction of glycolytic gene expression and stimulation of lactate dehydrogenase activity [121, 122]. Moreover, the use of $CoCl_2$ enables studies of the hypoxia response that is affected by HIF-1α independently from other hypoxia effects. However, it is difficult to determine the oxygen level corresponding to a certain $CoCl_2$ concentration. It is therefore difficult to compare the results with studies performed under true hypoxic conditions. Furthermore, $CoCl_2$ has been found to affect transcription of genes not affected by hypoxia [123]. However, it is generally considered a reliable model for studies of the HIF-related part of the hypoxia response [52].

High lactate concentration is a common feature of tumours [53]. Lactate can be present in up to 40mM concentrations in tumour tissue, while values in normal tissue and blood is typically 1.5-3mM [43, 53]. A study on cervical cancer by Walenta *et al*. (2000) carried out at the Norwegian Radium hospital shows that cervical tumours with metastasis had lactate concentrations of approximately 10mM, while in non-metastatic tumours the concentrations were approximately 6.3mM [88]. A model with 10mM lactate, which was used for the lactosis and lactic acidosis conditions in this study, reflects the high lactate concentrations found in metastatic cervical cancers and is therefore clinically relevant. This concentration has also been used in other studies of cervical cancer [61].

A pH of 6.6 was chosen as it is in the middle of the low pH-range found in cancer [53]. This pH has also been used in other studies, where cells are grown under conditions of low pH or lactic acidosis [89-91]. In fact, as the extracellular pH in tumours typically lie between 6.3 and 6.9, a model where pH is within this range reflects the microenvironment better than the normal culturing condition with pH between 7 and 7.6 [53]. This suggests that a culturing condition with low pH would be a better *in vitro* tumour model in general and should be adopted as the normal condition for culturing cancer cell lines.

## 5.2 Evaluation of methods

### 5.2.1 Proliferation assay

Proliferation was assessed based on the change in cell number after 24 hours of culturing. This method was chosen as it was easy, reliable and a common way to evaluate cell proliferation [124]. However, this assay cannot give information on whether the change in proliferation was caused by an alteration in the proliferation rate or be an effect of cell death. To get insight into the causes of the alterations, flow cytometry is an appropriate method. Flow cytometry can be used to determine cell cycle arrest, cell cycle time as well as apoptotic fraction [125]. Another proliferation assay which could have been useful is an MTT (3-(4,5-dimethylthiazol-2-yl)-2,5-diphenyltetrazolium bromide) assay, as it can evaluate proliferation, viability, and cytotoxicity. The assay is based on the reduction of MTT by cells that are metabolically active causing a shift in colour, where proliferation can be evaluated by measuring the absorbance [126]. However,

since a purpose of this work was to prepare for metabolic studies with Seahorse, the expected cell numbers for the TME models was essential to know, justifying the choice of assay in this study.

### 5.2.2 Mitochondrial mass

Mitochondrial mass was assessed using MitoTracker Green and a plate reader. The literature provides no or few examples where MitoTracker Green has been used specifically with a plate reader, but a Tecan plate reader can be used to detect fluorescence in cell monolayers, and MitoTracker Green stains mitochondria [105, 127]. The advantages of this method are that it is quick and offers a way to detect mitochondrial mass in adherent cells seeded in cell microplates. For this study seahorse plates were used, but the instrument can also be used with a variety of other plates [127]. As shown by the results in Figure 4.2 and 4.3, MitoTracker Green seemed to localize specifically to mitochondria and the fluorescence signal increased linearly with increasing cell numbers. This method can therefore be said to provide reliable data on mitochondrial mass *in vitro*. However, this method demands accuracy, and most likely more replicates to identify small differences between samples. As the detected signals can vary between different plates, the values should also be normalised against the same condition on each plate. Furthermore, Doherty and Perl (2017) underline the importance of knowing the reactive oxygen and nitrogen species levels in the cells as this could impact the accuracy of Mitotracker Green measurements of mitochondrial mass [128].

Methods where Mitotracker Green is frequently used to study mitochondrial mass are fluorescence microscopy and flow cytometry [129]. As plate readers are typically less sensitive, utilising microscopy and flow cytometry could provide useful information as they may detect changes in mitochondrial mass more easily [105]. Furthermore, studies with these methods would be useful, as it could provide information on the accuracy of our assay and confirm our results. There is also a range of other mitochondrial dyes that can be utilised and are optimal for different methods. MitoTracker Green was chosen as it localizes best in mitochondria of live unfixed cells, unlike some other typical dyes [105, 130]. The method used was chosen as it could further provide an opportunity for Seahorse normalization, as a higher mitochondrial mass could affect the cells' capacity for oxygen consumption.

### 5.2.3 Seahorse

Seahorse is an established method, but optimization is needed to achieve accurate results. The Mito stress assay applied in this study is useful for investigating mitochondrial function and metabolism and was found to give consistent results between runs. The results showed that OCR and ECAR increased with increasing cell number and that all the drugs had the desired effect on oxygen consumption. The seeding density chosen for HeLa and SiHa was 20 000 cells based on recommended OCR and ECAR ranges. It can therefore be concluded that the presented protocol for Seahorse measurements is adequate for procuring data on mitochondrial function in HeLa and SiHa cells.

However, there were some adjustments that could be done for further experiments. It is possible that a seeding density between 20 000 and 40 000 should be tested for the SiHa cells, as the ECAR values were just within the desired range. Furthermore, the most common final injection in the Mito stress assay is the combination of Rotenone and Antimycin A. However, for the experiments included in this study Myxothiazol was used due to availability. The OCR curves presented in the results show that the last injection does decrease the OCR considerably. However, the values should lie below the values obtained after oligomycin injection. Therefore, Rotenone and Antimycin A should be tested. Alternatively, a combination of Myxothiazol and Rotenone, as Antimycin A and Myxothiazol inhibit the same mitochondrial complex (complex III) (Figure 1.12). Another alternative could be to increase the number of measurements after the last injection to investigate if the values drop further. The non-mitochondrial oxygen consumption presented in the results could therefore be inaccurate, as inhibition of mitochondrial respiration may not be complete. The results presented support this idea, as the metformin treated cells showed a concentration dependent decrease in non-mitochondrial oxygen consumption when, in theory, metformin should only affect the mitochondrial oxygen consumption.

## 5.3 Biological characterization of the TME models

The present study provided information on HeLa and SiHa under normal growth conditions and under the presented TME models.

### 5.3.1 Cells in normal culturing conditions

HeLa and SiHa were found to have similar doubling times under normal growth conditions, 26 hours and 30 hours respectively. It is important to note that the doubling times were calculated from the number of cells after 24 hours compared to the number of cells seeded. Since the cells were still in the lagging phase at this stage and had not yet reached exponential growth, the doubling times at a later stage might differ more [131]. Furthermore, cell culturing can be done under different culturing conditions, and therefore doubling times are not always like those in other findings. Other studies show that HeLa and SiHa doubling times vary, but that HeLa cells multiply faster than SiHa cells, and that the difference is typically larger than what was found in the present study [132, 133]. Reported doubling times vary between 20 and 31 hours for HeLa cells, and 34 to 55 for SiHa cells [131-133]. Caspersen (2006), who utilised the same culturing conditions used in this study, found a doubling time of 22 hours for HeLa cells and 34 hours for SiHa cells in the exponential phase, and that the lag phase lasted approximately 3 days [131].

Further, the results show that HeLa and SiHa in normal culturing conditions have similar OCR and mitochondrial ATP production rate values, while the ECAR values differ. The similar OCR and ATP production rate values corroborate the similar mitochondrial mass in HeLa and SiHa using MitoTracker Green. Similar mitochondrial content between the two cell lines has also been found by others using quantification of mitochondrial DNA [134]. A study done with HeLa and SiHa cells using Seahorse technology found similar ATP-production rates for the two cell lines under normal conditions, reflecting a similar OCR. They found that SiHa used approximately 75% oxidative phosphorylation for production of ATP, while HeLa used approximately 50% [62]. These percentages were not calculated in this study, as ATP-production from glycolysis was not calculated, but SiHa was found to be more oxidative, which can be seen from comparing the OCR and ECAR rates as well as the OCR/ECAR ratios. These consistent results in two different laboratories support the reliability of the Seahorse technology.

The OCR/ECAR ratios for HeLa and SiHa cells show that the cell lines differ metabolically. This difference in ratios has also been found by Pérez-Escuredo *et al*. (2016), where the ratios for HeLa and SiHa were found to be approximately 2 and 6 respectively [61]. It is possible that this makes SiHa cells better targets for treatment with metformin, as their metabolism seem to

rely more on oxidative phosphorylation. However, both cell lines are shown to have similar oxygen consumption and respiratory capacity. Further, metformin was shown to have notable effects in HeLa cells. Future studies should therefore investigate these effects further in both cell lines, to determine therapeutic potential.

### 5.3.2 Cells in hypoxia TME model

The results presented in this study showed that chemically induced hypoxia reduced the number of SiHa cells compared to normal conditions. This suggests that $CoCl_2$ inhibits cell growth and division or leads to cell death. Rana, Singh, and Koch (2019) studied breast cancer cell lines and found that $CoCl_2$ leads to cell line specific apoptotic death at a certain concentration [135]. They further showed that $CoCl_2$ can lead to an increase in proliferation at lower doses than those that induce cell death. This corroborates the positive effect that HIF-1α upregulation is shown to have on proliferation [136, 137]. A decrease in proliferation has also been observed in other cancer cell lines, including colorectal cancer and pancreatic cancer [138, 139]. Studies have shown that treatment with $CoCl_2$ leads to increased formation of ROS, which causes oxidative damage in the cells [140]. ROS can lead to cell death at high doses through activation of apoptotic pathways, including mitochondrial induction of apoptosis [141, 142]. This indicates that the lower cell number caused by 200μM $CoCl_2$ could be due to apoptotic death in SiHa cells.

HeLa cells were seemingly unaffected by the chosen concentration of $CoCl_2$. However, cells were counted as soon as 24 hours after seeding in media containing $CoCl_2$, and it is possible that it would impact HeLa cell numbers as well if the cells were cultured for a longer time period. To understand how $CoCl_2$ impacts HeLa and SiHa cells, further studies using methods like flow cytometry could be used to determine possible arrest or retardation in cell cycle or induction of apoptosis. This will reveal whether the decrease in cell number is caused by a decrease in the proliferation rate per cell or by cell death. The only practical implications of the lower cell number after 24 hours in SiHa cells were that the data on mitochondrial mass, OCR and ECAR after chemically induced hypoxia should be normalised on expected cell numbers if the data is compared across cell lines or across TME models.

The results showed no significant impact of $CoCl_2$ on mitochondrial mass. However, the average signal was lower compared to Control in both cell lines. As $CoCl_2$ has been shown to increase ROS formation, which can damage mitochondrial function, mitochondrial mass could be impacted by this [143]. Furthermore, it has been found that MitoTracker Green does not accurately measure mitochondrial mass under conditions with oxidative stress, which could have impacted the readings [128]. Since metabolism is altered under hypoxic conditions, it is logical that the environment would also impact the mitochondria.

Prolonged true hypoxia has been shown to act on mitochondria in multiple ways, and the activation of HIF-1 is associated with mitochondrial function [144]. Hypoxia can alter mitochondrial morphology and mass, as well as the protein composition of the ETC. Furthermore, mitochondria has been shown to undergo fission, which could further promote autophagy of mitochondria and therefore also a reduction in mitochondrial mass [145]. A study on periodontal ligament cells treated with $CoCl_2$ found that the mitochondria collapsed away from the mitochondrial network and became fragmented and misshapen. The study also found an approximately 50% decrease in cell ATP levels in the cells treated with 200μM $CoCl_2$ [146]. However, the OCR results found in this study for cells treated with $CoCl_2$ do not indicate a decrease in mitochondrial ATP production.

The OCR/ECAR ratio was somewhat lower for the HeLa cells treated with $CoCl_2$ compared to normal conditions, but if this is significant or not cannot be said as the result is based on only one independent replicate. $CoCl_2$ treatment should in theory lead to increased glycolysis as it stabilises HIF-1α which further leads to HIF-1 upregulation of glycolytic genes [48]. Moreover, an increase in glycolysis has been observed using Seahorse in cells treated with $CoCl_2$ [147]. It would therefore be of interest to further evaluate the effects of chemically induced hypoxia as well as true hypoxia in HeLa and SiHa, by use of Seahorse.

### 5.3.3 Cells in lactosis TME model

The results showed no significant impact of lactosis on proliferation in either cell line, but did lead to an increase in mitochondrial mass compared to control conditions in HeLa cells. Proliferation in the lactosis condition has not been studied extensively. However, similar

proliferation results have been found in lung carcinoma cells, where cell counting revealed that lactosis and normal growth conditions led to similar cell numbers after 24 hours [148]. Fluorescence signals from MitoTracker Green showed a significant increase in mitochondrial mass in HeLa cells cultured in the lactosis condition. Interestingly, it has been found that fermenting HeLa cells use lactate to synthesise a big part of their lipids, and that there is a link between lactate metabolism and mitochondria [149]. This could be a possible explanation for the increase in mitochondrial mass seen in this study.

There could be an interesting link between the increase in mitochondrial mass and observations found in other studies. Walenta *et al*. (2000) found increased lactate concentrations in metastatic cervical tumours [88]. Furthermore, it has been found that cancer cells with high metastatic potential are dependent on oxidative phosphorylation [28]. The increase in mitochondrial mass found in this study for the lactosis model, could suggest a higher oxidative phosphorylation in these cells and be further evidence of a link between lactosis and metastasis in cervical tumours. High extracellular lactate concentrations have also been found to upregulate oxidative phosphorylation through increased OCR measurements by Seahorse in both HeLa and SiHa cells [61], supporting this hypothesis.

### 5.3.4 Cells in lactic acidosis TME model

The results showed that lactic acidosis led to less HeLa and SiHa cells compared to normal conditions after 24 hours. Other studies have also found that lactic acidosis at similar pH changes cell viability and lowers cell growth [150, 151]. HeLa cells grown at a pH of 6.3 has been shown to exhibit a loss of half the seeding population after 24 hours [151]. HeLa cells grown at a pH of 6.7 also exhibited a significant reduction in growth [151]. This corroborates the proliferation results found in the present study. However, contradictory results on the effects of lactic acidosis on proliferation in cancer cells have been presented, where some suggest that an acidic environment induces apoptosis, while others suggest a promotion in tumour progression [152]. Due to the decrease in cell growth found in this study, experiments on cells cultured in lactic acidosis should also be normalised on cell number if compared across cell lines or TME models.

Lactic acidosis was not found to effect mitochondrial mass in the present study. However, others have found increased mitochondrial biogenesis in lung and breast cancer cells cultured under lactic acidosis compared to lactosis through measurements of mitochondrial mass using Mitotracker Green and flow cytometry, as well as studies of mitochondrial DNA [153]. This could indicate that different types of cancer cells may react differently regarding mitochondrial biogenesis under these conditions. Future studies should also aim to investigate this further in cervical cancer cell lines using alternative methods for detection of mitochondrial mass.

In contrast to hypoxia, lactic acidosis has been shown to repress glycolysis, glucose consumption and lactate production in tumour cells [56]. Cancer cells, including HeLa and SiHa, cultured under lactic acidosis have been shown to revert from aerobic glycolysis (Warburg effect) to oxidative phosphorylation [62]. Like lactosis, lactic acidosis has been shown to increase OCR in HeLa and SiHa cells [62]. HeLa showed a higher ATP-production rate and OCR than SiHa, and both cell lines mainly used oxidative phosphorylation (approximately 90%) under the lactic acidosis conditions [62]. Further experiments should therefore be done to verify these results, and the implications of this should be determined. Furthermore, experiments with lactic acidosis in combination with metformin might give interesting results, as an upregulated oxidative phosphorylation is an attractive target for therapeutical treatment with metformin.

## 5.4 Treatment of TME models with metformin

The results showed that metformin had an effect on mitochondrial function through measurements by Seahorse. This was evident from the decrease in OCR with increasing metformin doses. The increase in ECAR with metformin suggests a compensatory switch to glycolysis. Metformin undoubtedly effects metabolism, also in cervical cancer cells, as shown by this study. A decreased OCR and increased ECAR has also been shown in other cancer cells lines treated with metformin [73, 154, 155]. The results show that 3mM metformin was found to inhibit mitochondrial function to a degree where no basal or ATP-production coupled respiration was detected.

Metformin has been shown to have negative effects on cancer cells, and many *in vitro* studies have been done showing the effects of metformin. Clinical trials have also been carried out, and

more are in progress. However, it is unclear whether metformin can be accumulated in the tumour tissue to the concentrations used in many *in vitro* studies, and it could be relevant to study more realistic doses. Uptake and accumulation in the liver is facilitated by exposure to orally administered metformin and expression of OCT1 transporters [66]. It has been shown that metformin's antitumour effect is dependent on OCT expression, and that loss of OCT3 is correlated with tumour cell resistance to metformin. This could explain metformin sensitivity heterogeneity within tumours, and the variability in clinical trials [36].

There is little data on metformin concentrations *in vivo*, but a study of plasma concentrations in 467 patients by Lalau, Lemaire-Hurtel and Lacroix (2011) found a median value of 1.3mg/mL and values ranging between 0 and 133mg/L [156]. The highest value corresponds to a concentration of 1mM metformin, while the median concentration corresponded to 10μM or 0.01mM. Normal plasma levels of metformin are therefore far below typical concentrations used for *in vitro* studies. In a study of 120 publications, most of the proposed therapeutical ranges of metformin were between 0.1 and 4mg/mL, which corresponds to 774nM and 31μM [157]. The chosen concentration of 3mM metformin for this study is therefore high when compared to clinically relevant doses and should therefore reveal any relevant effects of metformin.

Despite the relatively high dose, metformin had no significant effect on proliferation or mitochondrial mass in HeLa and SiHa cells under any of the microenvironmental conditions. HeLa and SiHa treated with metformin at higher doses (20mM) have been shown to increase apoptosis, as well as induce arrest in the $G_0/G_1$ phase [158]. Other studies have shown that metformin inhibits cancer cell proliferation both *in vitro* and *in vivo*. However, inhibition of proliferation only occurs at high concentrations *in vitro*, and is therefore possibly due to indirect effects *in vivo*, where doses are notably lower [159]. However, the dose needed for reduced tumour growth is likely to be almost twice the dosage in diabetes mellitus patients [36]. A study by Sivalingham *et al*. (2020) found that metformin significantly increases mitochondrial mass in endometrial tumours and cell lines. They also found a reduction in mitochondrial function, and therefore hypothesize a compensatory biogenesis of mitochondria in response to this [160]. A study in mice with a high-fat diet also found an increase in mitochondria in the mice livers [161].

Metformin had no effect on HIF-1α stabilisation in the chemically induced hypoxia model. However, this is not necessarily unexpected as $CoCl_2$ targets the PHDs in charge of hydroxylating HIF-1α by substituting their cofactor $Fe^{2+}$ with $Co^{2+}$. Metformin would under true hypoxia in theory release oxygen for this process, as less $O_2$ would be used for oxidative phosphorylation. This could consequently lead to destabilisation of HIF-1α. A study in multiple myeloma showed that metformin, at a concentration of 5mM, was able to inhibit stabilisation of HIF-1α and subsequent HIF-1 gene upregulation [162]. Under chemically induced hypoxia, stabilisation of HIF-1α remains because there is no change in the $CoCl_2$ level. Little research has been done on HIF-1α stabilisation under treatment with both $CoCl_2$ and Metformin, and no clear evidence of an effect on HIF-1α under these conditions has been presented.

As theorised in the introduction, metformin treatment could be a way of decreasing hypoxia, as it could lower the oxygen consumption of the cells. Metformin has shown promising results on improved tumour oxygenation and inhibition of hypoxic effects [73, 162, 163]. However, Sivalingham *et al*. (2020) showed in a study of endometrial cancer, that hypoxia might lead to decreased metformin response, as cell metabolism will be reprogrammed towards glycolysis [160]. Other studies have also found that cells utilizing mostly glycolysis are resistant to metformin treatment [38]. This underlines the importance of understanding the metabolism of the cancer being targeted, as it could predict response to the treatment.

To increase the effects, the more potent biguanide phenformin has been proposed as a cancer therapeutic drug and has also shown promising results. Despite increased potency it is no longer used in diabetes mellitus patients, making it less clinically relevant compared to metformin. Phenformin is not dependent on OCTs for uptake into the cell, as it is able to cross the cellular membranes without active transport. It therefore has an increased bioavailability and can more easily reach sufficient concentrations in the tumour. Phenformin has also been shown to inhibit cell proliferation in multiple cancers [164].

## 5.5 The usefulness of Seahorse

The results of this study show that Seahorse reliably detects an increase in OCR and ECAR with an increase in cell number as well as the difference in OCR/ECAR between the two cell lines.

The results exhibit some of the possibilities that come with Seahorse data, reflecting the usefulness of this technology when studying metabolism *in vitro*. The parameters can be used to characterize different cell lines, or the same cell line under different conditions. The Mito stress assay data can also be used to look at possible damage to the mitochondria by assessing how much of the OCR that is not part of the ATP-linked respiration. For further studies of cervical cancer cell lines, Seahorse could therefore provide novel and important information on cellular metabolism in cervical cancer cell lines.

Advantages to using Seahorse for studies of metabolism include fast, real-time kinetic measurements of small amounts of cells compared to other assays with high -throughput capability. It also allows processing of multiple replicates and conditions as the instrument can process 96-well plates. The procedure is also simple and time efficient, as most of the process is automated. Since live cells are used, the cells can also be used for further selected experiments after the Seahorse assay or for normalizations of results. Seahorse also allows for measurement of more parameters than alternative methods like the non-automated Oroboros O2k, which measures oxygen consumption but not extracellular acidification [78]. The Seahorse can also be used with cells under hypoxia in a hypoxia chamber, and the Wave software has a separate workflow and template for hypoxia [80].

Limitations of Seahorse include cost, as the equipment and materials used are expensive and are often only used once before being discarded. Another limitation is the need for optimization, which also involves using more materials, increasing the cost. Furthermore, the assay has a limit of four injections, which can be inconvenient if testing more than four injection solutions on one plate. The injected compounds may also interfere with the plate or sensor fluorescence, giving misleading results. Moreover, cellular function would probably change after being exposed to the different compounds in the assay, and further experiments using the same cells may give misleading results [78].

# 6. CONCLUSION

This thesis presents a way to study cervical cancer cell metabolism using *in vitro* TME models consisting of HeLa and SiHa cells cultured under different microenvironmental conditions with a Seahorse metabolic analyser. Furthermore, it presents effects on proliferation and mitochondrial mass in three TME models compared to normal culturing conditions in cells treated with and without metformin. Different results were achieved for the different TME models showing the importance of using these models rather than cells grown under normal conditions for clinically relevant results. Moreover, it presents the effects of metformin on HIF-1α stabilisation, in addition to the effects on HeLa metabolism in two microenvironmental conditions with Seahorse.

The findings can be summarised as follows:

- Protocols for chemically induced hypoxia, detection of mitochondrial mass and Seahorse Mito stress assay were successfully established.
- Proliferation was inhibited in the hypoxia model (SiHa cells), the lactic acidosis model (both cell lines), but not in the lactosis model.
- Mitochondrial mass increased in the lactosis model (HeLa cells), but no significant increase or decrease was found in any of the other TME models.
- Metformin had no significant effect on HIF-1α stabilisation in the hypoxia model.
- Metformin had no effect on proliferation or mitochondrial mass in any TME models.
- Metformin decreased OCR in a dose dependent manner under normal conditions and in the hypoxic model (HeLa cells)
- Metformin increased ECAR under normal conditions and in the hypoxic model (HeLa cells).
- HeLa and SiHa cells were found to differ metabolically through measurements by Seahorse, which showed that SiHa cells had lower ECAR than HeLa cells. This difference makes them useful for metabolic studies.
- Seahorse provides reliable data on the metabolism of both cell lines under normal conditions and can be used for metabolic studies in TME models.

# 7. FUTURE PERSPECTIVES

While the herein presented findings show that metformin does have interesting effects on cervical cancer cell metabolism regarding OCR and ECAR, there is still much to learn about its effects on the tumour biology and its therapeutical potential. Future work should obtain more data on OCR and ECAR under the different microenvironmental conditions using the Mito stress assay. Other Seahorse assays, like the glycolysis stress assay or the ATP rate assay could also be implemented to obtain a broader insight into the metabolism in the microenvironment models with and without metformin. The effects of true hypoxia with and without metformin on the metabolism, using a Seahorse instrument placed inside a hypoxia chamber should also be investigated if possible. Furthermore, metformin treatment should be studied *in vivo* in mouse xenograft cervical cancer models with different microenvironmental characteristics and in clinical trials, like the ongoing trial at the Norwegian Radium Hospital. Future work could also investigate the effects of the microenvironment models on cell proliferation and mitochondrial mass using alternative methods. Furthermore, more cervical cancer cell lines could be included in the study to better model the biological variation found in cervical cancer in patients.

# Literature


1. National Cancer Institute. *NCI Dictionary of Cancer Terms; Cancer*. [cited 2021 January]; Available from: https://www.cancer.gov/publications/dictionaries/cancer-terms/def/cancer.
2. Bertram, J.S., *The molecular biology of cancer.* Molecular Aspects of Medicine, 2000. **21**(6): p. 167-223.
3. Hanahan, D. and R.A. Weinberg, *Hallmarks of Cancer: The Next Generation.* Cell, 2011. **144**(5): p. 646-674.
4. Hanahan, D. and R.A. Weinberg, *The Hallmarks of Cancer.* Cell, 2000. **100**(1): p. 57-70.
5. Alberts, B., *Molecular Biology of the Cell*. 2017: W.W. Norton.
6. Caviglia, J.M. and R.F. Schwabe, *Experimental Hepatocarcinogenesis*, in *Pathobiology of Human Disease*, L.M. McManus and R.N. Mitchell, Editors. 2014, Academic Press: San Diego. p. 1866-1880.
7. Nathan, C., *Points of control in inflammation.* Nature, 2002. **420**(6917): p. 846-852.
8. Bhatia, S. and K. Sharma, *Chapter 10 - Microenvironmentation in Micropropagation*, in *Modern Applications of Plant Biotechnology in Pharmaceutical Sciences*, S. Bhatia, et al., Editors. 2015, Academic Press: Boston. p. 345-360.
9. Coussens, L.M. and Z. Werb, *Inflammation and cancer.* Nature, 2002. **420**(6917): p. 860-7.
10. Singh, N., et al., *Inflammation and cancer.* Ann Afr Med, 2019. **18**(3): p. 121-126.
11. World cancer research fund. *Worldwide cancer data Global cancer statistics for the most common cancers*. 2018 [cited 2020 Dec 17th]; Available from: https://www.wcrf.org/dietandcancer/cancer-trends/worldwide-cancer-data.
12. Harvard Health Publishing. *Cervical Cancer*. 2019 [cited 2020; Available from: https://www.health.harvard.edu/a_to_z/cervical-cancer-a-to-z.
13. Cancer Research UK. *Types and grades*. 2020 [cited 2020; Available from: https://www.cancerresearchuk.org/about-cancer/cervical-cancer/stages-types-grades/types-and-grades.
14. Moscicki, A.-B., *Impact of HPV infection in adolescent populations.* Journal of Adolescent Health, 2005. **37**(6, Supplement): p. S3-S9.
15. Moody, C.A. and L.A. Laimins, *Human papillomavirus oncoproteins: pathways to transformation.* Nature Reviews Cancer, 2010. **10**(8): p. 550-560.
16. NHI. *Livmorhalskreft*. 2020 [cited 2020; Available from: https://nhi.no/sykdommer/kreft/gynekologisk-kreft/livmorhalskreft/?page=all.
17. Brisson, M., et al., *Impact of HPV vaccination and cervical screening on cervical cancer elimination: a comparative modelling analysis in 78 low-income and lower-middle-income countries.* Lancet, 2020. **395**(10224): p. 575-590.
18. World Health Organization. *Cervical cancer*. Available from: https://www.who.int/health-topics/cervical-cancer#tab=tab_1.
19. Pal, A. and R. Kundu, *Human Papillomavirus E6 and E7: The Cervical Cancer Hallmarks and Targets for Therapy.* Frontiers in Microbiology, 2020. **10**(3116).
20. WHO. *Human papillomavirus (HPV) and cervical cancer*. 2020; Available from: https://www.who.int/en/news-room/fact-sheets/detail/human-papillomavirus-(hpv)-and-cervical-cancer.
21. Cancer registry of norway. *Cancer in Norway. Cancer incidence, mortality, survival*

*and prevalence in Norway*. 2018 [cited 2020; Available from: https://www.kreftregisteret.no/globalassets/cancer-in-norway/2018/cin2018_and_special_issue.pdf.
22. Hafiz, A., et al., *Frequency and Severity of Acute Toxicity of Pelvic Radiotherapy for Gynecological Cancer.* J Coll Physicians Surg Pak, 2015. **25**(11): p. 802-6.
23. Jhingran, A. and P. Eifel, *Radiation Therapy for Cervical Carcinoma.* Glob. libr. women's med., 2008.
24. Cancer Treatment Centers of America. *Cervical cancer stages*. 2020.
25. El Bacha, T., M. Luz, and A. Da Poian, *Dynamic Adaptation of Nutrient Utilization in Humans.* Nature Education, 2010.
26. Schönenberger, M.J. and W.J. Kovacs, *Hypoxia signaling pathways: modulators of oxygen-related organelles.* Front Cell Dev Biol, 2015. **3**: p. 42.
27. Chandel, N.S., *Mitochondria as signaling organelles.* BMC Biology, 2014. **12**(1): p. 34.
28. Ashton, T.M., et al., *Oxidative Phosphorylation as an Emerging Target in Cancer Therapy.* Clinical Cancer Research, 2018. **24**(11): p. 2482.
29. Bhagavan N.V., C.-E. Ha., *Essentials of Medical Biochemistry*. 2011.
30. Grasso, D., et al., *Mitochondria in cancer.* Cell stress, 2020. **4**(6): p. 114-146.
31. Agnello, M., G. Morici, and A.M. Rinaldi, *A method for measuring mitochondrial mass and activity.* Cytotechnology, 2008. **56**(3): p. 145-149.
32. Jornayvaz, F.R. and G.I. Shulman, *Regulation of mitochondrial biogenesis.* Essays Biochem, 2010. **47**: p. 69-84.
33. Gureev, A.P., E.A. Shaforostova, and V.N. Popov, *Regulation of Mitochondrial Biogenesis as a Way for Active Longevity: Interaction Between the Nrf2 and PGC-1α Signaling Pathways.* Frontiers in Genetics, 2019. **10**(435).
34. Jin, M.-Z. and W.-L. Jin, *The updated landscape of tumor microenvironment and drug repurposing.* Signal Transduction and Targeted Therapy, 2020. **5**(1): p. 166.
35. Ferreira, L.M.R., A. Hebrant, and J.E. Dumont, *Metabolic reprogramming of the tumor.* Oncogene, 2012. **31**(36): p. 3999-4011.
36. Vasan, K., M. Werner, and N.S. Chandel, *Mitochondrial Metabolism as a Target for Cancer Therapy.* Cell Metab, 2020. **32**(3): p. 341-352.
37. Ju, Y.S., et al., *Origins and functional consequences of somatic mitochondrial DNA mutations in human cancer.* Elife, 2014. **3**.
38. Sancho, P., D. Barneda, and C. Heeschen, *Hallmarks of cancer stem cell metabolism.* British Journal of Cancer, 2016. **114**(12): p. 1305-1312.
39. Prusinkiewicz, M.A. and J.S. Mymryk, *Metabolic Reprogramming of the Host Cell by Human Adenovirus Infection.* Viruses, 2019. **11**(2).
40. Martínez-Ramírez, I., et al., *Regulation of Cellular Metabolism by High-Risk Human Papillomaviruses.* Int J Mol Sci, 2018. **19**(7).
41. Walker, C., E. Mojares, and A. Del Río Hernández, *Role of Extracellular Matrix in Development and Cancer Progression.* Int J Mol Sci, 2018. **19**(10).
42. Bremnes, R.M., et al., *The role of tumor stroma in cancer progression and prognosis: emphasis on carcinoma-associated fibroblasts and non-small cell lung cancer.* J Thorac Oncol, 2011. **6**(1): p. 209-17.
43. de la Cruz-López, K.G., et al., *Lactate in the Regulation of Tumor Microenvironment and Therapeutic Approaches.* Frontiers in oncology, 2019. **9**: p. 1143-1143.

44. Zhang, Q., et al., *Role of hypoxia inducible factor-1 in cancer stem cells (Review).* Mol Med Rep, 2021. **23**(1): p. 17.
45. Bhandari, V., et al., *Divergent mutational processes distinguish hypoxic and normoxic tumours.* Nature Communications, 2020. **11**(1): p. 737.
46. Secomb, T.W., et al., *Analysis of the effects of oxygen supply and demand on hypoxic fraction in tumors.* Acta Oncol, 1995. **34**(3): p. 313-6.
47. Al Tameemi, W., et al., *Hypoxia-Modified Cancer Cell Metabolism.* Front Cell Dev Biol, 2019. **7**: p. 4.
48. Hompland, T., C.S. Fjeldbo, and H. Lyng, *Tumor Hypoxia as a Barrier in Cancer Therapy: Why Levels Matter.* Cancers (Basel), 2021. **13**(3).
49. Graham, A.M. and J.S. Presnell, *Hypoxia Inducible Factor (HIF) transcription factor family expansion, diversification, divergence and selection in eukaryotes.* PloS one, 2017. **12**(6): p. e0179545-e0179545.
50. Novus Biologicals. *FAQs - Hypoxia and HIFs.* [cited 2021; Available from: https://www.novusbio.com/support/hypoxia-and-hif-faqs.
51. Matsuura, H., et al., *Inhibition of prolyl hydroxylase domain-containing protein downregulates vascular angiotensin II type 1 receptor.* Hypertension, 2011. **58**(3): p. 386-93.
52. Muñoz-Sánchez, J. and M.E. Chánez-Cárdenas, *The use of cobalt chloride as a chemical hypoxia model.* J Appl Toxicol, 2019. **39**(4): p. 556-570.
53. Pérez-Tomás, R. and I. Pérez-Guillén, *Lactate in the Tumor Microenvironment: An Essential Molecule in Cancer Progression and Treatment.* Cancers (Basel), 2020. **12**(11).
54. Hao, G., Z.P. Xu, and L. Li, *Manipulating extracellular tumour pH: an effective target for cancer therapy.* RSC Advances, 2018. **8**(39): p. 22182-22192.
55. García-Cañaveras, J.C., L. Chen, and J.D. Rabinowitz, *The Tumor Metabolic Microenvironment: Lessons from Lactate.* Cancer Res, 2019. **79**(13): p. 3155-3162.
56. Chen, J.L., et al., *The genomic analysis of lactic acidosis and acidosis response in human cancers.* PLoS Genet, 2008. **4**(12): p. e1000293.
57. Kato, Y., et al., *Acidic extracellular microenvironment and cancer.* Cancer Cell International, 2013. **13**(1): p. 89.
58. Swietach, P., *What is pH regulation, and why do cancer cells need it?* Cancer and Metastasis Reviews, 2019. **38**(1): p. 5-15.
59. Pastorekova, S., P.J. Ratcliffe, and J. Pastorek, *Molecular mechanisms of carbonic anhydrase IX-mediated pH regulation under hypoxia.* BJU Int, 2008. **101 Suppl 4**: p. 8-15.
60. Molavian, H.R., et al., *Deriving mechanisms responsible for the lack of correlation between hypoxia and acidity in solid tumors.* PLoS One, 2011. **6**(12): p. e28101.
61. Perez-Escuredo, J., et al., *Lactate promotes glutamine uptake and metabolism in oxidative cancer cells.* Cell Cycle, 2016. **15**(1): p. 72-83.
62. Wu, H., M. Ying, and X. Hu, *Lactic acidosis switches cancer cells from aerobic glycolysis back to dominant oxidative phosphorylation.* Oncotarget, 2016. **7**(26): p. 40621-40629.
63. Parks, S.K., W. Mueller-Klieser, and J. Pouysségur, *Lactate and Acidity in the Cancer Microenvironment.* Annual Review of Cancer Biology, 2020. **4**(1): p. 141-158.
64. Pollak, M., *Potential applications for biguanides in oncology.* The Journal of clinical investigation, 2013. **123**(9): p. 3693-3700.

65. Graham, G.G., et al., *Clinical Pharmacokinetics of Metformin.* Clinical Pharmacokinetics, 2011. **50**(2): p. 81-98.
66. Luengo, A., L.B. Sullivan, and M.G. Heiden, *Understanding the complex-I-ty of metformin action: limiting mitochondrial respiration to improve cancer therapy.* BMC Biol, 2014. **12**: p. 82.
67. National Center for Biotechnology Information *PubChem Compound Summary for CID 4091, Metformin*. 2020 [cited 2020; Available from: https://pubchem.ncbi.nlm.nih.gov/compound/Metformin.
68. Brunetti, L. and J. Kalabalik, *Management of type-2 diabetes mellitus in adults: focus on individualizing non-insulin therapies.* P & T : a peer-reviewed journal for formulary management, 2012. **37**(12): p. 687-696.
69. Sanchez-Rangel, E. and S.E. Inzucchi, *Metformin: clinical use in type 2 diabetes.* Diabetologia, 2017. **60**(9): p. 1586-1593.
70. Kurelac, I., et al., *The multifaceted effects of metformin on tumor microenvironment.* Seminars in Cell & Developmental Biology, 2020. **98**: p. 90-97.
71. Liu, X., et al., *Metformin Targets Central Carbon Metabolism and Reveals Mitochondrial Requirements in Human Cancers.* Cell Metab, 2016. **24**(5): p. 728-739.
72. Janzer, A., et al., *Metformin and phenformin deplete tricarboxylic acid cycle and glycolytic intermediates during cell transformation and NTPs in cancer stem cells.* Proceedings of the National Academy of Sciences, 2014. **111**(29): p. 10574.
73. Zannella, V.E., et al., *Reprogramming metabolism with metformin improves tumor oxygenation and radiotherapy response.* Clinical cancer research, 2013. **19**(24): p. 6741-6750.
74. Buchner, E., *Cell-Free Fermentation.* Nobel Lectures, Chemistry 1901-1921, 1907.
75. Kornberg, H., *Metabolism.* Encyclopedia Britannica, 2020.
76. Agilent. *Seahorse XFe96 Analyzer*. [cited 2020; Available from: https://www.agilent.com/en/product/cell-analysis/real-time-cell-metabolic-analysis/xf-analyzers/seahorse-xfe96-analyzer-740879.
77. Agilent. *How Agilent Seahorse XF Analyzers Work*. Available from: https://www.agilent.com/en/products/cell-analysis/how-seahorse-xf-analyzers-work.
78. Horan, M.P., N. Pichaud, and J.W.O. Ballard, *Review: Quantifying Mitochondrial Dysfunction in Complex Diseases of Aging.* The Journals of Gerontology: Series A, 2012. **67**(10): p. 1022-1035.
79. Agilent. *How to run an assay*. [cited 2020; Available from: https://www.agilent.com/en/product/cell-analysis/how-to-run-an-assay.
80. Agilent. *Conducting an XFe Assay in an Hypoxia Chamber at ≥3% O2**. 2016; Available from: https://www.agilent.com/cs/library/technicaloverviews/public/XFe-Assay-Hypoxia-Chamber.pdf
81. Wettmarshausen, J. and F. Perocchi, *Assessing Calcium-Stimulated Mitochondrial Bioenergetics Using the Seahorse XF96 Analyzer*, in *Calcium Signalling: Methods and Protocols*, A. Raffaello and D. Vecellio Reane, Editors. 2019, Springer New York: New York, NY. p. 197-222.
82. Agilent. *Agilent Seahorse XF Cell Mito Stress Test Kit*. 2019; Available from: https://www.agilent.com/cs/library/usermanuals/public/XF_Cell_Mito_Stress_Test_Kit_User_Guide.pdf.

83. ATCC. *HeLa (ATCC® CCL-2™)*. 2020 [cited 2020; Available from: https://www.lgcstandards-atcc.org/products/all/CCL-2.aspx?geo_country=no#generalinformation.
84. ATCC. *SiHa (ATCC® HTB-35™)*. 2020 [cited 2020; Available from: https://www.lgcstandards-atcc.org/Products/All/HTB-35.aspx.
85. ATCC. *ATCC Animal Cell Culture Guide*. 2012; Available from: https://www.atcc.org/~/media/AnimCellCulture_Guide.ashx.
86. Brunner, D., et al., *Serum-free cell culture: the serum-free media interactive online database.* Altex, 2010. **27**(1): p. 53-62.
87. Merck. *Why Use Antibiotics in Cell Culture?* ; Available from: https://www.sigmaaldrich.com/technical-documents/articles/biology/antibiotics-in-cell-culture.html.
88. Walenta, S., et al., *High lactate levels predict likelihood of metastases, tumor recurrence, and restricted patient survival in human cervical cancers.* Cancer Res, 2000. **60**(4): p. 916-21.
89. Bosticardo, M., et al., *Biased activation of human T lymphocytes due to low extracellular pH is antagonized by B7/CD28 costimulation.* European Journal of Immunology, 2001. **31**(9): p. 2829-2838.
90. Tannock, I.F. and D. Rotin, *Acid pH in tumors and its potential for therapeutic exploitation.* Cancer Res, 1989. **49**(16): p. 4373-84.
91. Rauschner, M., et al., *Impact of the acidic environment on gene expression and functional parameters of tumors in vitro and in vivo.* Journal of Experimental & Clinical Cancer Research, 2021. **40**(1): p. 10.
92. Thermo Fisher Scientific. *Freezing Cells*. [cited 2020; Available from: https://www.thermofisher.com/no/en/home/references/gibco-cell-culture-basics/cell-culture-protocols/freezing-cells.html.
93. Day, J. and G. Stacey, *Cryopreservation and Freeze-Drying Protocols*. Vol. 368. 2007.
94. Santos, N.C., et al., *Multidisciplinary utilization of dimethyl sulfoxide: pharmacological, cellular, and molecular aspects.* Biochem Pharmacol, 2003. **65**(7): p. 1035-41.
95. Shu, Z., et al., *Development of a reliable low-cost controlled cooling rate instrument for the cryopreservation of hematopoietic stem cells.* Cytotherapy, 2010. **12**(2): p. 161-169.
96. Rhyner, M.N., *The Coulter principle for analysis of subvisible particles in protein formulations.* The AAPS journal, 2011. **13**(1): p. 54-58.
97. Graham, M., *The Coulter Principle: Foundation of an Industry.* JALA: Journal of the Association for Laboratory Automation, 2003. **8**: p. 72-81.
98. Thermo Fisher Scientific, *User guide: M-PER® Mammalian Protein Extraction Reagent.* 2011.
99. Thermo Fisher Scientific. *Bradford Assay*. [cited 2020; Available from: https://www.thermofisher.com/no/en/home/life-science/protein-biology/protein-assays-analysis/protein-assays/bradford-assays.html.
100. Abcam, *Definitive guide to western blot.* abcam.com.
101. Caprette, D.R. *Preparing Protein Samples for Electrophoresis*. 2012 [cited 2020; Available from: https://www.ruf.rice.edu/~bioslabs/studies/sds-page/denature.html.
102. Bio-Rad Laboratories. *Image Lab Software User Guide* 2020; Available from: https://www.bio-rad.com/webroot/web/pdf/lsr/literature/10000076953.pdf.

103. Tocris. *Certificate of Analysis / Product Datasheet for Metformin hydrochloride*. [cited 2020; Available from: https://resources.rndsystems.com/pdfs/tocris_coa/2864_3_coa.pdf?t=1600859617.
104. Integrated DNA Technologies. *Fluorescence and Fluorescence Applications*. 2011 [cited 2021; Available from: https://sfvideo.blob.core.windows.net/sitefinity/docs/default-source/technical-report/applications-of-fluorescent-oligonucleotides.pdf?sfvrsn=544b3407_6.
105. Thermo Fisher Scientific. *MitoTracker™ Green FM - Special Packaging*. [cited 2021; Available from: https://www.thermofisher.com/order/catalog/product/M7514#/M7514.
106. Agilent. *Advanced Cell Culture Solutions for Your Seahorse XF Analyzer*. 2021; Available from: https://www.agilent.com/cs/library/brochures/5991-8657EN_seahorse_plastics_brochure.pdf.
107. Agilent. *Why is a 1-hour non-CO2 incubation necessary for the cell plate?* [cited 2020; Available from: https://www.agilent.com/en/support/cell-analysis/why-non-co2-incubation.
108. Agilent. *Characterizing Your Cells*. 2017; Available from: https://www.agilent.com/cs/library/technicaloverviews/public/5991-7994EN.pdf.
109. van der Windt, G.J.W., C.-H. Chang, and E.L. Pearce, *Measuring Bioenergetics in T Cells Using a Seahorse Extracellular Flux Analyzer.* Current protocols in immunology, 2016. **113**: p. 3.16B.1-3.16B.14.
110. Agilent. *Report generator user guide*. 2020; Available from: https://www.agilent.com/cs/library/usermanuals/public/Report_Generator_User_Guide_Seahorse_XF_Cell_Mito_Stress_Test_Single_File.pdf.
111. Natalia Romero, G.R., Andy Neilson, Brian P. Dranka. *Quantifying Cellular ATP Production Rate Using Agilent Seahorse XF Technology* 2018; Available from: https://www.agilent.com/cs/library/whitepaper/public/whitepaper-quantify-atp-production-rate-cell-analysis-5991-9303en-agilent.pdf.
112. Katt, M.E., et al., *In Vitro Tumor Models: Advantages, Disadvantages, Variables, and Selecting the Right Platform.* Front Bioeng Biotechnol, 2016. **4**: p. 12.
113. Jonsson, M., et al., *Mitochondrial Function of CKS2 Oncoprotein Links Oxidative Phosphorylation with Cell Division in Chemoradioresistant Cervical Cancer.* Neoplasia, 2019. **21**(4): p. 353-362.
114. Erices, R., et al., *Metformin, at concentrations corresponding to the treatment of diabetes, potentiates the cytotoxic effects of carboplatin in cultures of ovarian cancer cells.* Reprod Sci, 2013. **20**(12): p. 1433-46.
115. Mroz, E.A. and J.W. Rocco, *The challenges of tumor genetic diversity.* Cancer, 2017. **123**(6): p. 917-927.
116. Arantes-Rodrigues, R., et al., *In Vitro and In Vivo Experimental Models as Tools to Investigate the Efficacy of Antineoplastic Drugs on Urinary Bladder Cancer.* Anticancer Research, 2013. **33**(4): p. 1273.
117. Asghar, W., et al., *Engineering cancer microenvironments for in vitro 3-D tumor models.* Mater Today (Kidlington), 2015. **18**(10): p. 539-553.
118. Groenman, F.A., et al., *Effect of chemical stabilizers of hypoxia-inducible factors on early lung development.* Am J Physiol Lung Cell Mol Physiol, 2007. **293**(3): p. L557-67.

119. Bartoszewska, S. and J.F. Collawn, *Unfolded protein response (UPR) integrated signaling networks determine cell fate during hypoxia.* Cellular & Molecular Biology Letters, 2020. **25**(1): p. 18.
120. Chee, N.T., I. Lohse, and S.P. Brothers, *mRNA-to-protein translation in hypoxia.* Molecular Cancer, 2019. **18**(1): p. 49.
121. Marti, H.H., et al., *Hypoxia and cobalt stimulate lactate dehydrogenase (LDH) activity in vascular smooth muscle cells.* Pflügers Archiv, 1994. **429**(2): p. 216-222.
122. Semenza, G.L., et al., *Transcriptional regulation of genes encoding glycolytic enzymes by hypoxia-inducible factor 1.* J Biol Chem, 1994. **269**(38): p. 23757-63.
123. Vengellur, A., et al., *Gene expression profiling of hypoxia signaling in human hepatocellular carcinoma cells.* Physiological Genomics, 2005. **22**(3): p. 308-318.
124. Wiepz, G.J., et al., *Methods for determining the proliferation of cells in response to EGFR ligands.* Methods Mol Biol, 2006. **327**: p. 179-87.
125. Pozarowski, P. and Z. Darzynkiewicz, *Analysis of Cell Cycle by Flow Cytometry*, in *Checkpoint Controls and Cancer: Volume 2: Activation and Regulation Protocols*, A.H. Schönthal, Editor. 2004, Humana Press: Totowa, NJ. p. 301-311.
126. Sigma-Aldrich. *Protocol Guide: MTT Assay for Cell Viability and Proliferation*. [cited 2021; Available from: https://www.sigmaaldrich.com/technical-documents/protocols/biology/roche/cell-proliferation-kit-i-mtt.html.
127. Tecan. *Master the challenges of cell-based fluorescence assays.* [cited 2021; Available from: https://www.tecan.com/blog/master-the-challenges-of-cell-based-fluorescence-assays.
128. Doherty, E. and A. Perl, *Measurement of Mitochondrial Mass by Flow Cytometry during Oxidative Stress.* Reactive oxygen species (Apex, N.C.), 2017. **4**(10): p. 275-283.
129. Clutton, G., et al., *A Reproducible, Objective Method Using MitoTracker® Fluorescent Dyes to Assess Mitochondrial Mass in T Cells by Flow Cytometry.* Cytometry Part A, 2019. **95**(4): p. 450-456.
130. Thermo Fisher Scientific. *Assays for Mitochondria Function*. [cited 2021; Available from: https://www.thermofisher.com/no/en/home/life-science/cell-analysis/cell-viability-and-regulation/apoptosis/mitochondria-function.html.
131. Caspersen, E.F., *Cell cycle distribution and CKS2 protein content in cervical carcinoma cell lines after exposure to ionizing radiation*. 2006, UiO.
132. Kalu, N.N., et al., *Genomic characterization of human papillomavirus-positive and -negative human squamous cell cancer cell lines.* Oncotarget, 2017. **8**(49): p. 86369-86383.
133. Banáth, J.P., S.H. MacPhail, and P.L. Olive, *Radiation Sensitivity, H2AX Phosphorylation, and Kinetics of Repair of DNA Strand Breaks in Irradiated Cervical Cancer Cell Lines.* Cancer Research, 2004. **64**(19): p. 7144.
134. You, Y., et al., *Silibinin Induces G2/M Cell Cycle Arrest by Activating Drp1-Dependent Mitochondrial Fission in Cervical Cancer.* Front Pharmacol, 2020. **11**: p. 271.
135. Rana, N.K., P. Singh, and B. Koch, *CoCl(2) simulated hypoxia induce cell proliferation and alter the expression pattern of hypoxia associated genes involved in angiogenesis and apoptosis.* Biol Res, 2019. **52**(1): p. 12.
136. Tang, B., et al., *In vitro effects of hypoxia-inducible factor 1alpha on the biological characteristics of the SiHa uterine cervix cancer cell line.* Int J Gynecol Cancer, 2009. **19**(5): p. 898-904.

137. Weidemann, A. and R.S. Johnson, *Biology of HIF-1α.* Cell Death & Differentiation, 2008. **15**(4): p. 621-627.
138. Yang, G., et al., *The hypoxia-mimetic agent $CoCl_2$ induces chemotherapy resistance in LOVO colorectal cancer cells.* Mol Med Rep, 2016. **13**(3): p. 2583-9.
139. Dai, Z.J., et al., *Up-regulation of hypoxia inducible factor-1α by cobalt chloride correlates with proliferation and apoptosis in PC-2 cells.* J Exp Clin Cancer Res, 2012. **31**(1): p. 28.
140. Tripathi, V.K., S.A. Subramaniyan, and I. Hwang, *Molecular and Cellular Response of Co-cultured Cells toward Cobalt Chloride (CoCl2)-Induced Hypoxia.* ACS Omega, 2019. **4**(25): p. 20882-20893.
141. Redza-Dutordoir, M. and D.A. Averill-Bates, *Activation of apoptosis signalling pathways by reactive oxygen species.* Biochimica et Biophysica Acta (BBA) - Molecular Cell Research, 2016. **1863**(12): p. 2977-2992.
142. Lee, J.-H., et al., *CoCl2 induces apoptosis through the mitochondria- and death receptor-mediated pathway in the mouse embryonic stem cells.* Molecular and Cellular Biochemistry, 2013. **379**(1): p. 133-140.
143. Guo, C., et al., *Oxidative stress, mitochondrial damage and neurodegenerative diseases.* Neural Regen Res, 2013. **8**(21): p. 2003-14.
144. Solaini, G., et al., *Hypoxia and mitochondrial oxidative metabolism.* Biochimica et Biophysica Acta (BBA) - Bioenergetics, 2010. **1797**(6): p. 1171-1177.
145. Fuhrmann, D.C. and B. Brüne, *Mitochondrial composition and function under the control of hypoxia.* Redox Biol, 2017. **12**: p. 208-215.
146. He, Y., et al., *CoCl2 induces apoptosis via a ROS-dependent pathway and Drp1-mediated mitochondria fission in periodontal ligament stem cells.* American Journal of Physiology-Cell Physiology, 2018. **315**(3): p. C389-C397.
147. Agilent. *Identifying Metabolic Phenotype Switches in Cancer Cells Using the Agilent Seahorse XF Analyzer in an Hypoxic Environment*. 2016; Available from: https://www.agilent.com/cs/library/applications/5991-7146EN.pdf.
148. Kolesnik, D.L., O.N. Pyaskovskaya, and G.I. Solyanik, *Impact of lactic acidosis on the survival of Lewis lung carcinoma cells.* Exp Oncol, 2017. **39**(2): p. 112-116.
149. Chen, Y., Jr., et al., *Lactate metabolism is associated with mammalian mitochondria.* Nature Chemical Biology, 2016. **12**(11): p. 937-943.
150. Huang, W., et al., *A proposed role for glutamine in cancer cell growth through acid resistance.* Cell Research, 2013. **23**(5): p. 724-727.
151. Trebinska-Stryjewska, A., et al., *Impact of Medium pH on DOX Toxicity toward HeLa and A498 Cell Lines.* ACS omega, 2020. **5**(14): p. 7979-7986.
152. Sharma, V., et al., *Low-pH-induced apoptosis: role of endoplasmic reticulum stress-induced calcium permeability and mitochondria-dependent signaling.* Cell Stress Chaperones, 2015. **20**(3): p. 431-40.
153. Romero-Garcia, S., et al., *Lactic Acidosis Promotes Mitochondrial Biogenesis in Lung Adenocarcinoma Cells, Supporting Proliferation Under Normoxia or Survival Under Hypoxia.* Frontiers in Oncology, 2019. **9**(1053).
154. de Mey, S., et al., *Antidiabetic Biguanides Radiosensitize Hypoxic Colorectal Cancer Cells Through a Decrease in Oxygen Consumption.* Frontiers in Pharmacology, 2018. **9**(1073).

155. Ariaans, G., et al., *Anti-tumor effects of everolimus and metformin are complementary and glucose-dependent in breast cancer cells.* BMC Cancer, 2017. **17**(1): p. 232.
156. Lalau, J.-D., A.-S. Lemaire-Hurtel, and C. Lacroix, *Establishment of a Database of Metformin Plasma Concentrations and Erythrocyte Levels in Normal and Emergency Situations.* Clinical Drug Investigation, 2011. **31**(6): p. 435-438.
157. Kajbaf, F., M.E. De Broe, and J.-D. Lalau, *Therapeutic Concentrations of Metformin: A Systematic Review.* Clinical Pharmacokinetics, 2016. **55**(4): p. 439-459.
158. Xia, C., et al., *Metformin inhibits cervical cancer cell proliferation by modulating PI3K/Akt-induced major histocompatibility complex class I-related chain A gene expression.* Journal of Experimental & Clinical Cancer Research, 2020. **39**(1): p. 127.
159. Birsoy, K., D.M. Sabatini, and R. Possemato, *Untuning the tumor metabolic machine: Targeting cancer metabolism: a bedside lesson.* Nature Medicine, 2012. **18**(7): p. 1022-1023.
160. Sivalingam, V.N., et al., *Hypoxia and hyperglycaemia determine why some endometrial tumours fail to respond to metformin.* British Journal of Cancer, 2020. **122**(1): p. 62-71.
161. Wang, Y., et al., *Metformin Improves Mitochondrial Respiratory Activity through Activation of AMPK.* Cell Reports, 2019. **29**(6): p. 1511-1523.e5.
162. Kocemba-Pilarczyk, K.A., et al., *Influence of metformin on HIF-1 pathway in multiple myeloma.* Pharmacological Reports, 2020. **72**(5): p. 1407-1417.
163. Zhou, X., et al., *Metformin suppresses hypoxia-induced stabilization of HIF-1α through reprogramming of oxygen metabolism in hepatocellular carcinoma.* Oncotarget, 2016. **7**(1): p. 873-84.
164. Li, J., et al., *Targeting Metabolism in Cancer Cells and the Tumour Microenvironment for Cancer Therapy.* Molecules, 2020. **25**(20).

# APPENDIX

## Table of contents for Appendix

# Appendix A

Appendix A contains cell lines, instruments, software, kits, reagents, equipment, and antibodies used for this study.

**Table A.1 Cell line characteristics for HeLa and SiHa.**

| Name | Origin | HPV status | Phenotype | Culturing medium used | Split ratio | ATCC cat # |
|---|---|---|---|---|---|---|
| HeLa | Cervical adenocarcinoma | HPV18 | Adherent | DMEM | 1:10 | CCL-2 |
| SiHa | Cervical squamous cell carcinoma | HPV16 | Adherent | DMEM | 2:10 | HTB-35 |

**Table A.2 Instruments.**

| Instrument | Supplier |
|---|---|
| Hera Safe (LAF-bench) | Heraeus |
| Nikon Diaphot Light Microscope with LWD 0,52 Phase Contrast condenser | Nikon Corporation |
| Z2 Coulter Counter Analyzer | Beckman Coulter |
| Cell incubator NuAire 5810E | NuAire |
| PowerWave XS2, Microplate Spectrophotometer | BioTek |
| ChemiDoc MP Imaging System | Bio-Rad |
| Extracellular Flux Analyzer XFe96 | Seahorse Bioscience |
| 827 pH lab | Metrohm |
| Trans-Blot Turbo Transfer System | Bio-Rad |
| Tecan Spark 10M | Tecan |
| Zeiss cell observer microscope | Zeiss |
| Memmert Cell incubator (not hooked up to $CO_2$) | Memmert |

**Table A.3 Software**

| Name | Developer |
|---|---|
| Agilent Seahorse Wave Desktop | Agilent |
| Microsoft Word | Microsoft |
| Microsoft Excel | Microsoft |
| EndNote | Clarivate Analytics |
| Seahorse Analyzer | Agilent |
| Spark Control Magellan | Tecan |
| Gen5 2.09 | BioTek |

**Table A.4 Kits**

| Kit | Supplier | Cat # |
|---|---|---|
| Coomassie Plus (Bradford) Assay Kit | Thermo Fisher Scientific | 23236 |
| SuperSignal West Dura Extended Duration Substrate | Thermo Fisher Scientific | 34075 |
| Trans-Blot Turbo RTA Mini 0.2µm PVDF Transfer Kit | Bio-Rad | 1704272 |
| Agilent Seahorse XFe96 Extracellular Flux assay kit | Agilent | 102416-100 |

**Table A.5 Reagents**

| Name | Supplier | Cat # |
|---|---|---|
| 1,1-Dimethylbiguanide hydrochloride (metformin) | Sigma-Aldrich | D150959 |
| $CoCl_2$ 0.1M | Sigma-Aldrich | 15862 |
| NaCl 9mg/mL | Fresenius Kabi | 824862 |
| Coulter Clenz Cleaning agent | Beckman Coulter | 8448188 |
| Halt Protease Inhibitor Coctail, EDTA-Free | Thermo Fisher Scientific | 87785 |
| M-PER Mammalian Protein Extraction reagent | Thermo Fisher Scientific | 78503 |
| Pierce Lane Marker Reducing Sample Buffer (5X) | Thermo Fisher Scientific | 39000 |
| 10x premixed electrophoresis buffer Tris/Glycine/SDS | Bio-Rad | 1610772 |

| | | |
|---|---|---|
| 20X TBS-T | Santa Cruz | SC-362311 |
| Skim Milk Powder | Sigma-Aldrich | 70166 |
| 99.9% EtOH | Antibac | 600068 |
| Precision Plus Protein Dual Color Standards | Bio-Rad | 1610374 |
| Oligomycin A | Sigma-Aldrich | 75351 |
| FCCP | Sigma-Aldrich | C2920 |
| Myxothiazol | Sigma-Aldrich | T5580 |
| Seahorse Calibrant | Agilent | 100840-000 |
| MitoTracker Green FM | Thermo Fisher Scientific | M7514 |
| Dimethyl sulfoxide (DMSO) | Sigma-Aldrich | 41639 |

**Table A.6 Culturing media, sterile solutions, and supplements**

| **Name** | **Supplier** | **Cat #** |
|---|---|---|
| Dulbecco's Modified Eagles Medium (DMEM) | Thermo Fisher Scientific | 31966-021 |
| Dulbecco's Phosphate Buffered Saline | Sigma-Aldrich | D8537 |
| Trypsin-EDTA solution | Sigma-Aldrich | T3924 |
| Penicillin-Streptomycin | Sigma-Aldrich | P4333 |
| Fetal Bovine Serum | Thermo Fisher Scientific | 16000044 |
| RPMI 1640 (1x) | Thermo Fisher scientific | 11835-063 |
| Seahorse XF DMEM, pH 7.4 | Agilent | 103575-100 |
| D-Glucose | Sigma-Aldrich | G7528 |
| Sodium Pyruvate | Sigma-Aldrich | P5280 |
| L-Glutamine | Thermo Fisher Scientific | 25030-081 |
| HEPES | Thermo Fisher Scientific | 15630-106 |
| HCl | Sigma-Aldrich | H9892 |
| Calcium L-lactate hydrate | Sigma-Aldrich | L4388 |

**Table A.7 Equipment**

| Name | Supplier | Cat # |
|---|---|---|
| Fisherbrand™ Sterile Polystyrene Disposable Serological Pipets | Thermo Fisher Scientific | 13-676-10K<br>13-676-10H<br>13-676-10J |
| T75 EasYFlask | Thermo Fisher Scientific | 156499 |
| T25 EasYFlask | Thermo Fisher Scientific | 156367 |
| Sterile tubes | Sarstedt | 62.554.502<br>62.547.254 |
| 60mm Easy-Grip Style Cell Culture Dish | Falcon | 353004 |
| Nunc MicroWell 96-Well Flat-Bottom Microplate | Thermo Fisher Scientific | 167008 |
| 7.5% Mini-PROTEAN TGX Gel, 12 well and 10 well | Bio-Rad | 4561025<br>4561023 |
| Cell scraper | Sarstedt | 83.1832 |
| Eppendorf multipette plus | Sigma-Aldrich | Z374563 |
| Combitips advanced Eppendorf Biopur 5mL | VWR | 613-2072 |
| Seahorse XF96 Cell Culture Microplates | Agilent | 101085-004 |
| Syringe filters acrodisc Supor 0.2µm | Pall corporation | 4602 |
| µ-slide 8 well coverslip | ibidi | 80826 |
| Mr. frosty freezing unit | VWR | 479-3200 |

**Table A.8 – Primary and secondary antibodies used for Western Blotting.**

| | Name | Host | Supplier | Cat # |
|---|---|---|---|---|
| **Primary antibodies** | HIF-1α | Mouse | BD Biosciences | 610958 |
| | γ-Tubulin | Mouse | Sigma-aldrich | T6557 |
| **Secondary antibody** | Donkey Anti-Mouse | Donkey | Jackson Immunoresearch | 715-035-150 |

# Appendix B

Appendix B contains protocols for the methods used in this study.

### Appendix B.1 Cell splitting

To prepare medium add 50mL FBS and 5mL PS to a 500mL bottle of DMEM medium. The DMEM used already contained glutamine, negating the necessity to add it. The cells are grown in T75 EasYFlask cell bottles. Clean gloves and a LAF bench should be used during work with cells. The cells were kept in the exponential growth face. HeLa was usually split in a 1:10 ratio and SiHa was usually split in a 2:10 ratio when confluent. Cells were kept for approximately 25 passages before switching to new cells.

1. Medium, PBS and Trypsin should be warmed up to 37°C in a water bath for 30 minutes.
2. Wipe down the LAF bench and equipment with 70% ethanol. Wipe the water off the medium, PBS and trypsin before also wiping these down with 70% ethanol.
3. Examine the cells under the microscope and determine what split ratio to proceed with.
4. Remove the old medium and wash the cell surface with approximately 5 mL PBS to remove remnants from the growth medium and dead cells. Remove the PBS.
5. Add trypsin (1mL to the HeLa cells and 2mL to the SiHa cells) and gently tilt the bottle to ensure that the entire cell surface is covered.
6. Incubate at 37ºC until you can see that the cells no longer adhere to the bottle. The time of incubation varies between the different cell types.
7. To neutralize the trypsin, add medium to reach a total volume of 10mL. Mix to create a homogenous cell suspension.
8. To a new bottle add cell suspension (1mL if HeLa and 2mL if SiHa) and add medium to a total volume of 10mL. Tilt the bottle gently back and forth. Label the bottle, and incubate at 37°C. The cells should be confluent again in approximately 4 days.

### Appendix B.2 Treatment with Cobalt(II)Chloride for chemically induced hypoxia

Two concentrations of $CoCl_2$ were used: 100µM and 200µM. Four incubation times were used: 4, 6, 18 and 24 hours. Before working with $CoCl_2$ make sure you take the appropriate security measures, and collect solutions containing $CoCl_2$ and discard in designated place.

Day 1

1. Seed out desired number of cells to 60mm cell culture dishes.

Day 2

1. Prepare medium with desired concentrations of $CoCl_2$.
2. Remove the old medium from the cells without disturbing the cell layer.
3. Carefully add 3mL of $CoCl_2$ medium to the 18- and 24-hour dishes.

Day 3

1. Add 3mL of $CoCl_2$ medium to the 4- and 6-hour dishes.
2. After ended incubation time, remove the medium and wash the cells with 1mL of PBS.
3. Lysate the cells. A control dish was left untouched between seeding and lysing.

**Appendix B.3 Preparation of lactosis and lactic acidosis media**

1. Make a small amount of fresh supplemented DMEM-medium by adding 1% PS and 10% FBS (e.g. 0.3mL and 3mL to 30mL medium)
2. Make the lactosis and lactic acidosis media according to the recipe below.

| Lactosis medium:<br>To a 50mL tube add:<br>• 30mL of freshly made medium<br>• 750µL HEPES<br>• 1308µL lactate stock (200mg calcium lactate in 4mL $ddH_2O$) | Lactic acidosis medium:<br>To a 50mL tube add:<br>• 30mL of freshly made medium<br>• 750µL HEPES<br>• 1308µL lactate stock (200mg calcium lactate in 4mL $ddH_2O$)<br>• 928µL 1M HCl<br><br>(pH should be approximately 5.83) |
|---|---|

3. Gently mix the media by turning the tube upside down a few times.
4. Filter both media and transfer to T75 bottles (15mL in each bottle). Place the bottles in the cell incubator for 4 hours.
5. pH should now be approximately 6.6 for the lactic acidosis medium.
6. Cells were seeded in the correct medium by spinning the correct number of cells down at 1000g (force) for 5 min before resuspending the cell pellet in the desired medium.
7. Incubate cells at 37°C for 24 hours.

**Appendix B.4 Freezing of cells**

For this procedure you need 2 bottles of 80-90% confluent cells, growth medium at 37°C, PBS at 37°C, trypsin at 37°C, DMSO, cryotubes and a Mr. Frosty freezing unit at room temperature.

1. Wash and trypsinize the cells as usual.
2. Label 8 cryotubes with date, cell line, amount (1/4 T75 bottle) and name.
3. Inactivate the trypsin with 5mL growth medium. Transfer the cell suspension from each bottle into the same 15mL tube and spin the cells down at 1000 rpm for 5 minutes at room temperature.
4. Remove the supernatant and resuspend the pellet in 2.1 mL growth medium.
5. Prepare 20% DMSO solution by carefully adding 2mL DMSO to 8mL FBS.
6. Add 2.1mL FBS to the cell suspension, and 4.2mL of the 20% DMSO solution. The total volume should now be 8,4mL.
7. Mix carefully, but quickly and aliquot 1mL solution to each cryotube.
8. Place the cryotubes in Mr. Frosty, which is immediately placed at -80°C.
9. After 24 hours, transfer the cryotubes to a liquid nitrogen tank for long time storage.

**Appendix B.5 Thawing of cells**

Preparations:

1. Heat up growth medium in water bath at 37°C and fill up a small box with ice for retrieval of cells. Place a filtered T25 bottle and a 15mL tube in the LAF bench.

Protocol:

1. Thaw the frozen cells in the water bath at 37°C until you see that almost everything has thawed.
2. Transfer the thawed cells into the 15mL tube (if there is still frozen cells, use some medium to thaw it completely and transfer to the 15mL tube). Carefully add 10mL medium to the 15mL tube.
3. Centrifuge the tube at 1000g (force) for 6 minutes. Remove the supernatant.
4. Add 5-6mL of medium to the 15mL tube and dissolve the cell pellet.
5. Mix well, and transfer to the T25 bottle. Place in a cell incubator.

**Appendix B.6 Cell quantification**

1. Add 1mL of cell suspension to a small plastic cup.
2. Turn on the Coulter Counter and lower the platform to remove the cup of Coulter Clenz® cleaning agent and replace it with a cup of NaCl solution and submerge the aperture.
3. Flush the instrument twice using the "Flush Aperture" function. Repeat this step once.
4. Add 9mL of NaCl solution to the cup with the cells and mix thoroughly.
5. In "Set-Up" put the upper and lower size of the particles to 24µm and 8µm, respectively. Also set the dilution factor to the correct number (in this case 10).
6. Ensure that your solution is well mixed and lower the sample platform to replace the NaCl solution with your cell solution. Submerge the aperture.
7. Push the "start/stop" button to count the cells. The Coulter Counter will give you the number of cells per mL.
8. When done, replace the cell solution with a cup of Coulter Clenz® cleaning agent and flush the aperture once. Turn off the Coulter Counter and dispose of your sample.

**Appendix B.7 Lysing of cells**

Preparations:

1. Let Halt protease inhibitor cocktail reach room temperature. Vortex and spin quickly down before use for homogenous solution. Right before use: Add 10µl Halt protease inhibitor cocktail per mL M-PER Mammalian Protein Extraction Reagent lysis buffer.

Protocol:

1. Remove medium and wash the cells with 1mL cold PBS. Remove PBS.
2. Use a fitting amount of lysis buffer. The recommended amount is approximately 100µL per 1 million cells, but it is possible to use less if you want a more concentrated lysate. Here 150µL was used for dishes containing around 2 million cells.
3. Scrape off the cells using a cell scraper and transfer the solution to an Eppendorf tube using a pipette. Pipette the cell suspension up and down to mix and remove lumps.
4. Place tubes on a shaker for around 10 minutes.
5. Spin down at 14 000 g (force) for 15 minutes to remove cell debris.
6. Transfer the supernatant to a new Eppendorf tube and freeze at -80°C.

## Appendix B.8 Protein Quantification with Coomassie Plus (Bradford) Assay kit

Preparations:

1. Dilute BSA (2mg/mL) according to the table below for making the standard curve.
2. Before use: Tilt the bottle with Coomassie Plus back and forth to dissolve any aggregates that may occur during storage. Take out what you need and let it reach room temperature before further use. Wrap in tin foil as the solution is light sensitive.
3. When testing a new cell line, use undiluted and diluted samples to make sure the concentrations are within the range of the standard curve. HeLa cells were diluted 1:4 and SiHa cells were diluted 1:3.

Dilutions for standard curve using BSA with a concentration of 2mg/mL:

| Sample | $ddH_2O$ (µL) | BSA (µL) | Final concentration (µg/mL) | Comment |
|---|---|---|---|---|
| A | 80 | 120 | 1200 | Take BSA from 2mg/mL stock |
| B | 33 | 167 | 1000 | Take BSA from A |
| C | 50 | 150 | 750 | Take BSA from B |
| D | 67 | 133 | 500 | Take BSA from C |
| E | 100 | 100 | 250 | Take BSA from D |
| F | 100 | 100 | 125 | Take BSA from E |

Protocol:

1. Pipette 10µl of each standard or lysate to each well in a 96-well plate. Use triplets.
2. Add 300µl Coomassie Plus to each well and mix using a plate shaker for 30 seconds.
3. Cover the plate with tin foil and incubate at room temperature for 10 minutes.
4. Mix using a plate shaker for 30 seconds and measure absorbance using the PowerWave XS2, Microplate Spectrophotometer.
5. Calculate concentrations using the BSA standard curve.

## Appendix B.9 Western Blotting

Preparation of samples

1. Add 5x sample loading buffer to your samples in a 1:4 ratio.
2. Boil the samples for 5 min at 95°C. Spin down to collect vapour and put samples on ice.

Electrophoresis

1. Place the gel in the electrophoresis cell. If only running one gel, use a dummy gel.

2. Use approximately 400mL cold 1xRunning buffer. Fill the space between the gels first, and then in the cell itself if there is no leak.
3. Remove the gel comb and wash the wells with running buffer.
4. Add 5µL of Precision Plus Protein™ Dual Color Standards to the first (and last) well. Add the desired amount of sample (cell lysate) to the other wells.
5. Run gel at 200V for approximately 40-45 min. Put the finished gel in dd$H_2O$.

Blotting with Trans-Blot Turbo Transfer system

1. Put filter stacks in transfer buffer.
2. Activate the membrane by covering it in 100% ethanol for 30 seconds, and then transfer it to the transfer buffer with the filter stacks.
3. Remove all excess liquid from the filter stacks and assemble the transfer pack in the following order in the cassette: 1. Filter stack 2. Membrane 3. Gel 4. Filter stack. When blotting two mini gels place them so that the bottoms of the gels face each other. Always use gloves to prevent contamination of gel or membrane and use tweezers to move and adjust the membrane. Be careful during assembly to avoid air bubbles. Use a blot roller on the assembled transfer pack to remove bubbles and to make sure all layers have consistent contact. Carefully place the lid on the cassette and place it in the instrument.
4. Turn on the Trans-Blot instrument and choose the desired protocol and press Run.
5. Rinse all parts in the sink after use.
6. The membrane can be put in TBS-T until the next step.

Blocking

1. Block in room temperature for 15 minutes in 25-30mL skim milk solution (5% in TBS-T).
2. Using a scalpel, mark the membrane(s) so that identification is easy. Cut the membrane in the desired spot so that primary antibodies can be added to the correct part of the membrane.

Addition of primary antibody

1. 50 mL tubes with 3mL skim milk solution (5% in TBS-T) and desired antibody are prepared. Carefully place the membrane with the protein side facing inwards into the tube.
2. Place the tubes on a roller at 4°C overnight.

3. Wash the membrane for 3x 5 min with TBS-T.

Addition of secondary antibody

1. 10 mL skim milk solution (5% in TBS-T) is added to a 50mL tube along with 1µL of secondary antibody (here, Donkey anti-mouse (DAM)). Carefully place the membrane with the protein side facing inwards into the tube.
2. Place the tubes on a "roller" for 1 hour in room temperature.
3. Wash the membrane(s) for 3x 5 min with TBS-T.

Development using Chemidoc

1. Prepare the developing solution. Use 1mL per membrane (0,5 mL of each reagent).
2. Place the membrane on transparent and add the solution. Place another piece of transparent on top to avoid spill. Let the solution work for approximately 5 min (without movement). Make sure the protein side is facing up.
3. Take pictures of the membrane using the chemidoc. The Image Lab software can then be used to merge and analyze the pictures further.
4. If it is desirable to keep the membrane for further experiments, wash it in TBS-T and wrap it in saran wrap. Store at -20°C.

Recipes for solutions used for the western blot protocol.

| **Solution** | **Reagents** |
|---|---|
| 1x Running buffer | 100 mL 10 x runningbuffer (Bio-Rad)<br>900 mL $ddH_2O$ |
| Transblot buffer | 200 mL Transblot buffer (5x) (Bio-Rad)<br>600 mL $ddH_20$<br>200 mL Abs EtOH |
| 1 x TBS-T | 50 mL 20 x TBS-T<br>1000 mL $ddH_2O$ |
| 5% skim milk solution | 5g skim milk powder in 100mL 1 x TBS-T |

**Appendix B.10 Preparation of Metformin stock solution**

A stock of 100mM metformin was made using sterile water and 1,1-Dimethylbiguanide hydrochloride from Sigma-Aldrich. The stock was kept at -20°C for 1 month.

1. Weigh out 165.62mg metformin and add it to a 50mL tube.
2. Add 10mL sterile water, and vortex the solution.

3. Using a syringe filter (0.2µm) to filtrate the solution before adding it to 1.5mL autoclaved Eppendorf tubes. Place tubes at -20°C.

**Appendix B.11 Detection of mitochondrial mass**

MitoTracker Green Stock concentration: 1mM. MitoTracker Green is light sensitive, work with the lights off.

1. To 5µl of MitoTracker stock, add 45µL DMSO to dilute it further.
2. To make MitoTracker medium add the 50µL of diluted Mitotracker solution to 25mL RPMI medium (without phenol red). Final MitoTracker concentration: 200nM.
3. Remove the seeding media from the cells and replace it with 100µL MitoTracker medium.
4. Incubate under growth conditions for 30 minutes.
5. Remove MitoTracker media and replace it with PBS.
6. Measure fluorescence using Tecan plate reader at excitation 485 and emission 530. Settings were: 30 flashes, plate read from the top and gain calculated from the well with the assumed highest signal.

**Appendix B.12 Seahorse Protocol for Mito Stress Test**

Day 1

1. Turn on the Seahorse instrument (to let it warm up and stabilise) and open the Wave software on the computer. Turn the heater on, and make sure that it is connected.
2. Open the XFe96 extracellular Flux assay kit and put the guide plates to the side. Remove the sensor cartridge from the utility plate and carefully place it upside down on the bench. Add 200µL Seahorse XF Calibrant to each well of the utility plate and place the sensor cartridge back onto the utility plate. Place in non-CO2 incubator overnight.
3. Seed the cells in 100µL medium in an Agilent Seahorse XFe96 Cell culture Micro plate. Keep the bottom row empty. This is typically done the afternoon before starting the experiment so the cells have time to adhere, but approximately 6 hours should also be enough time for the cells to adhere.

Day 2

1. Heat up the Agilent Seahorse XF DMEM Medium pH 7.4 to 37°C using a water bath and turn on the LAF bench.
2. Prepare the medium by adding appropriate amounts of glucose, sodium pyruvate, glutamine and Agilent Seahorse XF DMEM Medium to a glass bottle. For one plate you need: 72,5mg glucose, 9mg sodium pyruvate, 400µL glutamine and 40mL XF Base Medium. Keep at 37°C until use.
3. Remove the medium from the seeded cells and add 180uL to each well of the freshly made seahorse medium (also to the wells without cells). Place in the non-$CO_2$ incubator for 1 hour.
4. Prepare the A, B and C solutions.
    - ➔ Solution A: 5µL Oligomycin + 5mL Seahorse medium (Final concentration: 10µM)
    - ➔ Solution B: 5µL FCCP + 5mL Seahorse medium (Final concentration: 10µM)
    - ➔ Solution C: 10µL Myxothiazol + 5mL Seahorse medium (Final concentration: 20µM)
5. Add the A (20µL to each well), B (22.5µL to each well) and C (25µL to each well) solutions to the hydrated cartridge using the guide plates in the assay kit.
6. Start a new protocol in Wave and set up the experiment by adding injections, type of media used, no. of desired measurements. The plate map is also set up, letting the instrument know which wells contain what. When this is done the experiment is ready to be run. Follow the instructions given by the instrument.
7. Carefully place the Cartridge without the lid in the instrument when asked to.
8. Place the cell plate without the lid in the instrument when asked to.
9. The instrument will do the measurements. This takes approximately 1h and 40 minutes.
10. Throw away the plate and cartridge.

## Appendix C

Appendix C contains the western blots done to verify stabilisation of HIF-1α in cells treated with $CoCl_2$, and the western blots done to investigate the effect of metformin on chemically induced stabilisation of HIF-1α.

| | Cell line | HeLa | | | | | | | | |
|---|---|---|---|---|---|---|---|---|---|---|
| | Treatment | Control | 100μM (4h) | 200μM (4h) | 100μM (6h) | 200μM (6h) | 100μM (18h) | 200μM (18h) | 100μM (24h) | 200μM (24h) |
| 1 | HIF-1α (120kDa) | | | | | | | | | |
| | γ-tubulin (48kDa) | | | | | | | | | |
| 2 | HIF-1α (120kDa) | | | | | | | | | |
| | γ-tubulin (48kDa) | | | | | | | | | |
| 3 | HIF-1α (120kDa) | | | | | | | | | |
| | γ-tubulin (48kDa) | | | | | | | | | |

**Figure C.1 Western blots for optimization of chemical stabilisation of HIF-1α in HeLa.** The cells were treated with the indicated $CoCl_2$ concentrations for the indicated incubation times. The figure shows Western blots from three biological replicates. h: hours.

| | Cell line | SiHa | | | | | | | | |
|---|---|---|---|---|---|---|---|---|---|---|
| | Treatment | Control | 100μM (4h) | 200μM (4h) | 100μM (6h) | 200μM (6h) | 100μM (18h) | 200μM (18h) | 100μM (24h) | 200μM (24h) |
| 1 | HIF-1α (120kDa) | | | | | | | | | |
| | γ-tubulin (48kDa) | | | | | | | | | |
| 2 | HIF-1α (120kDa) | | | | | | | | | |
| | γ-tubulin (48kDa) | | | | | | | | | |
| 3 | HIF-1α (120kDa) | | | | | | | | | |
| | γ-tubulin (48kDa) | | | | | | | | | |

**Figure C.2 Western blots for optimization of chemical stabilisation of HIF-1α in HeLa.** The cells were treated with the indicated $CoCl_2$ concentrations for the indicated incubation times. The figure shows Western blots from three biological replicates h: hours.

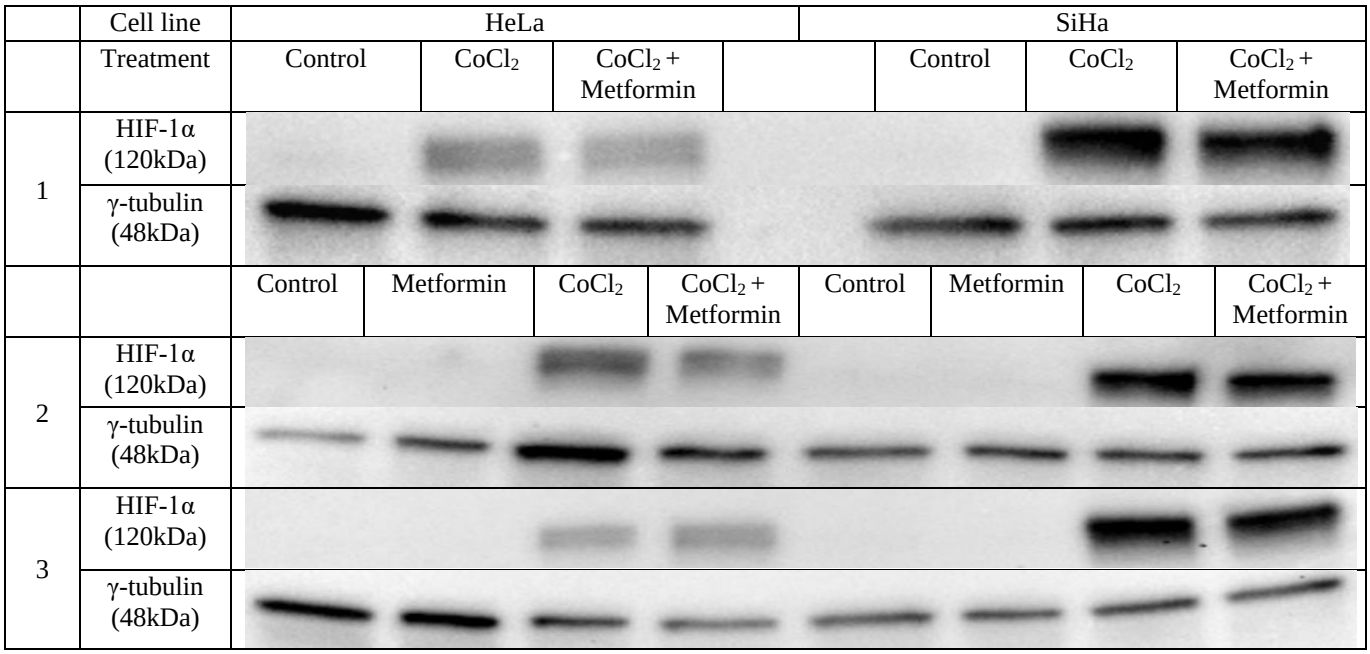


**Figure C.3 Western blots showing effect of metformin on chemically stabilised HIF-1α in HeLa and SiHa cells.** The cells were treated with 200μM $CoCl_2$ for 24 hours, where the last 18 hours also included treatment with 3mM metformin. New lysates was made for each experiment, giving three biological replicates. h: hours.

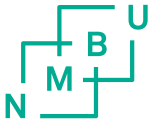


**Norges miljø- og biovitenskapelige universitet**
Noregs miljø- og biovitskapelege universitet
Norwegian University of Life Sciences

Postboks 5003
NO-1432 Ås
Norway